UNIVERSITY OF THE WITWATERSRAND, JOHANNESBURG

Effect of gas flow rate on the welding of ferritic stainless steel using alternative electrode 308L for railway coal wagons

MSC RESEARCH DISSERTATION

Prepared by

Audrey Maleka

607731

Submitted to

School of Chemical and Metallurgical Engineering, Faculty of Engineering and the Built Environment, University of the Witwatersrand, Johannesburg, South Africa

Declarations

I declare that this dissertation is my own, unaided work. It is being submitted for the Master of Science in the University of the Witwatersrand, Johannesburg. It has not been submitted before for any degree or examination in any other University.

____

(Signature of candidate)

__________29th _______day of_ September ____2022___________

Abstract

In this study 3Cr12 stainless steel was welded using 308L as an alternative consumable electrode using Gas Metal Arc Welding (GMAW) process. The electrode was selected because it is relatively cheap compared to the currently used 309L electrode. The aim of the study was to investigate the effect of varying shielding gas (helium) flow rate (10L/min, 15L/min, 20L/min, and 25L/min) on the quality of the weld, microstructural, mechanical and corrosion properties. Magnetic particle inspection fluorescent testing is the non-destructive test that was performed to evaluate the soundness of the welds. Subsequent tests were performed on defect free samples. Surface properties and morphologies of the samples were analysed by stereoscope, optical microscope and scanning electron microscope (SEM). Phases were characterised by X-ray diffraction (XRD). Mechanical tests were evaluated by conducting hardness, tensile and Charpy V-notch tests. Huey corrosion test was used to study the corrosion behaviour of the welded samples in a boiling solution of 65% HNO_3 for 48 hours. The microstructural results showed that the parent metal had a fully ferritic structure, while the HAZ contained coarse grained ferrite with intergranular martensite. The weld consisted of austenite, ferrite, and martensite, obtained phases were further confirmed by XRD.As the gas flowrate was increasing it was observed that the martensite content increased on the heat affected zone and the weld leading to increased hardness and ultimate tensile strength however reducing the % elongation. In addition, all flowrate managed to exceed the absorbed energy expected for the material. No intergranular corrosion (sensitization) was observed on any of the samples on both Huey corrosion test and electro-etching.

Dedication

In loving memory of my father

Mohube Moses Maleka

1962 – 2006

Acknowledgement

- I thankfully acknowledge my academic supervisor Prof Nthabiseng Maledi for her consistent support financially, mentally, and emotionally throughout my study. Her politeness, technical support and encouraging words carried me throughout the study.

- I would also love to appreciate the availability of the Transnet laboratory and thankfully acknowledge Dr Velaphi Matjeke under his leadership for making all the resources available to me whenever I needed them and providing me with in-depth sight of the study.

- My appreciation goes to my supportive mother (Lephepane Lorraine Maleka) who had been my consistent pillar of strength in all my studies, her support is overwhelming and unmatched.

- My affectionate gratitude goes to my little family, my fiancé (Brian Malapane) for his support always as well as my baby boy Bahumi for offering me all the smiles that kept me going.

- My siblings (Kgaladi, Mosa and Letago Maleka) whom made things easier for me by helping out whenever I needed their assistance.

Table of Contents

List of figures

List of Tables

List of symbols

A_1: the eutectoid temperature, 723°C (lowest temperature for stable austenite).

A_3: lower limit of austenite field for hypo-eutectoid steels (< 0.8wt% C).

A_{cm}: lower limit of austenite field for hyper-eutectoid steels (> 0.8wt% C).

(α-Fe)-Alpha Ferrite

(δ-Fe)-Delta Ferrite

(ɣ-Fe)-Gamma Austenite

°C-Degrees Celsius (measurement of temperature)

mm^2-milimeters squared (Area measurement)

Nomenclature

A

Al-Aluminium

A-Ampere

AISI-American Iron and Steel Institute

Ar-Argon

AHW-Atomic Hydrogen Welding

B

BCC-Body Cubic Centre

BCT-Body-Centred Tetragonal

C

C-Carbon

Cr-Chromium

Cu-Copper

D

DBTT-Ductile-Brittle Transition Temperature

E

EGW-Electro Gas Welding

ESW-Electro Slag Welding

F

FCAW-Fluxed Cored Arc Welding

FCC-Face Cubic Centre

Fe-Iron

FF-Ferrite factor

FSS-Ferritic Stainless Steel

G

GMAW-Gas Metal Arc Welding

GTAW-Gas Tungsten Arc Welding

H

HAZ-Heat Affected Zone

He-Helium

HI-Heat Input

HTHAZ-High Temperature Heat Affected Zone

Hv-Vickers hardness

I

IGC-Intergranular corrosion

J

J-Joules

K

KJ-kilo joules

KFF-Kalhuester Ferrite Factor

L

LTHAZ-Low Temperature Heat Affected Zone

M

MAG

Max-Maximum

MIG-Metal Inert Gas

MS&A- Middleburg Steel and Alloy

Min-Minimum

MIP-Magnetic Particle Inspection

MPA-Mega pascal

Mn-Manganese

MM-Millimetres

Mo-Molybdenum

N

Nb-Niobium

NDT-Non-Destructive Testing

Ni-Nickel

N-Nitrogen

S

SAW-Shielded Arc Welding

SEM-Scanning Electron Microscope

SMAW-Shield Metal Arc Welding

SS-Stainless steel

T

Ti-Titanium

TIG-Tungsten Inert Gas

U

UTS-Ultimate Tensile Strength

UV-Ultra violet

V

V-Voltage

X

XRD-X-ray Diffraction

Y

YS-Yield strength

Chapter 1: Introduction

1.1 Background of study

Ferritic stainless steels are widely used for structural and railway wagons application. The coal line wagons are fabricated using ferritic stainless steel. The 3Cr12 ferritic stainless steel is a chromium containing corrosion resisting steel developed as an alternative material of construction to mild steel and aluminium, with improved mechanical and corrosion properties. Ferritic stainless steel was developed specifically as a utility grade, combining low cost with good resistance to wet abrasion in mildly corrosive environments. In addition, the ferritic grade stainless steel has good weldability of up to 30 mm thickness (Oy, 2014). Typical applications of 3Cr12 ferritic stainless steel includes furnace and oven parts, mining and minerals processing transportation and rail wagon for coal and iron ore (SASSDA, 2013).

The 3Cr12 coal wagons in South Africa and Australia have always been fabricated using the austenitic 309L welding consumable electrode, since the first batch that was put into service in 1985 (SASSDA, 2013). One of the biggest cost drivers for manufacturing railway vehicles with ferritic stainless steels is the welding operation and consumables. The cost rate of 309L and 308L welding wires is 17.5 and 13.9 US dollars per kg respectively. Therefore, using the 308L welding wire to fabricate the jumbo wagon will results in 21% decrease in costs.

Due to an increased payload, and high traffic demand of wagon fleet depicted in Figure 1-1, the manufacturing process must be robust in a way that the obtained wagon joints will increase the lifespan of the wagon leading to reduced cycle cost as well as maintenance costs.

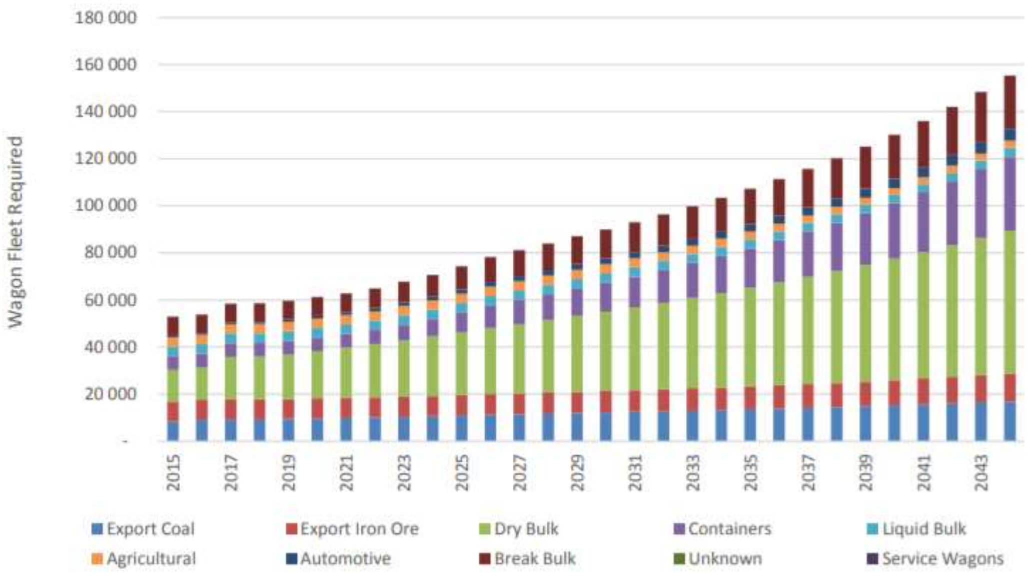

Figure 1-1: Wagon demand for transporting of goods (Plan, 2017).

Welding processes and consumables plays a major role in the rolling stock fabrication of steels. Furthermore, welding joints of a wagon plays a crucial role on the lifespan of the wagon and locomotives. Hence, the life cycle cost of the wagon joints is highly depended on the quality, production turnaround time, consumables, and labour. Welding is dependent on several process parameters (i.e. heat input, current, shielding gas, and shielding gas flow rate) which must be optimised to obtain good quality welds. Varying these process parameters affect the quality of the welds as well as the resulting microstructure (Chuaiphan, 2020) .

Different kinds of shielding gases are often preferred for different processes and applications. The primary function of shielding gases used in welding process, such as argon, helium, carbon dioxide and their mixtures, is to protect the weld pool against harmful contaminants that could generate defects (Mvola and Kah, 2017). In addition, shielding gases significantly affect the shape of the weld, weld geometry, metallurgical and mechanical properties, welding speed, metal transfer and arc stability (Lincoln, 2014). Hence shielding gas is a key factor in determining weld joint properties as well as process efficiencies (Bergquist, 2011).

Incorrect choice of a shielding gas can lead to weak welds, excessive spatter, or defective welds. This further leads to decreased productivity due to a need to remove the scattered drops. Only two of the noble gases, helium and argon are the most cost effective gases to be used in welding (Bolarinwa, 2018). Important characteristics of these noble gases include thermal conductivity, heat transfer and their relative density to air. Gases heavier than air such as argon blankets the weld and require lower flow rates than gases that are lighter than air (Mvola and Kah, 2017).

Gas Metal Arc Welding (GMAW) process will be utilized to join ferritic stainless steel using 308L welding wire. Helium will be used as the shielding gas and its flow rate will be varied. Gas flow rate influences the cooling rate of the material. At lower gas flow rate, lower cooling rates are expected whereas at high gas flow rates fast cooling rates are expected. Thus, different gas flow rates will lead to the formation of different microstructures in the welded joints. Gas flow rate also influence the transfer frequency of the welding wire, mode of transfer, dilution and chemical composition of the weld metal (Chuaiphan, 2020).

This study sought to investigate the effect of shielding gas (helium) flow rate on the welding of railway coal wagon with the intention of observing the effect it has on the mechanical properties, microstructure, corrosion properties, quality, and soundness of the welds.

1.2 Problem statement

Railway transport is significant and strategic in the development of the modern economy. Therefore, products and components such as wagons, coaches and locomotives are expected to be of high quality and not to fail unexpectedly. It is against this background that scientists and engineers interest was driven towards finding fast, efficient, and cost-effective methods to produce good quality welds (Kah *et al.*, 2014) since the quality of welds is becoming increasingly important as customer expectations rise.

Improving productivity is a major focus for the welding industry and its associated research community, especially in the push for higher weld quality and reduced manufacturing costs. Weld quality is dependent on arc stability and minimizing the effects of disturbances or changes in the operating condition that commonly occur during welding (Kang *et al.*, 2009a). Recent trends of welding systems are focused on the development of new processes in order to achieve better quality, higher productivity and cost savings in welding (Kang *et al.*, 2009b).

1.3 Research Objectives

The main aim of the study is to obtain good quality joints for the wagon panels on a laboratory scale which will further enable production of wagons prototypes and enhance the in-house production of good quality and cost-effective wagons. This area of research is interesting now and for the future, due to the requirement of good mechanical properties and predominantly a low-cost material for fabrication of wagons.

The aim of the study will be achieved through the following objectives:

- Investigate the compatibility of varied helium flowrate on welding of the 3Cr12 stainless steel with 308L as the alternative welding wire and obtain sound quality welds.
- Evaluate the effect of microstructural evolution on the phases that form in the weld and the heat affected zone.
- To examine the mechanical properties of the welded samples.
- To investigate the effect of sensitization/intergranular corrosion on the welded samples.

1.4 Research questions

- What effect does the GMAW welding process parameters have on the samples during the welding of 3Cr12 material with 308L welding wire?
- Are there any welding challenges that can lead to unwanted welding defects because of different gas flow rates?
- Are there any microstructural differences when comparing the gas flow rates on the welds? And what microstructures phases will form on the HAZ and the weld at different gas flowrate?
- Are there any distinct differences on mechanical properties such as hardness, tensile and impact on the welded samples when shielding gas flow rate is varied?
- Is there any pronounced difference in corrosion resistance of the welded samples at different gas flow rates?

1.5 Hypothesis

It is postulated that the increase in gas flow rate increases the cooling rate of the material during welding hence more martensite is expected as high gas flowrate is introduced leading to higher hardness.

1.6 Outline of the dissertation

Chapter 1 of this dissertation introduces the research, background, problem statements, the aim and objectives, research questions, hypothesis, as well as the scope of the dissertation.

Chapter 2 presents a detailed literature review on the railway wagons, the description of the welding phenomena occurring during the welding process, the development of 3Cr12 and the description of ferritic stainless steel in depth. It also focused on the weldability of 3Cr12, the welding parameters, explanation on the welding consumables. Elaborated on the defects that are associated with welding, the effect of alloying elements, explaining sensitization. It also incorporated the literature survey on the work done on shielding gas as well as gas flowrates.

Chapter 3 outlines the experimental procedures that were followed to achieve the objectives of the research study. The material sample selection and sample characterisation applied on the samples. These methods include the welding process, parameters used, cleaning of the samples after welding, non-destructive testing, metallographic preparation, microstructural and macrostructural analysis, XRD, hardness testing, tensile testing, impact testing as well as the corrosion testing.

Chapter 4 presents the analysis of results and discussion of all the test conducted, including the analysis and characterisation that was carried out in this research. The findings and discussion are focusing on the NDT on welds, microstructural and macrostructural analysis, XRD diffractions, micro hardness test results, tensile tests and charpy impact tests obtained results from the tests conducted together with the comparison of the previous work done in the literature.

Chapter 5 presents the conclusions of the study based on the work done and recommendations for future studies.

Chapter 2: Literature Review

2.1 Introduction

This chapter is a review of the literature relevant to this study. This survey addresses the railway wagons applications, the welding processes description, classification of stainless steel, development of 3Cr12,the effect of alloying elements, discussion of the ferritic stainless steel, weldability of 3Cr12, microstructural evolution, welding parameters, welding consumables suitable for 3Cr12, defects associated with welding, in depth explanation of sensitization and finally, the effect of the shielding gas which discusses the previous work done on the effect of gas flow rate that was varied to obtain the optimum gas flow rate to be utilized.

2.2 Railway wagons

Materials for railway applications are required to maintain the integrity of the structure (i.e., to be sufficiently robust to withstand their service environment) and to be inert (i.e., corrosion resistant). As a result, iron and steel are the most commonly used fabrication materials for railway wagons due to its good strength, easy to fabricate, cast and forge, furthermore, these material has the ability to enhance its properties by adding alloying elements and performing heat treatment processes on them. The following examples may serve to indicate the considerations made in selecting a suitable grade of stainless steel for railway applications(Oy, 2014).

Austenitic stainless steel grades 1.4301 (AISI 304) and 1.4310 (AISI 301) are suitable for mild service environments and have been used in the construction of railway carriages, while ferritic stainless steel 1.4003 (ASTM S41050) has been used for freight wagons (Oy, 2014). Stainless steel is selected for both applications because it does not need protective paint coatings and thus maintenance costs are reduced. Stainless steel is also used extensively in railway buildings and construction applications. In particular, the fire resistant properties of stainless steel have been utilised in underground railway stations (e.g. wall cladding and tunnel linings) (Oy, 2014).

Ferritic stainless steels are a good substitute to the regular austenitic and mild steels due to their superior properties such as corrosion resistance (Shojaati and Beidokhti, 2017). The ferritic stainless-steel wagon has lower life cycle costing as compared to the mild steel wagons.

Coal wagons are currently built using 3Cr12 ferritic stainless-steel plates made up of low-carbon, 10.5 to 12.5 wt.% chromium and a maximum of 0.6% titanium and 309L welding electrode. Titanium attract carbon atom, due to carbon having higher affinity to titanium (Sundqvist *et al.*, 2018). This result in reducing the possible precipitation of chromium carbides on the grain boundaries (Keskitalo *et al.*, 2015). The loss of corrosion resistance due to chromium depletion within the heat affected zone (HAZ) is called sensitisation (Dahmen et al., 2015).

The chromium depletion theory states that sensitization is promoted by the intergranular precipitation of chromium-rich $M_{23}C_6$-type carbides resulting in chromium depletion in the matrix adjacent to the precipitated carbides. The reduction in chromium concentration levels increases the inability of chromium passivation to occur hence the material becomes sensitized which consequently leads to intergranular corrosion (Du Toit *et al*., 2007).

Titanium which is contained in 3Cr12 has higher affinity of reactivity as compared to chromium, as a result it attracts the carbon and form titanium carbides which depletes the carbon and less chromium carbides results and subsequently corrosion resistance reduces. Many stainless steels generally have good corrosion resistance and mechanical properties (Sundqvist *et al.*, 2018). The 3Cr12 stainless steels have good formability and they are cheaper compared to the larger stainless-steel family (Keskitalo *et al.*, 2015) such as austenitic stainless steel . The 308L welding electrode was selected over other welding consumable due to its distinct properties and cost efficiency. The 308L welding wire properties includes excellent corrosion resistance, its low carbon prevents cracking and its capability of welding all the low-grade stainless steel alloys.

2.3 Welding process: Phenomena occurring during the process

Welding is a process in which materials of the same fundamental type or class are brought together and caused to join and become one through the formation of primary and occasionally secondary chemical bonds under combined action of heat and pressure (Messler Jr, 1999). Welding is the most economical and efficient way to join metals permanently, it plays a major role in steel fabrication and repair. It is also used in the fabrication of spacecraft, fighter planes, submarines and atomic power plants. Welding ranks highly among industrial processes and involves more scientific principle and variables than those involved in any other industrial processes (Duffey, 2016). There are many different kinds of welding methods, some processes causes spark and others do not even require extra heat. Numerous welding methods or techniques are in common use for a wide range of application

Welding falls under two categories namely: homogeneous and heterogeneous welding. Homogeneous welding describes the process of joining two identical materials whereas heterogeneous welding joins two dissimilar types of material. However, the heterogeneous welding requires the materials to be joined to be of the same atomic structure so that the chemical bonds can be formed such as metallic, covalent and ionic bonds (Welding metallurgy, 2012).

Arc welding is a process whereby heat is generated by an electric arc struck between two electrodes or between electrode and a workpiece. An electrical arc is a luminous electrical discharge between two electrodes through ionized gas. The electric arc between electrode and the workpiece closes the electric circuit and creates a temperature of up to 5500°C which is enough for fusion to take place that enables the workpiece edges to join (Molabe, 2018).

Arc welding can typically be broken down into two categories non consumable electrode and consumable electrode welding. Non-consumable electrode arc welding includes Gas Tungsten Arc Welding (GTAW, TIG), Plasma arc welding (PAW), Carbon Arc Welding (CAW), Stud Arc Welding (SAW), and Atomic Hydrogen Welding (AHW).

2.3.1 Gas Tungsten Arc Welding (GTAW, TIG)

In the GTAW process, an arc is established between a tungsten electrode and the base metal(s) as shown in Figure 2-1. Under the correct conditions, the electrode does not melt, although the work does at the point where the arc contacts and produces a weld pool. The filler metal is thin wire that’s fed manually into the pool where it melts. Since tungsten is sensitive to oxygen in the air, good shielding with oxygen-free gas is required. The same inert gas provides a stable, inert environment to protect the weld pool as it solidifies. Consequently, GTAW is commonly known as TIG (tungsten inert gas) welding. The welds produced are sound, free of contaminants and slags, and as corrosion-resistant as the parent metal. Tungsten's extremely high melting temperature and good electrical conductivity make it the best choice for a non-consumable electrode. The arc temperature is typically around 11,000° F. Typical shielding gasses are Ar, He, N, or a mixture of the two. Similar to GMAW, the filler material usually is the same composition as the base metal (Florida, 2006).

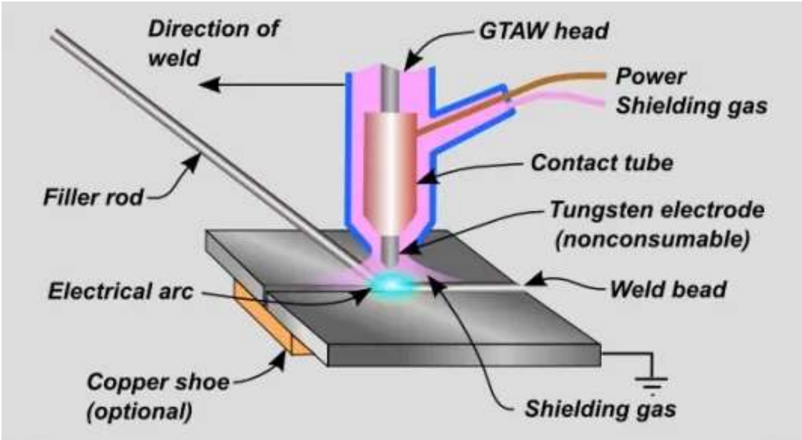

Figure 2-1: Gas Tungsten Arc Welding (Weldingis, 2021)

GTAW is easily performed on a variety of materials, from steel and its alloys to aluminium, magnesium, copper, brass, nickel, titanium, etc. Virtually any metal that is conductive lends itself to being welded using GTAW. Its clean, high-quality welds often require little or no post-weld finishing. This method produces the finest, strongest welds out of all the welding processes. However, it is also one of the slower methods of arc welding (Florida, 2006).

2.3.2 Plasma arc welding (PAW)

Plasma arc welding (PAW) is an arc welding process very similar to TIG welding as the arc is formed between a pointed tungsten electrode and the workpiece. However, by positioning the electrode within the body of the torch, the plasma arc can be separated from the shielding gas envelope. Plasma is then forced through a fine-bore copper nozzle which constricts the arc (TWI, 2003). This process is mainly used in a mechanized system where high speed and high productivity autogenous welding of square edged butt joints off up to 8 mm is required (Molabe, 2018). For the welding of thicker squared butt joints, a combination off PAW or TIG and filler wire becomes necessary to ensures full profile weld surface. Thickness greater than

10 mm require a partial V-penetration PWA W root weld, which is followed by multi-pass joint filing (Molabe, 2018).The corrosion resistance of the under bead is maintained using argon-backing gas protection.

2.3.3 Carbon Arc Welding (CAW)

Carbon Arc Welding is a process in which the joining of metals is produced by heating with an arc between a carbon electrode and the work (Ethan, 2021). No shielding is used, pressure and filler metal may or may not be used. The welding circuit for carbon arc welding is the same as for shielded metal arc welding. The difference in the apparatus is a special type of electrode holder used only for holding carbon electrodes. This type of holder is used because the carbon electrodes become extremely hot in use, and the conventional electrode holder will not efficiently hold and transmit current to the carbon electrode (Ethan, 2021). The power source is the conventional or constant current type with drooping volt-amp characteristics. Normally, a 60 percent duty cycle power source is utilized. The power source should have a voltage rating of 50 volts since this voltage is used when welding copper with the carbon arc (Ethan, 2021).Figure 2-2 illustrates the operating principle.

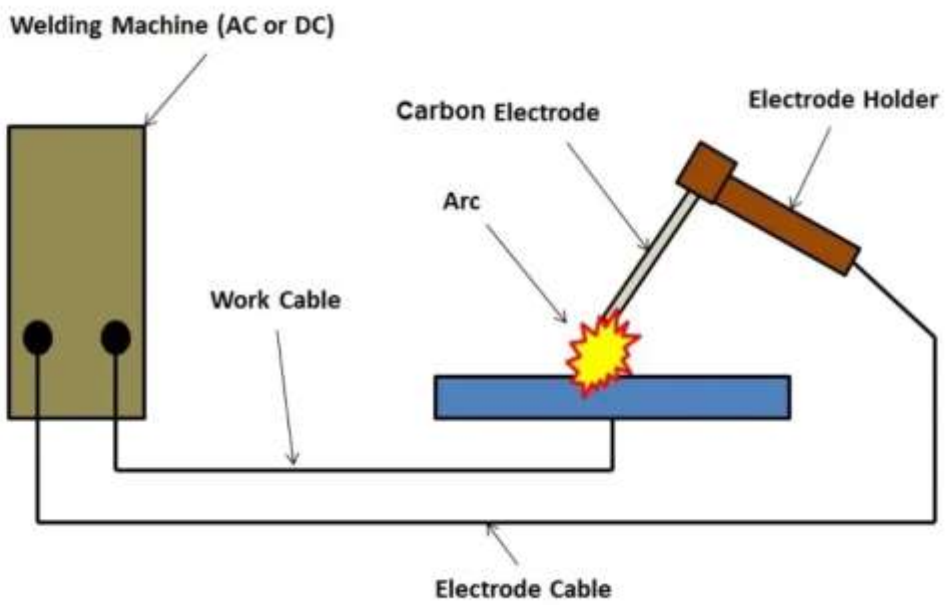

Figure 2-2: Carbon arc welding principle (Ethan, 2021)

The main use of carbon arc welding of steel is making edge welds without the addition of filler metal. This is done mainly in thin gauge sheet metal work, such as tanks, where the edges of the work are fitted closely together and fused using an appropriate flux. Galvanized steel can be braze welded with the carbon arc. A bronze welding rod is used. The arc is directed on the rod so that the galvanizing is not burned off the steel sheet. The arc should be started on the welding rod or a starting block. Low current, a short arc length, and. rapid travel speed should be used. The welding rod should melt and wet the galvanized steel (Enterprise, 2002).

2.3.4 Stud Arc Welding (SAW)

Stud arc welding is a reliable method of fastening for a wide variety of applications. It can quickly weld any size, and create strong, one-sided welds on the base metal, even as thin as 0.048 inches (Lesson, 2020). It uses a DC power supply to create the arc, which produces the joint in just 0.06 seconds that is shown in Figure 2-3. The technique is used in the automotive industry to weld heat shields, power steering, and dashboard components. It is also used in instrument panels, exhaust systems, insulation, electrical wire routing, lighting system, brake lines, and trim (Lesson, 2020).

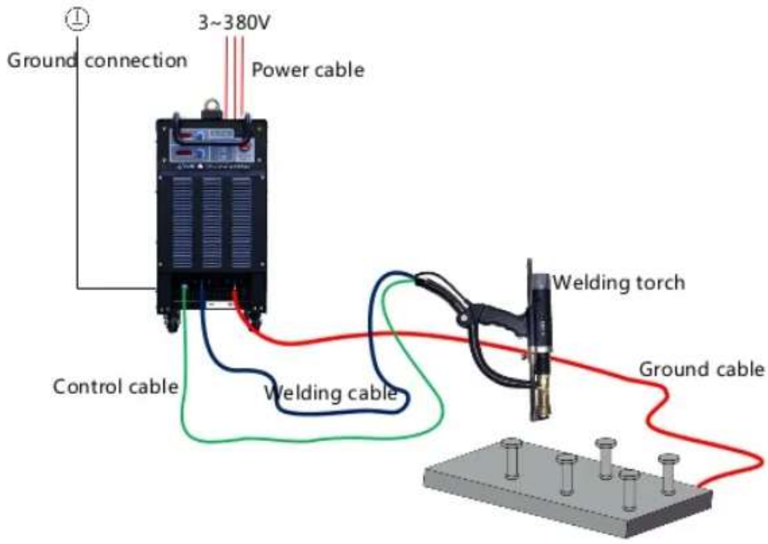

Figure 2-3: Welding sketch for stud arc welding (Lesson, 2020)

2.3.5 Atomic Hydrogen Welding (AHW)

Atomic Hydrogen Welding (AHW) is a combination of electric are and gas welding technique. It is a thermo-chemical arc welding process in which the work pieces are joined by heat obtained on passing a stream of hydrogen through an electric are struck between two tungsten electrodes, Figure 2-4 illustrates the principle of AHW.

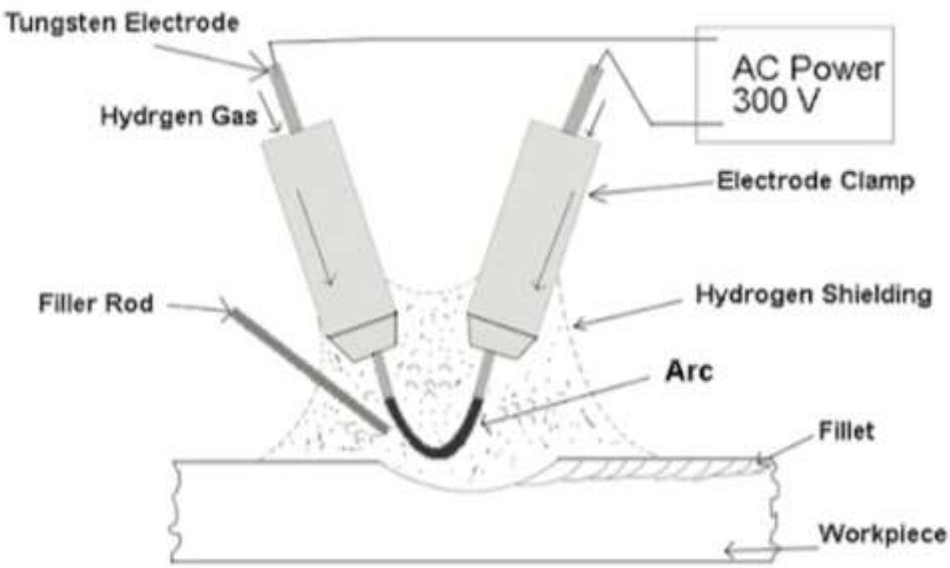

Figure 2-4: Atomic hydrogen welding setup (Thorat, 2016)

The arc is independently maintained for the workpiece or parts being welded. The hydrogen gas is normally diatomic (H_2) but where the temperatures are over 6000°C near the arc. When the hydrogen strikes a relatively cold surface, it will recombine into its diatomic form releasing the energy associated with the formation of bond. The energy in AHW can easily be varied by changing the distance between arc stream and workpiece surface. This process is being replaced by gas metal-arc welding mainly because of the availability of inexpensive inert gases. (Thorat, 2016).Consumable electrode welding includes: Gas Arc Welding (GMAW, MIG), Shielded Metal arc welding (SMAW), Flux Cored Arc Welding (FCAW), Submerged Arc Welding (SAW), Electro Gas Arc Welding (EGW) and Electro Slag Welding (ESW).

2.3.6 Gas Arc Welding (GMAW, MIG)

The GMAW welding process is easily found in any industry whose products require metal joining on a large scale. It establishes an electrical arc between a continuous filler metal electrode and the weld pool, with shielding gas from an externally supplied gas, which may be inert, active or a gas mixture. The heat of the arc melts the surface of the base metal and the end of the electrode. GMAW is a welding process which joins metals by heating the metals to their melting point with an electric arc. The arc is between a continuous, consumable electrode wire and the metal being welded.

The arc is shielded from contaminants in the atmosphere by a shielding gas. Generally, the quality of a weld joint is directly influenced by the welding input parameters during the welding process; therefore, welding can be considered as a multi-input multi-output process. Unfortunately, a common problem that has faced the manufacturer is the control of the process input parameters to obtain a good welded joint with the required bead geometry and weld quality with minimal detrimental residual stresses and distortion (Chaudhari and More, 2014)

In the GMAW process, an arc is established between a continuous wire electrode (which is always being consumed) and the base metal, Figure 2-5 illustrates this properly. Under the correct conditions, the wire is fed at a constant rate to the arc, matching the rate at which the arc melts it. The filler metal is the thin wire that’s fed automatically into the pool where it melts. Since molten metal is sensitive to oxygen in the air, good shielding with oxygen-free gases is required. This shielding gas provides a stable, inert environment to protect the weld pool as it solidifies. Consequently, GMAW is commonly known as MIG (metal inert gas) welding. Since fluxes are not used, the welds produced are sound, free of contaminants, with corrosion resistance that is similar to the parent metal. The filler material is usually the same composition (or alloy) as the base metal (Florida, 2006).

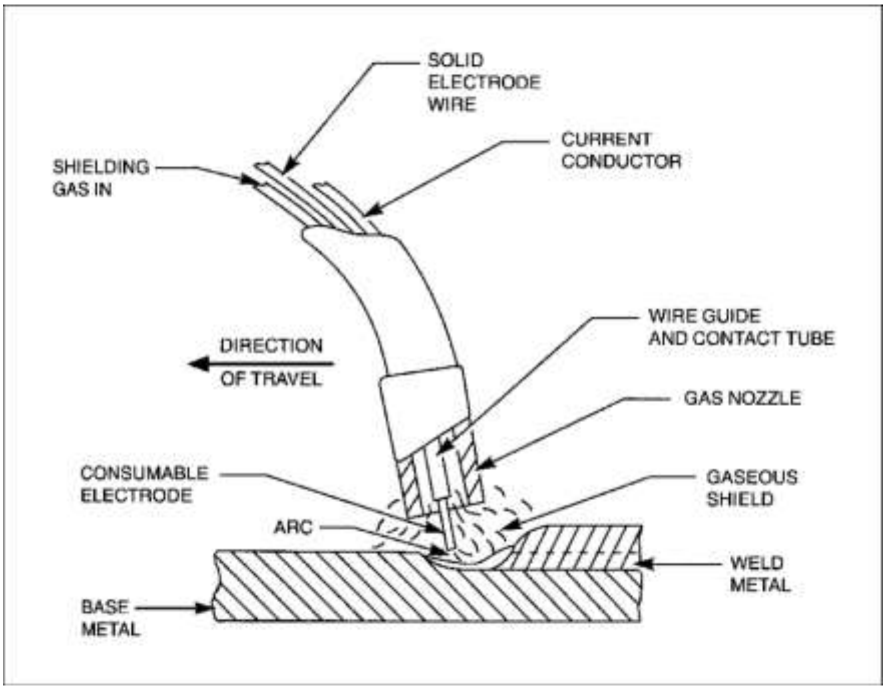

Figure 2-5: Gas arc welding GMAW (Malcom, 2000)

GMAW is extremely fast and economical. This process is easily used for welding on thin-gauge metal as well as on heavy plate. It is most commonly performed on steel (and its alloys), aluminium and magnesium, but can be used with other metals as well. It also requires a lower level of operator skill than the other two methods of electric arc welding discussed in these notes. The high welding rate and reduced post-weld clean-up are making GMAW the fastest growing welding process.

2.3.6.1 GMAW welding process

The gas metal arc welding (GMAW) process uses four basic modes to transfer metal from the electrode to the work piece. Each mode of transfer depends on the welding process, the welding power supply, and the consumable, and each has its own distinct characteristics and applications. Different transfer modes include short circuit transfer mode, globular transfer mode spray transfer mode as well as pulse spray transfer mode.

2.3.6.2 Short circuit transfer mode:

In short-circuit transfer mode, the electrode touches the work and short circuits, causing the metal to transfer because of the short. The advantage of the short circuit transfer includes its ability to be used to weld in all positions as well as the low energy that it consumes (Kang *et al.*, 2009). This mode of metal transfer typically supports the use of (0.6 - 1.1 mm) diameter electrodes shielded with either 100% CO_2 gas or a mixture of 75-80% argon, plus 25-20% CO_2 (Metal and Welding, 2013).

2.3.6.3 Globular transfer mode:

Globular transfer mode means the weld metal transfer across the arc are in large droplets usually larger than the diameter of the electrode used. This method is typically used to weld in flat and horizontal position. Globular transfers uses inexpensive CO_2 shielding gas, but is frequently used with argon/CO_2 blends (Metal and Welding, 2013).

2.3.6.4 Spray transfer mode:

Spray transfer mode is characterised by the formation of tiny molten droplets across the arc that are similar to spray coming out of a garden hose pipe when the opening is restricted. Spray transfer mode is usually smaller than the diameter of the wire used. The spray transfer mode uses high voltage and wire feed. This method produces very little splatter and most often used on thick metals in flat and horizontal positions (Metal and Welding, 2013).

2.3.6.5 Pulse spray transfer mode:

In the pulse-spray transfer mode, the power supply cycles between a high spray transfer current and a low background current. It can be used to lower heat input and reduce distortion when high travel speeds are not needed or cannot be achieved because of equipment or throughput limitation. Argon based shielding gas selection with a maximum of 18%CO_2 supports the use of pulsed spray metal transfer with carbon steel (Metal and Welding, 2013).

2.3.7 Shielded Metal arc welding (SMAW)

Shielded metal arc welding (SMAW) is a welding process that uses a flux covered metal electrode to carry an electrical current. The current forms an arc that jumps a gap from the end of the electrode to the work. The electric arc creates enough heat to melt both the electrode and the base material(s). Molten metal from the electrode travels across the arc to the molten pool of base metal where they mix together. As the arc moves away, the mixture of molten metals solidifies and becomes one piece. The molten pool of metal is surrounded and protected by a fume cloud and a covering of slag produced as the coating of the electrode burns or vaporizes, see Figure 2-6. Due to the appearance of the electrodes, SMAW is commonly known as 'stick' welding (Florida, 2006).

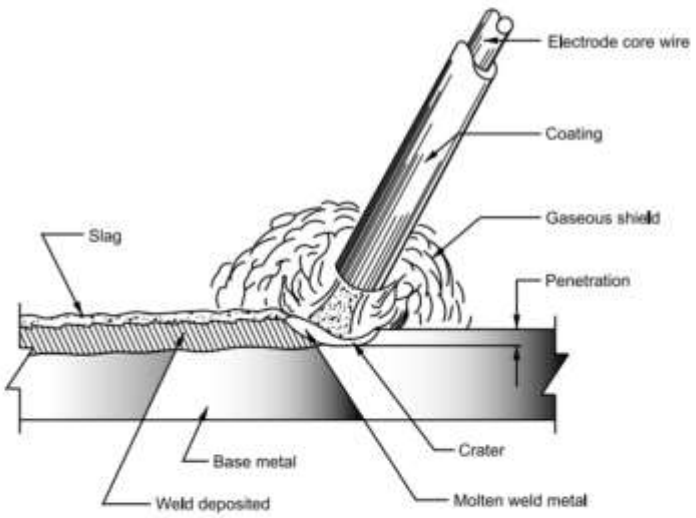

Figure 2-6: Shielded metal arc welding (Paktechpoint, 2016)

SMAW is one of the oldest and most popular methods of joining metal. Moderate quality welds can be made at low speed with good uniformity. SMAW is used primarily because of its low cost, flexibility, portability and versatility. Both the equipment and electrodes are low in cost and very simple. SMAW is very flexible in terms of the material thicknesses that can be welded (materials from 1/16" thick to several inches thick can be welded with the same machine and different settings). It is a very portable process because all that's required is a portable power supply (i.e., generator). Finally, it's quite versatile because it can weld many different types of metals, including cast iron, steel, nickel & aluminium. Some of the biggest drawbacks to SMAW are (1) that it produces a lot of smoke and sparks, (2) there is a lot of post-weld clean-up needed if the welded areas are to look presentable, (3) it is a fairly slow welding process and (4) it requires a lot of operator skill to produce consistent quality welds (Florida, 2006).

2.3.8 Flux Cored Arc Welding (FCAW)

Flux cored arc welding (FCAW or FCW) is a version of the MIG or MAG process where the solid wire consumable is replaced with a flux or metal powder filled tubular wire as shown in Figure 2-7. Flux cored arc welding (FCAW), also known as dual shield welding, is a semi-automatic arc welding process that is similar to metal active welding(MAG). FCAW uses a continuous wire fed electrode, a constant-voltage welding power supply, and similar equipment to MAG welding. The process was first developed in the 1950s as an alternative to manual metal arc welding (MMA) which is also called stick welding. FCAW overcomes many of the restrictions associated with MMA, since it uses a continuously fed wire electrode. Flux core arc welding usually uses a shielding gas similar to that used by MAG welding, but it can also be performed without a shielding gas. It is more productive than MAG welding (TWI, 2003).

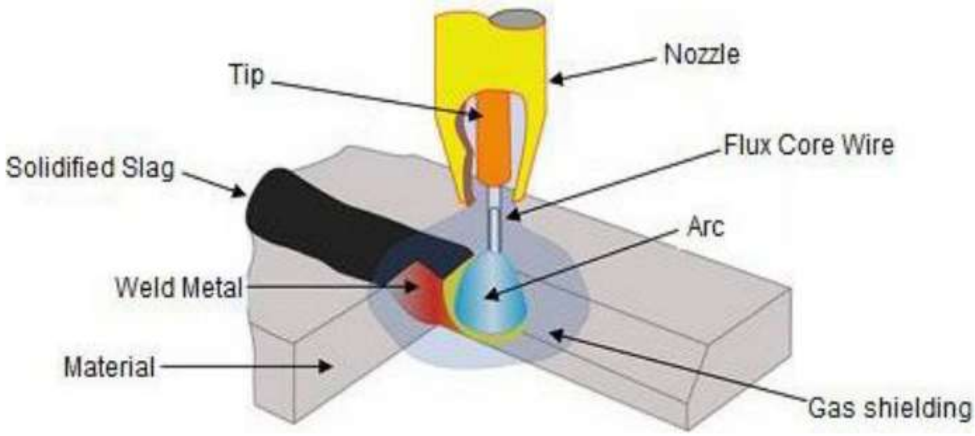

Figure 2-7: Flux cored arc welding (Joao, 2014)

2.3.9 Submerged Arc Welding (SAW)

Submerged arc welding (SAW) is a common arc welding process that requires a continuously fed consumable solid or tubular (flux cored) electrode. The molten weld and the arc zone are protected from atmospheric contamination by being "submerged" under a blanket of granular fusible flux consisting of lime, silica, manganese oxide, calcium fluoride, and other compounds. When molten, the flux becomes conductive, and provides a current path between the electrode and the work. This thick layer of flux completely covers the molten metal thus preventing spatter and sparks as well as suppressing the intense ultraviolet radiation and fumes that are a part of the SMAW (shielded metal arc welding) process (Enterprise, 2002). Figure 2-8 shows the schematic presentation of SAW process.

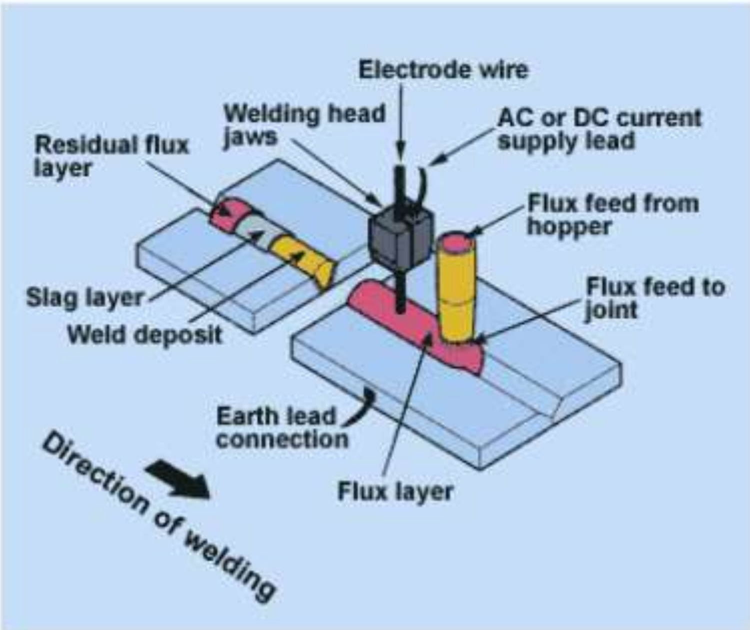

Figure 2-8: Schematic of submerged arc welding (TWI, 2003).

2.3.10 Electro Gas Arc Welding (EGW) and Electro Slag Welding (ESW)

Electro Gas Arc Welding (EGW) and Electro Slag Welding (ESW) comprise only a minor portion of all welding done in the country, but they are uniquely adapted to certain applications, primarily the joining of very thick materials. The joining of a 12 inch material along a 40 foot line is not an uncommon application for the Electroslag process. Electroslag Welding (See

Figure 2-9) is technically not an arc welding process, although it utilizes a current carrying consumable electrode. The only time there is an arc between the electrode and the work piece is when current is initially charged through the electrode. This initial charge heats a layer of loose flux that becomes molten and extinguishes the arc.

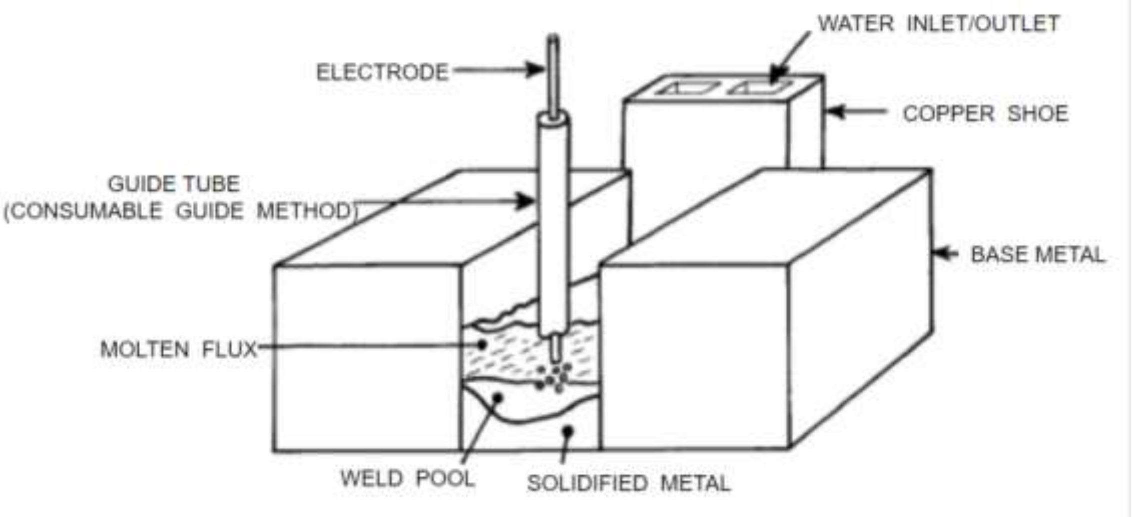

Figure2-9: Electro slag welding (TWI, 2003)

When using a consumable electrode, there are three predominant metal transfer modes namely; Free flight transfer, bridging transfer and slag protected transfer. Flight can further be broken down into spray and globular type transfer. Spray type metal transfer is characterized by the axial transfer of fine molten droplets at the rate of hundreds per second which leads to an essentially splatter free transfer. Globular type metal transfer causes large globules of molten metal to form at the tip of the consumables and joints the weld pool predominantly by gravity and arc forces. This is typically slower resulting in transfer rate of a few droplets per second.

Short circuiting metal transfer, the most common type of bridging transfer, it is characterized by low welding current and voltage. This leads to the slow formation of molten globules at the end of the consumable that will periodically encounter the weld pool. Slag protected metal transfer applies mainly to the ESW and SAW techniques. Due to the presence of a molten slag layer, resulting in protection from the environment and an overall higher heat efficiency.

The efficiency factor will depend on the welding process. Heat is commonly lost through radiation, conduction and convention (Poorhaydari, 2005).SAW is considered one of the most heat efficient process due to the protective flux layer that covers the developing weld pool leading with an efficiency of 0.9-0.99 as tabulated in Table 2-1.The 1-10% heat loss is attributed to the flux that does not melt during the welding process, which will allow some of the heat to escape.

Table 2-1: Efficiency factor for different welding process.

Welding process	**Efficiency factor**
Submerged arc welding	0.9-0.99
Manual metal arc/Shielded metal arc welding	0.8
Cored wire welding /Flux cored arc welding	0.8
Metal active gas /Metal inert gas	0.8
Tungsten inert gas /Gas metal arc welding	0.6
Plasma arc welding	0.6

2.4 Classification of stainless steel

Stainless steels are iron based alloys containing a minimum of about 10.5% chromium, this forms a protective self-healing oxide film, which is the reason why this group of steels have their characteristic "stainlessness" or corrosion resistance. Although all stainless steels depend on the presence of chromium, other alloying elements are often added to enhance their properties. The categorisation of stainless steels is unusual amongst metals in that it is based upon the nature of their metallurgical structure - the terms used denote the arrangement of the atoms which make up the grains of the steel, and which can be observed when a polished section through a piece of the material is viewed at high magnification through a microscope.

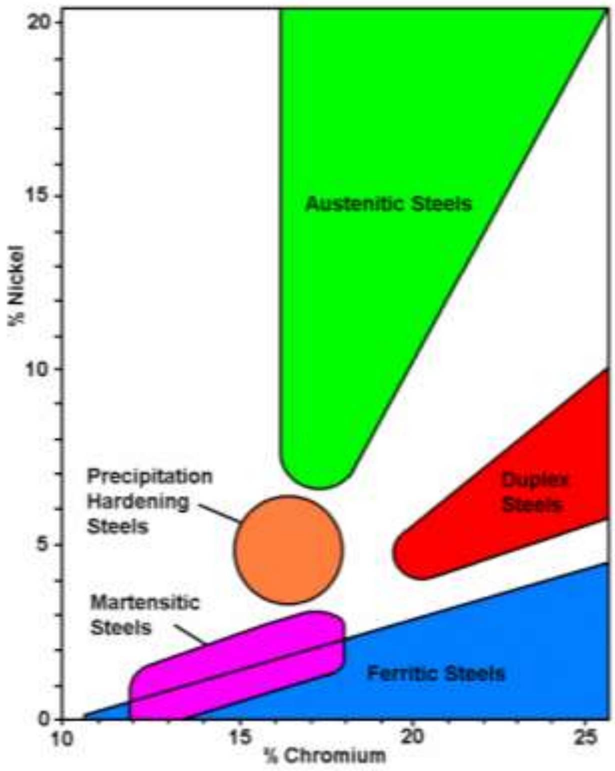

Figure 2-10: Families of stainless steel (Atlas, 2013).

Depending upon the exact chemical composition of the steel the microstructure may be made up of the stable phases of austenite or ferrite, a "duplex" mix of these two, the phase martensite created when some steels are rapidly quenched from a high temperature, or a structure hardened by precipitated micro-constituents. The relationship between the different families is as shown in Figure 2-10. A broad-brush comparison of the properties of the different families is given in Table 2-2.

Table 2-1: Comparison of properties for stainless steel families (Atlas, 2013).

Alloy Group	Magnetic Response (note1)	Work Hardening Rate	Corrosion Resistance (note2)	Hardenable	Ductility	High Temperature Resistance	Low Temperature Resistance (note 3)	Weldability
Austenitic	Generally No	Very high	High	By Cold work	Very high	Very High	Very High	Very high
Duplex	Yes	Medium	Very high	No	Medium	Low	Medium	High
Ferritic	Yes	Medium	Medium	No	Medium	High	Low	Low to High
Martensitic	Yes	Medium	Medium	Quench and Temper	Low	Low	Low	Low
Precipitation Hardening	Yes	Medium	Medium	Age hardening	Medium	Low	Low	High

Notes:

1. Attraction of the steel to a magnet. Note some austenitic grade can be attracted to a magnet if cold worked, cast or welded.
2. Varies significantly between grades within each group. E.g. free machining grades have lower corrosion resistances, those grades higher in chromium, molybdenum and nitrogen have higher resistances. Corrosion resistance is not primary related to the alloy group (structure) but more by composition.
3. Measured by toughness or ductility at subzero temperatures. Austenitic grades retain ductility to cryogenic temperatures.

2.4.1 Austenitic Stainless Steels

This group contain at least 16% chromium and 6% nickel (the basic grade 304 is sometimes referred to as 18/8) and range through to the high alloy or "super austenitics" such as 904L and 6% molybdenum grades. Additional elements can be added such as molybdenum, titanium or copper, to modify or improve their properties, making them suitable for many critical applications involving high temperature as well as corrosion resistance. This group of steels is also suitable for cryogenic applications because the effect of the nickel content in making the steel austenitic avoids the problems of brittleness at low temperatures, which is a characteristic of other types of steel (Atlas, 2013).

2.4. 2 Ferritic Stainless Steels

These are plain chromium (10½ to 29%) grades such as Grades 430 and 409. Their moderate corrosion resistance and poor fabrication properties are improved in the higher alloyed and stabilised grades such as 439 and 444 and in the proprietary grade 3Cr12.

2.4.3 Martensitic Stainless Steels

Martensitic stainless steels are also based on the addition of chromium as the major alloying element but with a higher carbon and generally lower chromium content (e.g. 12% in Grades 410 and 416) than the ferritic types; Grade 431 has a chromium content of about 16%, but the microstructure is still martensite despite this high chromium level because this grade also contains 2% nickel (Atlas, 2013).

2.4.4 Duplex Stainless Steels

Duplex stainless steels (DSS) such as 2205 and 2507 (these designations indicate compositions of 22% chromium, 5% nickel and 25% chromium, 7% nickel but both grades contain further minor alloying additions) have microstructures comprising a mixture of austenite and ferrite. Duplex ferritic - austenitic steels combine some of the features of each class. The alloys are resistant to stress corrosion cracking, albeit not quite as resistant as the ferritic steels; their toughness is superior to that of the ferritic steels but inferior to that of the austenitic steels, and their strength is greater than that of the (annealed) austenitic steels, by a factor of about two. In addition, the duplex steels have general corrosion resistances equal to or better than 304 and 316, and in general their pitting corrosion resistance is superior to 316. DSS suffer reduced toughness below about -50°C and after exposure above 300°C, and therefore only used between these temperatures (Atlas, 2013).

2.4.5 Precipitation Hardening Stainless Steels

These are chromium and nickel containing steels which can develop very high tensile strengths. The most common grade in this group is "17-4 PH"; also known as Grade 630, with the composition of 17% chromium, 4% nickel, 4% copper and 0.3% niobium. The great advantage of these steels is that they can be supplied in the "solution treated" condition; in this condition the steel is just machinable. Following machining, forming etc. the steel can be hardened by a single, fairly low temperature "ageing" heat treatment which causes no distortion of the component (Atlas, 2013). The elements chromium (Cr) and nickel (Ni) form major alloying additions to the steels investigated in this dissertation. An understanding of the phase equilibria in the Fe-Cr-Ni ternary system is therefore an important factor in predicting the transformation behaviour of these steels. The development of stainless steels over the years has resulted in the constitution of the Fe-Cr-Ni ternary system being one of the most thoroughly investigated among iron ternary systems, and a critical evaluation of original literature by Rivlin and Raynor (1980) from literature data, is also presented in the same format. More recently, a thermodynamic analysis and calculation of the Fe-Cr-Ni phase diagram has been presented by Chuang and Chang (1987) and their calculations show good agreement with previous experimental data over a wide range of temperature. However, a few discrepancies do occur, and where applicable, are noted in this section.

2.5 Development of 3Cr12

The 3Cr12 alloy was developed by Southern Cross Steel, the stainless steel producing division of Middelburg Steel and Alloys (Pty), Ltd. The "Cr" refers to chrome, while the 12 refers to the amount of chrome contained in the steel, that is, 12%. The "3" also refers to the amount of carbon in the steel (0.3%). Thus, 3Cr12 is a 12% chromium containing corrosion resisting steel. The chemical composition of 3Cr12 is shown in Table 2-3.

The development of 3Cr12 corrosion resistant steel was a result of the need to obtain a low chromium containing steel with better mechanical properties and weldability than that of AISI 409 stainless steel. The mechanical properties of this steel is tabulated in Table 2-4. 3Cr12 was developed as an alternative material where the mechanical properties, corrosion resistance and fabrication requirements of other materials such as mild steel, galvanised, aluminium, or pre-painted steels are unsuitable. 3Cr12 is used in material handling, road transport, rail transport, petrochemical, power generation, telecommunication cabinets and electrical enclosures and water and sewage-treatment plants (Columbus, 2007). The alloys was designed to fill the price and "technology" gap between stainless steels at the top of the market, and corrosion-prone carbon steel at the other end. 3Cr12 is a highly sophisticated steel which required 10 years of research and development to develop the qualities of weldability and toughness.3Cr12 is recommended to operate up to a maximum of 620°C, when operated continuously: and 730°C, when operated intermittently. Table 2-5 shows the creep properties of 3Cr12.

Table 2-2: Chemical composition for a typical 3cr12 (Columbus, 2007).

Type	%C	%Si	%Mn	%P	%S	%Cr	%Ni	%N	%Ti
3Cr12	0.030 max	1.00 max	2.00 max	0.040 max	0.030 max	10.50-12.50	1.50 max		4(C+N) 0.6

Table 2-3: Mechanical properties of 3Cr12 (Columbus, 2007).

Type	**Product form or Gauge(mm)**	**0.2% Proof Stress (MPa)**	**Tensile Strength (MPa)**	**Elongation (%)**	**Brinell Hardness**	**Impact Energy (J)**
3Cr12	<3	280 450	460 min	20 min	220 max	$35x10^4$
	3 to 4.5	300 450	460 min	20 min	220 max	$35x10^4$
	>4.5 to12	300 450	460 min	20 min	220 max	$35x10^4$
	>12	300 450	460 min	20 min	220 max	$35x10^4$

Table 2-4: Creep properties of 3Cr12 (Columbus, 2007).

	Stress to produce 1% strain (MPa)		
Temperature (°C)	**1000 hours**	**5000 hours**	**10 000 hours**
400	315	283	270
450	195	151	134
500	88	65	56
550	34	29	28

2.6 Ferritic stainless steel

Ferritic stainless steels are part of the steel family containing a minimum of 10.5% chromium. The utility grade stainless steel 3Cr12 will be used for wagon application, this is for more corrosion resistant than standard engineering steels yet less expensive than high alloy stainless steel. Good resistance to corrosion and abrasive wear. Ferritic stainless steel has good weldability, it is easy to fabricate, and can further be welded using all the known processes. Stainless steel shows excellent corrosion resistance in many atmospheres, due to a phenomenon known as passivation. The material protects itself from the environment by forming a very thin passive film or layer at its surface. This film further prevents further contact between the metal and the surroundings.

Strength, toughness, and ductility are the most important properties specified for structural steels. Due to corrosion also being prevalent in many engineering applications, a suitable structural steel would be one that combines these properties with good corrosion resistance. Sensible alloy selection requires the maintenance of a reasonable level of cost effectiveness within the system and in many instances protective coatings are applied to low cost -mild steels and related alloys (Knusten, 1989). However, these attempts to provide corrosion protection can often be very tedious and this has led a number of development organisations towards the consideration of ferritic grade stainless steels (Knusten, 1989).

Ferritic stainless steels represent the cheapest family of chromium containing corrosion resisting steels, but what these steels gain in their resistance to corrosive attack, they generally lose in terms of ductility, toughness, and forming and welding properties. The introduction of commercial methods of obtaining low interstitial levels in ferritic stainless steels has improved the properties of these steels remarkably, but it is well known that grain-coarsening occurs readily in these steels due to the greater atomic mobility (Knusten, 1989).

In body centred cubic structures, and poor toughness is a consequence. Furthermore, ferritic stainless steels, like mild steels, show a ductile-brittle cleavage transition, but their impact transition temperature is considerably higher than that for mild steel due to the embrittling effect of chromium dissolved in ferrite. This impact transition temperature can be reduced, whilst also increasing the upper shelf energy, by decreasing the grain size, but, due to the non-transformable nature of ferritic grades, the coarse grain size is a major problem. Because ferritic stainless steels are generally considered to have single phase microstructures, the ferrite formed during solidification of ferrite remains stable down to room temperature. This means that any refinement of the large grains produced at elevated temperatures generally only occurs due to the rolling and subsequent recrystallisation processes (Grobler, 1987).

Additional grain refinement, however, could be achieved by transformation reactions induced because of steel chemistry modification. Transformation, or partial transformation, of the large grained ferrite to austenite during cooling from the high temperature region may lead to either fully austenitic or duplex ferrite-austenite structures at intermediate temperatures. Further cooling to ambient can then result in either the regression of austenite to a-ferrite, the formation of martensite, or retention of stable austenite (Knusten, 1989).

These transformations will of course ultimately depend on the steel chemistry and the cooling rate. In this way the decomposition of the high temperature ferrite, by suitable minor alloy addition, can modify the properties of the original ferritic stainless steel both in terms of a more refined microstructure after rolling, and improved weldability due to the presence of a duplex structure at elevated temperature. The principle of transformation grain refining has been applied to the ferritic grade AISI 409 stainless steel and has resulted in the development of a transformable steel containing approximately 12 wt. % chromium (Grobler, 1987).

The alloy, designated 3Cr12 [Middelburg Steel and Alloys (Pty) Ltd, S. Afr. Pat. 78/4764, 1978], is titanium stabilised, and produces a ferritic grain structure much finer than the parent AISI 409 after sub-critical annealing. Mechanical properties in this condition are comparable to mild steel, but obviously the corrosion resistance is far superior to that of conventional carbon steels. In addition, the ductile-brittle cleavage transition temperature is much reduced compared to AISI 409. Reheating this alloy above the lower critical temperature (Ac1) gives rise to a duplex ferrite austenite microstructure which will transform to ferrite-martensite during air cooling to ambient. The improved weldability of 3Cr12 compared to AISI 409 is attributed to the formation of the duplex structure at elevated temperature.

2.7 Weldability of 3Cr12

Weldability is often described as the ease on the welding process and the feasibility of the weld obtained to their designed service (Anita and Heikkinen, 2014). The term includes mechanical and corrosion properties of the steel because it is important that the strength, ductility, and toughness are good enough for the application. In terms of corrosion the stress corrosion cracking, intergranular and overall corrosion should be considered (Anita and Heikkinen, 2014).

3Cr12 has good weldability and is suited to most standard welding methods (MMA/SMAW, MIG/GMAW, TIG/GTAW, FCAW and PAW). 3Cr12 can be welded to other ferrous metals e.g. mild, S355Jr and stainless steels quite satisfactorily. The recommended grade of electrode is the 309L austenitic welding wire. It is important that this type of over alloyed consumable is used, rather than one which matches either of the base metals, to avoid excessive weld metal dilution (Atlas, 2013). When welding 3Cr12 to itself, E308L and E316L can also be used. The heat input should be controlled to between 0.5 kJ/mm and 1.5 kJ/mm per pass (Atlas, 2013).

The successful weldability of 3Cr12 is attributed mainly to the occurrence of the second phase austenite (transforms to martensite) in the heat affected zone (HAZ) which restricts ferrite grain growth (Witness, 2004). The HAZ in 3Cr12 contains between 20% and 90% martensite, depending on the ferrite factor of the steel, the heat input per pass during welding and the number of passes. These factors all contribute towards determining the strength, ductility and toughness of the welded material. The grain size in the HAZ is determined by the heat input and the volume fraction of martensite. This means that steels with a high ferrite factor (i.e. approaching 12) will have a low martensite content and therefore ferrite grain growth is less likely to be inhibited (Witness, 2004).

The improvement of the weld HAZ toughness of 12 percent chromium ferritic stainless steels, e.g. AISI 409, is the critical factor in extending the applications of these steels to thicker plate material. Since 3Cr12 was developed from AISI 409, it is of some significance to consider attempts by Thomas and Apps (1980) to improve the weldability of 6 mm AISI 409 plate by compositional variations within the AISI 409 specification (Thomas, 1980). Table 2-6 shows the compositional range experimental steels together with the composition of one of (steel A) which contained up to 20% martensite in temperature HTHAZ.

Table 2-5: Chemical compositional range (wt%) of AISI 409 steels (Thomas, 1980).

	C	N	Mn	Si	S	Cr	Ni	Ti	Al
Range	0.020- 0.027	0.012- 0.015	0.72- 0.98	0.39- 0.51	0.015- 0.023	11.42- 11.57	0.32- 0.60	0.17- 0.30	0.09- 0.028
Steel	0.025	0.015	0.74	0.39	0.017	0.6	0.6	0.3	0.09

Hoffman published a comprehensive summary of research, down to September 1984, done on the weldability of 3CR12. Satisfactory results were obtained with reference to the following factors determining the weldability: joint strength, ductility, toughness, fatigue strength, corrosion resistance, ease of welding and susceptibility to hot cracking.

2.8 Welding parameters

The six welding parameters that influence the performance of welds are welding current, welding voltage, travelling speed, heat input, filler metal and shielding gas.

2.8.1 Welding current

Welding current is the most influential variable in arc welding process which controls the electrode burn off rate, the depth of fusion and geometry of the weldments. Current has direct influence on weld bead shape, on welding speed and quality of the weld. Most GTAW welds employ direct current on electrode negative (DCEN) (straight polarity) because it produces higher weld penetration depth and higher travel speed than on electrode positive (DCEP) (reverse polarity) (Bolarinwa, 2018). Besides, reverse polarity produces rapid heating and degradation of the electrode tip, because anode is more heated than cathode in gas tungsten electric arc. Higher current in GTA welding can lead to splatter and work piece become damage (Bolarinwa, 2018). Again, lower current setting in GTA welding led to sticking of the filler wire. Sometimes larger heat affected area can be found for lower welding current, as high temperatures need to apply for longer periods of time to deposit the same amount of filling materials. Fixed current mode will vary the voltage in order to maintain a constant arc current (Atma and Joy, 2004).

2.8.2 Welding voltage

This is the electrical potential difference between the tip of the welding wire and the surface of the molten weld pool. Welding voltage can be fixed or adjustable depending on the GTA welding equipment. It determines the shape of the fusion zone and weld reinforcement. A high initial voltage allows for easy arc initiation and a greater range of working tip distance. However, it produces wider, flatter and less deeply penetrating welds than low welding voltages, depth of penetration is maximum at optimum arc voltage, to high voltage on the other hand will lead to large variable in welding quality (Tewari et al.,2010).

2.8.3 Travelling speed

Speed of welding is defined as the rate of travel of the electrode along the seam or the rate of the travel of the work under the electrode along the seam (Abioye, 2017).

Weld Travel Speed = Travel of electrode/arc time, mm/min………….... (2-1)

Welding speed is an important parameter for GTAW welding. The effect of increasing the welding speed for the same current and voltage is to reduce the heat input. The welding speed does not influence the electromagnetic force and the arc pressure because they are dependent on the current (Bolarinwa, 2018). The weld speed increase produces a decrease in the weld cross section area, and consequently penetration depth (D) and weld width (W) also decrease, but the D/W ratio has a weak dependence on travel speed (Bolarinwa, 2018). These results suggest that the travel speed does not influence the mechanisms involved in the weld pool formation, it only influences the volume of melted material. Normal welding speeds are from 100 to 500 mm/min depending on current, material type and plate thickness (Janunkar et al., 2017).

2.8.4 Heat input

Heat input is a relative measure of the energy transferred per unit length of weld. The higher the heat input, the slower the cooling rate. Conversely, the lower the heat input, the faster the cooling rate. Hence, like preheat and interpass temperature, heat input is an important characteristic that influences the cooling rate, which may affect the mechanical properties and metallurgical structure of the weld and the HAZ (Yuri et al, 2000).In arc welding, it is well known that energy is transferred from the welding electrode to the base metal by an electric arc. Upon starting the arc, enough power (energy transferred per unit time) and energy density is supplied to the electrode. Consequently, both the base metal and the filler metal are melted to create the weld (Apurv and Vijaykumar, 2014). Heat input is typically calculated as the ratio of the power (i.e., voltage × current) to the velocity of the heat source (i.e. the arc). Heat input was calculated according to Equation 2-1.

$$Heat\ input(HI) = \frac{V*A*60}{s} * \eta \ldots\ldots\ldots\ldots\ldots\ldots\ldots\ldots\ldots\ldots\ldots (2\text{-}2)$$

Where:

HI = heat input in kJ/mm,

η = efficiency = 0.80 for GMAW,

V = voltage in V,

I = current in A,

ν = welding speed in mm/sec.

2.8.5 Filler metal

Filler metals are generally used for plate thickness above 2 mm, having chemical composition similar to that of the parent material. Filler metal diameter is between 1.6 and 3.2 mm and in automatic systems is normally added cold from a roll or a coil. Many, but not all austenitic stainless steels can be welded without filler metal and without any further heat treatment. Most of the super austenitic alloys require the use of filler metal to obtain proper corrosion resistance of the weld (Bolarinwa, 2018). Normally, the weld metal is able to meet the minimum yield and tensile strength requirements of the annealed base material. The ductility of the welds is generally lower than base metal, but they are still very ductile. Low carbon grades (L-grades) of filler metals are normally used for corrosion resistant service. For high-temperature service, the higher carbon filler metals may give better high-temperature strength. The compositions of many of the 300 series filler metals are adjusted so that they solidify with a certain amount of ferrite to prevent hot cracking during solidification (Bolarinwa, 2018). This allows for higher heat inputs and thus higher welding speeds. The presence of a certain amount of ferrite means that welds are slightly ferromagnetic. Those alloys that solidify fully or nearly fully austenitic must be welded with lower heat inputs. For certain applications, a low ferrite weld metal is desirable, and certain filler metals are produced for that purpose. For most 300 series stainless steels, a nominally matching filler metal is the most common filler metal used (Arun et al., 2013).

2.8.6 Shielding gas

Shielding gases are used in GTAW in order to prevent atmospheric contamination of the weld metal. This contamination can produce porosity, weld cracking, scaling and even change in the chemical composition of melted material (Bolarinwa, 2018). Besides shielding gas also has a large influence on the stability of the electric arc. Gases with low ionization potential facilitate the ignition of the electric arc and those with low thermal conductivity tend to increase the arc stability. Argon is the most used GTAW shielding gas. It has low ionization potential and is heavier than air, providing an excellent shielding of the molten weld pool (Bolarinwa, 2018). Furthermore, it is less expensive than helium, the other inert shielding gas used in the process.

Argon is used in welding of carbon and stainless steels and low thickness aluminium alloys components. For welding thick aluminium work-pieces and other high-conductive materials, such as copper alloys, helium is recommended because it has higher ionization potential than argon, needing higher voltage for arc initiation and maintenance, but producing higher heat-input (Sun et al., 2008). The shielding gas flows out of the welding torch, surrounding the hot tungsten and molten weld metal, and displaces the air (oxygen and nitrogen), thus preventing the air, in this way, the air is prevented from having contact with the molten metal or hot tungsten electrode (Ghazviloo, 2010).

Helium or helium/argon (30% - 80% He) mixtures allow increased welding speed and improved process tolerance. Mixtures of argon with up to 5% of hydrogen are frequently used in welding of austenitic stainless steels. Hydrogen increases arc-voltage and consequently heat input, increasing weld penetration and weld travel speed, as well as improving weld appearance (Kang et al, 2009). Argon/hydrogen mixtures are also used in welding of copper nickel alloys. Argon is also used as back side shielding gas, mainly in welding of stainless steels, aluminium alloys and reactive metals. Flow rates of shielding gases depend on weld thickness, being 4 - 10 L/min for argon and 10 - 15 L/min for helium, because it is lighter than argon, and consequently less effective in shielding purposes (Arun, 2013). Gases with a purity of 99.995% are used in welding most of the metals, though reactive materials such as titanium need contaminant level less than 50 ppm. The choice of shielding gas is very important as it affects weld penetration depth and surface profile, porosity, corrosion resistance, strength, hardness and brittleness of the weld material (Paniagua et al., 2007).

The choice of shielding gas dependent on the working metals and effects on the welding cost, weld temperature, arc stability, weld speed, splatter and electrode life. Argon or Helium may be used successfully for GTAW welding applications. For welding of extremely thin material pure argon is used (Bolarinwa et al., 2018). Argon generally provides an arc which operates more smoothly and quietly. Penetration of arc is less when Argon is used than the arc obtained by the use of Helium (Bolarinwa et al, 2018). For these reasons argon is preferred for most of the applications, except where higher heat and penetration is required for welding metals of high heat conductivity in larger thicknesses (Bang et al., 2008). Argon hydrogen mixture is used for welding of some grades of stainless steels and nickel alloys. Pure helium may be used for aluminium and copper. Helium argon mixtures may be used for low alloy steels, aluminium and copper (Zhang et al., 2006).

2.9 Welding consumables for 3Cr12

Welding consumables for ferritic stainless steel are generally of austenitic type, and type 309L with low carbon content is the most used consumable. This is to ensure that any dilution that occurs does not result in a low ductility austenitic, ferritic or martensitic weld metal microstructure. Austenitic consumables are preferred for welding the ferritic alloys. Although this leads to a property mismatch between the weld and the surrounding base metal, the tough austenitic weld metal improves the overall toughness of the weld by absorbing some of the impact that the joint may be exposed to during service (Du Toit *et al*., 2007). A matching welding electrode is commercially available (classified as E410NiMo, with modified chromium content), but it is not recommended in applications where impact, shock, fatigue or any other form of non-static loading is anticipated (Du Toit *et al*., 2007). Weld joints produced from austenitic stainless steel are strong and ductile in their as-welded condition. They do not require preheat or post weld heat treatment.

Although some ferritic filler metals are available for welding ferritic stainless steels, the resultant weld deposits are low in ductility. Austenitic steel fillers are therefore generally recommended for welding ferritic stainless steels (TWI, 2003). Hoffman investigated the influence of different MMA and MIG filler metals on the weldment properties of 3Cr12 and recommended that any austenitic filler metal may be used for welding 3Cr12. The use of AISI 308L, 309L and 309LMo is, however, preferred (TWI, 2003).

Taban and Kaluc (2009) also reported no significant differences in the weldment properties of welds on 3Cr12, welded with AISI 308L, 309 and 310 electrodes. A high strength matching (composition) electrode, E3Cr12, has also recently been developed. The evaluation of the mechanical properties of weldments, welded with the abovementioned filler metals, has been based on bend test and tensile test results only. These tests only evaluate the plane stress fracture behaviour of welds.

With the toughness of the HTHAZ lower than the toughness of the rest of the HAZ, the suitability of a filler metal for welding 3Cr12 should also be evaluated on the basis of its influence on the fusion line fracture behaviour of welds in the presence of a triaxial stress field. The HTHAZ is expected to have a significant effect on the fusion line fracture behaviour of welds on the presence of a triaxial stress field (Du Toit *et al*., 2007).

2.10 Defects, causes and remedies associated with welding

Welding Defects can be defined as the irregularities formed in the given weld metal due to wrong welding process or incorrect welding patterns, etc. (TVS, 2007). The defect may differ from the desired weld bead shape, size, and intended quality. Welding defects may occur either outside or inside the weld metal. Some of the defects may be allowed if the defects are under permissible limits but other defects such as cracks are never accepted. (TVS, 2007).

2.10.1 Lack of penetration

Incomplete penetration occurs when the root of the weld bead does not reach the root of the joint to weld the opposite surface in the part as shown in Figure 2-11. To correct this discontinuity, you can increase the current, decrease the welding speed, or change the joint geometry**.**

Figure 2-11: Lack of penetration defect (Baughurst, 2011).

2.10.2 Lack of fusion

Figure 2-12 illustrate Incomplete Fusion which occurs with localized lack of fusion, either at the joint edge or at the face of the previously deposited strand. To correct this discontinuity, you can increase the current, decrease the welding speed, change the joint geometry, or use some artifice to avoid magnetic blowing.

Figure 2-12: Lack of fusion defect (Baughurst, 2011).

2.10.3 Porosity

Porosity defect as shown in Figure 2-13 is a collective name describing cavities or pores caused by gas and non-metallic material entrapment in molten metal during solidification. There are many causes that include contamination, inadequate shielding, unstable arc or arc gap too short. Porosity can be minimized by enough shielding gas and proper selection of electrode.

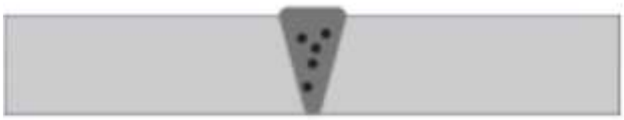

Figure 2-13: Porosity defect (Baughurst, 2011).

2.10.4 Undercut

When the base of metal melts away from the weld zone, then a groove is formed in the shape of a notch, then this type of defect is known as Undercut as shown in Figure 2-14 (Baughurst, 2011). It reduces the fatigue strength of the joint (Baughurst, 2011). This defect is caused by the utilisation of wrong electrode also when the arc voltage is too high. This can be eliminated by reducing the arc voltage and by making use of smaller electrode.

Figure 2-14: Undercut defect (Baughurst, 2011).

2.10.5 Slag inclusion

Slag is formed on the surface of the weld or between the welding turns as shown in Figure 2-15. If there is any slag in the weld, then it affects the toughness and metal weldability of the given material. This decreases the structural performance of the weld material (TVS, 2007). Slag is formed if the welding current density is very small, as it does not provide the required amount of heat for melting the metal surface, if the welding speed is too fast then slag may occur (TVS, 2007). Finally, slag occurs if the edges of the weld surface is not cleaned properly. This can be eliminated by increasing the current density, adjusting the speed so that the slag and the weld pool do not mix and clean the weld edges properly.

Figure 2-15: Slag fusion defect (Baughurst, 2011).

2.10.6 Crack

This is the most unwanted defect of all the other welding defects; Figure 2-16 demonstrate the defect. Welding cracks can be present at the surface, inside of the weld material or at the heat affected zones. Cracks are usually caused by material with high content of impurities, insufficient weld bead size or shape and shrinkage on solidification. Cracks can be limited by using appropriate material, cleaning of the plates before welding and reducing the gap between the weld joints by using reasonable weld joints.

Figure 2-16: Crack defect (Baughurst, 2011).

2.10.7 Overlap

When the weld face extends beyond the weld toe, then this defect occurs as shown in Figure 2-17. In this condition the weld metal rolls and forms an angle less than 90° (TVS, 2007). This is caused by improper welding technique, by using large electrodes and high welding current (TVS, 2007). This may be eliminated by using less welding current, smaller electrode and by making use of appropriate welding technique.

Figure 2-17: Overlap defect (Baughurst, 2011).

2.10.8 Spatter

When some metal drops are expelled from the weld and remain stuck to the surface, then this defect is known as Spatter (TVS, 2007)**.**Spatter is caused by high welding current and improper shielding gas. This may be eliminated by reducing the arc length and welding current in addition by choosing appropriate shielding gas (TVS, 2007).Figure 2-18 illustrate the defect.

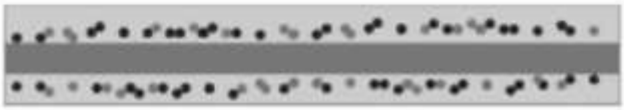

Figure 2-18: Spatter defect (Baughurst, 2011).

2.10.9 Warping

Warping is an unwanted change in the shape and position of the metal parts, Figure 2-19 illustrate the defect. It happens when the heat usage is wrong and is caused by the contraction/expansion of the welded parts (Gomes , 2020). The defect can be eliminated by maintaining the travelling speed and by making use of appropriate number of passes.

Figure 2-19: warping defect (Baughurst, 2011).

2.10.10 Burn through

If the weld metal penetrates the base metal, then burn through occurs as demonstrated in Figure 2-20. This is a common discontinuity when welding thin parts (Gomes , 2020). It happens when the root opening is too large or too much voltage is used. This can be eliminated by lowering the voltage or wire feed speed can help rectify the problem.

Figure 2-20: Burn through defect (Baughurst, 2011).

It is therefore important to conclude that defects have an impact on the weld performance hence is important to eliminate them.

2.11 Effect of alloying elements

Stainless steels are iron-based alloys, with the Iron content ranging from 50-88 wt. % of the composition (Lippold, 2005). To consider a steel "stainless", a minimum of approximately 10.5 wt% chromium must make up the composition. In ferritic and martensitic grade stainless steels, the major alloying elements are chromium and 11 carbon. The addition of nickel is common in austenitic and duplex grade stainless steels (Lippold, 2005). Most stainless steels contain a combination of manganese, silicon, molybdenum, niobium, titanium, aluminium, copper, tungsten, nitrogen, and others. This section discusses the role each alloying element plays on the properties of stainless steels (Duffey, 2016). The most common stainless steel alloys are chromium, nickel, molybdenum, copper, and titanium. Non-metal additions include carbon and nitrogen. Alloying elements enhance the characteristics, structure, and performance of the metal (Duffey, 2016).

2.11.1 Chromium (Cr)

This highly reactive element accounts for the “passive” nature of all stainless steels, protecting against chemical corrosion and the typical oxidation (rusting) that is common in unprotected steel. When stainless steel contains a minimum of 10.5% chromium, an instant and insoluble surface film is filmed, preventing oxidation.Chromium imparts corrosion resistance to steel; it combines with the oxygen in the atmosphere to form a stable non-metallic oxide film that acts as a protective coating, Figure 2-21 shows the relationship between chromium and corrosion resistance. (Bomi, 2018) .

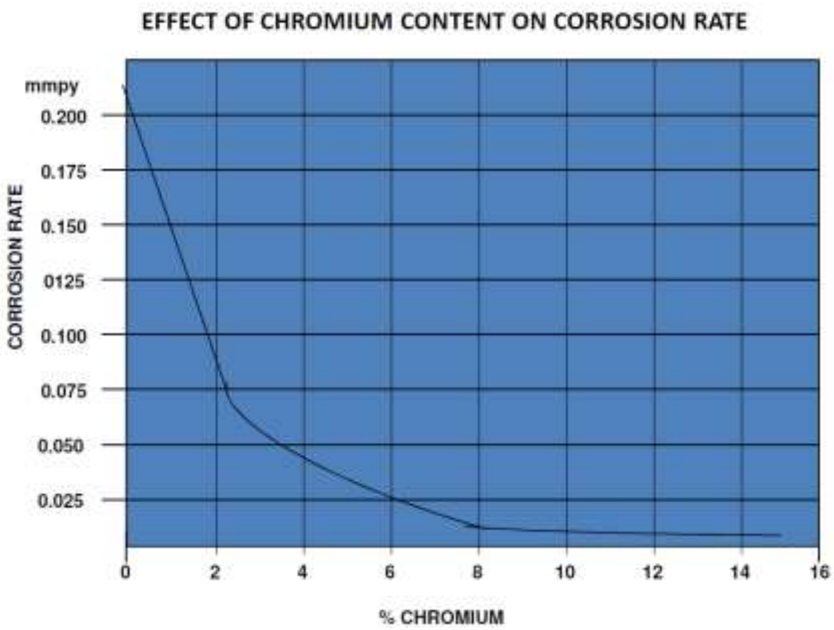

Figure 2-21: Effect of chromium on corrosion resistance *(Materia, 2022)*

2.11.2 Nickel (Ni)

In all grades within the 300 series of stainless steel, nickel is the essential alloying element, creating an austenitic structure known for ductility, toughness, and strength. Nickel also adds significant resistance to acids in general, but sulphuric acid, and helps to reduce distortion and cracking during the quenching phase of heat treatment (Atlas, 2013).

2.11.3 Molybdenum (Mo)

Molybdenum plays a different role in stainless steels depending on the grade. In ferritic, austenitic, and duplex grades, Molybdenum is added to improve corrosion resistance, specifically pitting and crevice corrosion. In austenitic grades, Molybdenum improves the strength of the alloy at elevated temperatures. In martensitic grades, Molybdenum forms carbides, which leads to secondary hardening of the alloy. Molybdenum is a ferrite promoter, and is generally undesirable in martensitic grades because ferrite can reduce the toughness and ductility at room temperature (Lippold, 2005). Molybdenum adds resistance to localised pitting, and, when mixed with chromium-nickel austenitic steels, gives better resistance to crevice corrosion. It also protects against the negative effects of chlorides, slows the critical quenching speed, and increases high temperature tensile strength.

2.11.4 Manganese (Mn)

Manganese was first added to stainless steels to avoid hot shortness during casting. This is a version of solidification cracking linked to the formation of Iron-Sulphide eutectic at low temperatures. Manganese combines with Sulphur much easier than Iron and forms a Manganese Sulphide that eliminated the hot shortness problem (Lippold, 2005). Manganese is an austenite promoter, although it is not a strong promoter compared to other elements (Lippold, 2005).

2.11.5 Carbon(C)

Carbon is the single most important alloying element in stainless steel. It is always present in all grades, and the amount of carbon in each grade is key to its performance. In all types of stainless steel except martensitic, carbon levels are kept quite low, but in martensitic grades, they are deliberately higher in order to increase hardness and strength. Low carbon content is particularly key in ferritic and austenitic stainless steels in order to avoid carbide precipitation when welding (Industries, 2021).

2.11.6 Copper (Cu)

Copper is often present as a residual element in stainless steel, but can also be intentionally added to improve corrosion resistance, especially in acidic or marine environments. Copper is not added for cutlery applications as it has a detrimental effect on surface quality and hot working behaviour (Industries, 2021).

2.11.7 Titanium (Ti)

Titanium merges with carbon to form titanium carbides that are stable and not easily dissolved. This helps to reduce inter-granular corrosion that could affect the formation of the passive (protective) layer of stainless steel (Industries, 2021).

2.11.8 Nitrogen

In a similar way to nickel, the addition of nitrogen to stainless steel increases the austenite stability of the metal, helping to protect against pitting and inter-granular corrosion – particularly in duplex stainless steel. Nitrogen also helps raise the yield strength (Industries, 2021).

2.11.9 Silicon

Small amounts of silicon are usually present in stainless steels (usually 0.3-0.6 wt. %). The primary role of silicon is to act as a deoxidizing agent during melting. Aluminium can be used as a deoxidizing agent in place of silicon if desirable. Some austenitic grade stainless steels have poor fluidity when in the molten state. The addition of silicon has also been shown to improve fluidity of molten steel. Therefore, Silicon is usually added to weld filler metals (Lippold, 2005)

2.12 Microstructure evolution

3Cr12 is a low carbon (0.03%), titanium stabilised, 12 percent chromium, duplex ferritic-martensitic steel which was developed by Southern Cross Steel, the stainless steel producing division of Middelburg Steel and Alloys (Pty), Ltd. The steel was developed from the ferritic stainless steel AISI 409 by careful balancing of the ferrite (Cr, Si, Ti) and austenite (Ni, Mn, C, N) stabilising elements using Kaltenhauser's (l) relationship:

Ferrite Factor (F.F.) = Cr + 6Si + 8Ti - 2Mn - 4Ni - 40(C+N) where

F.F. = 11.5 for 3Cr12.

The microstructure of the steel consists of slightly elongated to equiaxed ferrite and highly tempered martensite grains (grain size ASTM 7) with large blocky cubic titanium carbonitrides. This structure is obtained by tempering (700-770°C) of hot rolled plate of which the temperature during the final pass was within the dual-phase ferrite-austenite phase field. This results in a banded microstructure consisting of pancake shaped ferrite and martensite grains.

Two basic varieties of 3Cr12, one containing 0.6 percent nickel (3CrI2) and one containing 1.2 percent nickel (3CrI2Ni), are being marketed by Southern Cross Steel.

The lower nickel variety is intended for general applications, while the higher nickel variety is produced for high strength applications. 3CR12 has been developed as a relatively inexpensive corrosion resisting steel and replacement for mild and structural steels. Its application includes being utilized in mildly corrosive environments where the corrosion resistance of mild steel is inadequate.

Sheet and plate are presently being marketed respectively within the thickness ranges 0.55 to 3.0 mm and 3.5 to 30 mm. The steel is presently finding application in the South African gold and coal mines for construction of transport wagons, coal bunkers, railway masts, storage tanks, containers, etc. It is also increasingly being used in structural applications for petro-chemical, metallurgical, pulp and paper, and sugar industries.

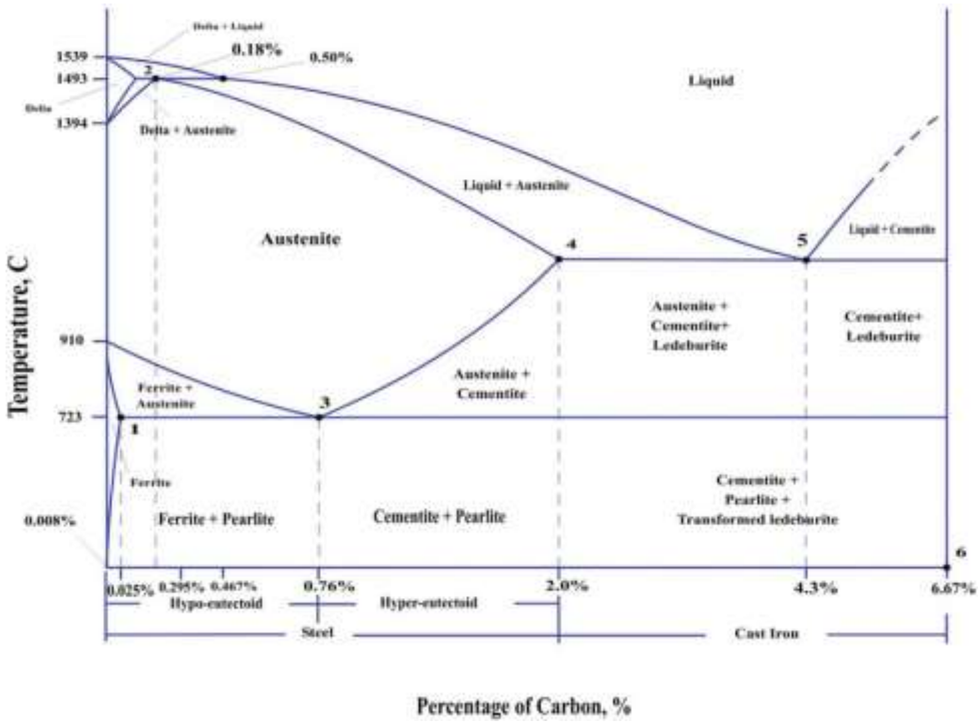

Figure 2-22: Iron based phase diagram *(Shamail, 2015)*

The 3Cr12 ferritic stainless steels are designed to transform to austenite partially upon cooling, passing through the dual-phase (austenite and ferrite) field on the Fe-Cr equilibrium phase diagram shown in both Figure 2-22 and zoomed in Figure 2-23 for carbon contents below 0.01 per cent (Du Toit *et al.*, 2007). This partial solid-state phase transformation of ferrite to austenite on cooling improves the weldability and as-welded toughness of these steels by restricting heat-affected zone grain growth (Meyer and Meyer, 2000).

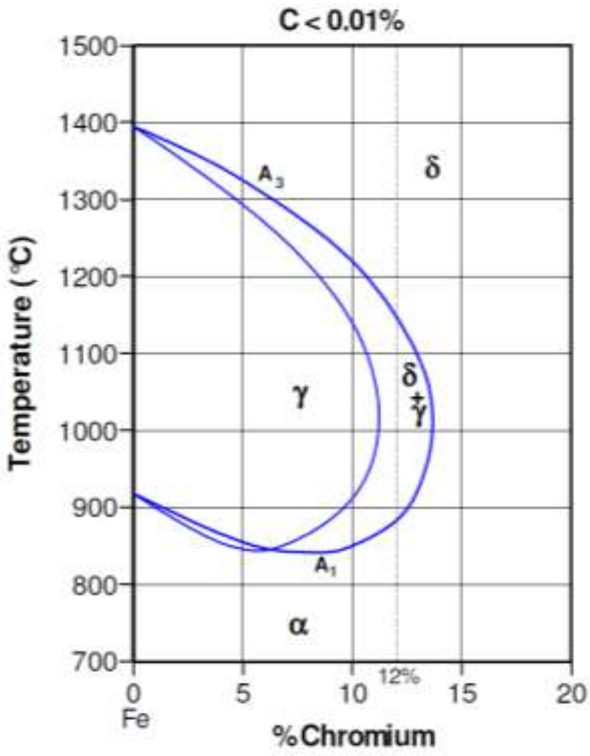

Figure 2-23: Phase diagram for steel with carbon contents below 0.1*(Du Toit et al., 2007)*

The 3Cr12 steels are usually supplied in the fully annealed and desensitized condition. Final annealing is performed at temperatures below the A_1 (normally between 700°C and 750°C) after air cooling or cold rolling (Steels, 2012). During the annealing treatment, any austenite formed during slow cooling through the dual-phase region, transforms completely to ferrite. Due to its low solubility in ferrite, the majority of the carbon precipitates as chromium-rich carbides or carbonitrides during annealing, but any chromium-depleted zones formed in the ferrite phase is healed through rapid chromium back-diffusion from the grain interiors (Du Toit *et al.*, 2007).

The rapid cooling rates associated with welding, however, prevent the transformation of austenite to ferrite at lower temperatures, and any austenite formed on cooling through the dual-phase (d and g) region transforms to martensite below the martensite start(M_s)-temperature

(Grobler, 1987). As a result of the high carbon solubility in austenite, the austenite phase that forms on cooling acts as a carbon sink, dissolving significant amounts of carbon (Du Toit *et al*., 2007).

When austenite transforms to martensite at lower temperatures, the amount of carbon retained in solid solution in the martensite phase is determined by the cooling rate. Martensite formed on fast cooling retains higher levels of the carbon in supersaturated solid solution. At slower cooling rates, the formation of martensite is preceded by carbide precipitation in the austenite, and less carbon is retained in solution in the martensite phase. The high temperature heat-affected zone (HTHAZ) adjacent to the fusion line represents parent metal heated above the A_3 temperature during the weld thermal cycle, and is characterized by d-ferrite grains surrounded by grain boundary martensite (Du Toit *et al*., 2007).

Despite the partial solid-state phase transformation from ferrite to austenite on cooling, the HTHAZ is normally characterized by a coarse grain size. This contrasts with the much finer grain size of the low temperature heat-affected zone (LTHAZ) further removed from the fusion line. This region has a structure consisting of ferrite and martensite, and represents parent metal heated to temperatures between the A_1 and A_3 temperatures during welding (Du Toit *et al*., 2007).

2.13 Sensitization

Ferritic stainless steel are iron-chromium alloys with body centered cubic crystal structure having chromium content usually in the range of 11-30 wt%. These steels exhibit good ductility, formability and moderately better yield strength relative to those of the austenitic grades but the higher the temperature strength is somewhat poor (Amuda, 2011).Due to the crystal structure, the toughness is low at the cryogenic temperature. Ferritic stainless steel it’s a candidate material in less severe corrosion atmosphere for chemical processing equipment, storage vessel, furnace parts, solar water heaters etc. They are more appropriate in caustic and chloride environment.

Sensitization refers to the formation of chromium carbides precipitates along the grain boundaries, which leads to a chromium depleted zone near the grain boundaries. Sensitization is due to stainless steel being exposed to high temperatures for a long period, this may be through heat treatment or welding. Sensitization results in increased susceptibility to intergranular stress corrosion cracking as chromium is the alloying element responsible for corrosion resistance in stainless steel (Doerr, *et al.*, 2017). Sensitization is represented by a ditch structure where one of more grains in the microstructure are surrounded by ditches whereas a dual structure is when there are some ditches along the grain boundaries, but no single grain is surrounded by ditches (Domankova, *et al.*, 2014). Figure 2-24 shows two microstructures, (a) being the normalized microstructure and (b) sensitized microstructures.

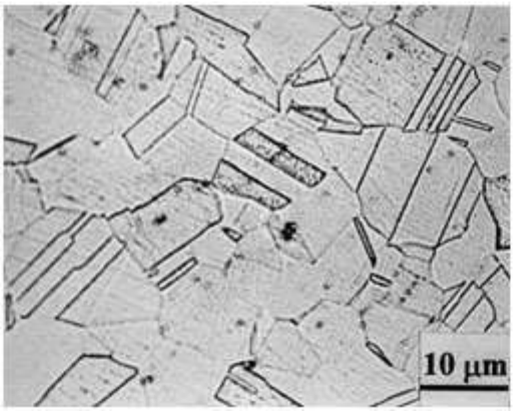

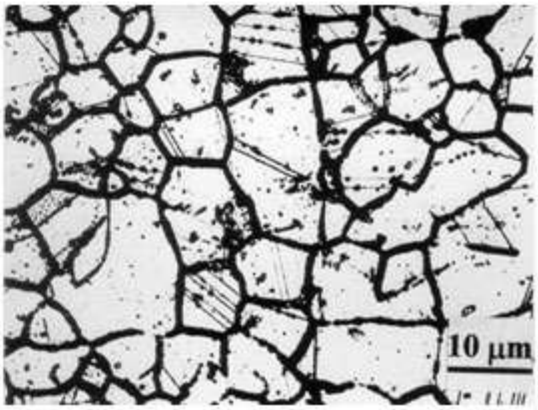

Figure 2-24: Example of a (a) Normalized microstructure and (b) Sensitized microstructure (Domankova, et al., 2014).

Sensitization is generally believed to promote stress cracking corrosion failure in some ferritic stainless steel. Several models have been proposed to explain the sensitization of stainless steel, however the chromium depletion model is the most widely accepted as shown in Figure 2-25 (Seong., 2013).Extensive studies had been undertaken to understand the mechanism, mode of sensitization and provides opinions for the control of sensitization problem by ensuring that chromium remain in the matrix (Van Warmelo, 2007).

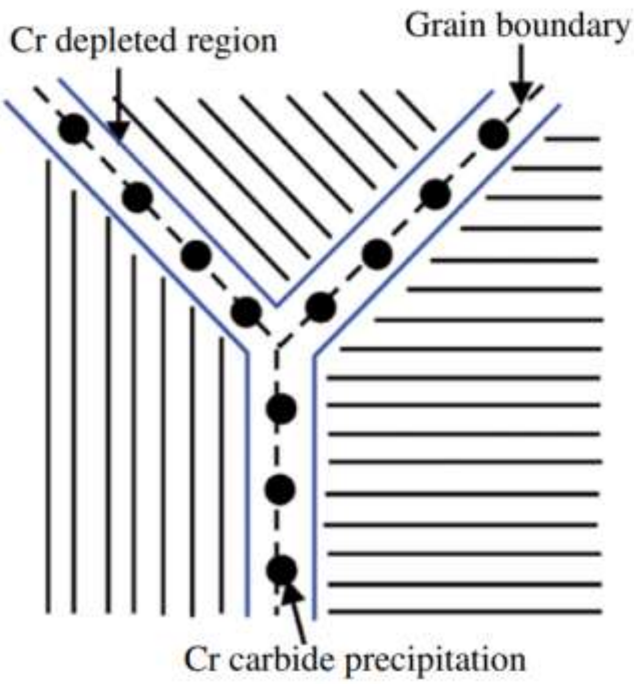

Figure 2-25: Schematic view of grain boundary carbide precipitation and association of grain boundary (Seong., 2013)

Sensitization is essentially a heat affected zone phenomena in fusion welding and has been reported a major cause of stress corrosion failure in most fusion welded alloys (Seong., 2013). The mechanism of sensitization-the mechanism by which sensitization occur varies and contrasts. These are: Chromium depletion theory, strain theory, electro-chemical theory and Solute segregation theory.

The chromium depletion theory states that sensitization is promoted by the intergranular precipitation of chromium rich.$M_{23}C_6$- type carbides resulting in chromium depletion in the matrix adjacent to the precipitated carbides. If the depletion leads to reduced chromium level below the concentration required for passivation, then the material become sensitized to intergranular corrosion. The chromium depletion theory is supported by the work of Straristion and Hillert (2009) who observed good agreement between experimental and theoretical results.

Strain theory however, presents a contradictory postulation to the chromium depletion mechanism. In the strain theory, severe plastic deformation at low temperature (cold work) leading to substantial increase in the dislocation density at the grain boundary compared to that in the matrix is believed to be driving force for sensitization. The presence of such imperfections lattice structure containing dislocations, stacking faults and stainless steel enhances overall diffusion of alloying elements resulting in faster sensitization (Amuda, 2011).

Electro-chemical theory on the other hand consider that the potential difference exists between the metallic carbide and the matrix, and that the metal carbide is nobler than the steel matrix, and hence, experience is accelerated. Intergranular attach particularly in the presence of residual stresses. However, Baumel *et al.,* (2000) in their work contradicted this theory because localized corrosion could not be confined to a very narrow zone, and that the corrosion must extend to the matrix (Amuda, 2011).

The solute segregation mechanism postulates that the intergranular corrosion occurs in the non-sensitized austenitic stainless steel when there is a continuous grain boundary path of a second phase, and soluble impurity segregates resulting from solute vacancy interactions. The model was, however, concerned mainly with intergranular attack on non-sensitized steel and only secondarily with carbide forming sensitized steel .On the basis of this theory, resistance to intergranular attack is improved if discontinuous carbides are precipitated through heating between 800-900°C followed by water quenching (Amuda, 2011).

Sensitization in the heat affected zone

Laboratory simulation and in-service inspection techniques have established four different manifestations in stainless steel, and these have been confirmed in ferritic stainless steel grades (Van Warmelo et al, 2007).This manifestations are called modes and are divided in to four namely: mode 1,mode 2,mode 3 and mode 4.These modes differentiates the dynamics of chromium depletion zones in terms of where and how the zones will be formed and thermal consideration for the onset of chromium depletion process (Amuda, 2011).

Mode 1

This occurs in single pass weld and is linked to the presence of untampered martensite in the stainless steel before exposure to the sensitization temperature. Sensitization through this mode is usually characterized by pitting corrosion and intergranular cracking within me the low temperature heat affected zone a few millimeters from the weld interface as shown in Figure 2-26. Mode 1 is initiated when the material is inappropriately annealed into the dual phase (ἀ+ɣ) region above the A_1temperatureduring thermal treatment before processing and this will produce substantial amount of untampered martensite. Martensite particularly in the low-chromium ferritic stainless-steel grade (Van Warmelo *et al.,* 2007). Since mode 1 is caused by the presence of untampered martensite, it is best prevented by ensuring that the base metal does not contain any untampered martensite (Amuda, 2011).

Figure 2-26: Mode 1 pitting corrosion and intergranular cracking (Amuda, 2011).

Mode 2

Sensitization in welds with overlapping heat affected zone. Sensitization via this mode presents similar mechanism to that described in mode 1 and also requires the application of double heating cycle however, the distinction in the two models lies in how the untampered martensite is produced because of incorrect annealing above A_1 temperature, it develops in mode 2 as a result of overlapping heat affected zone formed on the deposition of multiple weld passes. For mode 1 single pass is sufficient to initiate sensitization whereas mode 2 at least two weld passes must be realized such that the first pass creates untampered martensite in the heat affected zone, and the critical sensitizing isotherm from the second pass causes carbides precipitation in the first heat affected zone (Van Warmelo *et al.,* 2007). Mode 2 sensitization has been observed at double fillets welds, double butt welds, repair welds, weld stop/start position and tack welds. Figure 2-27 illustrates mode 2 type of sensitization in ferritic stainless steel.

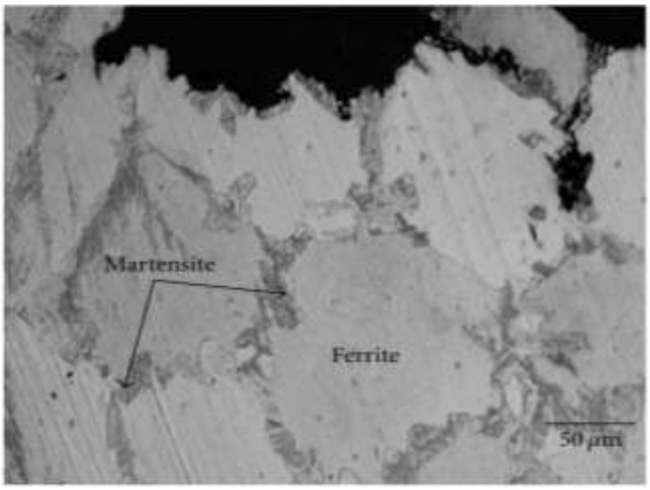

Figure 2-27: Preferential attack of the sensitized martensite phase in the HTHAZ of overlapping weld indicating Mode2 sensitization (Amuda, 2011).

Mode 3

Sensitization due to continuous cooling after welding at low heat input. This occurs in coarse grained region adjacent to the fusion line in material where the high temperature heat affected zone is predominately ferritic. Mode 3 type sensitization is independent of any previous heat treatment and material condition unlike Mode 1 and 2. It occur when low heat input during welding leads to a very fast cooling rates at the early stage of the weld thermal cycle. This rapid cooling rates can restrict or prevent austenitic nucleation as the heat affected zone cools through the dual phase (ἀ+ɣ) field resulting in almost fully ferritic high temperature heat affected zone microstructure. Mode 3 sensitization is illustrated in Figure 2-28.

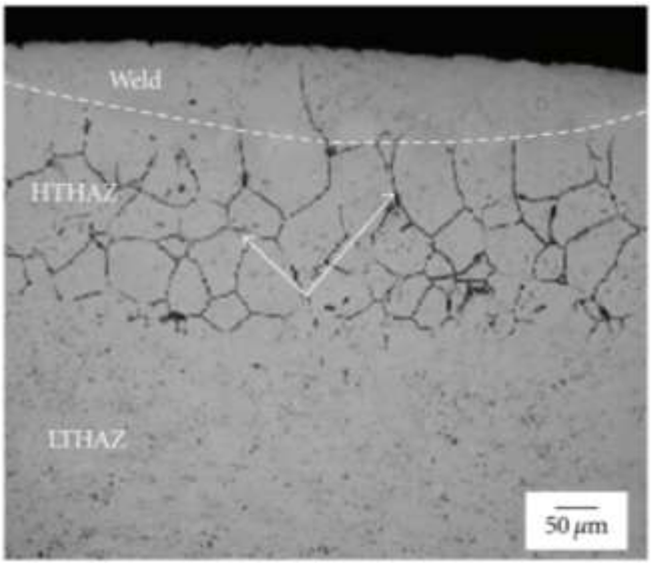

Figure 2-28: A continuous networks of ditched ferrite-ferrite grain boundaries in the HTHAZ due to mode 3 type sensitization (Amuda, 2011)

Mode 4

Sensitization on welding at excessive high heat input. The modes discussed above before showed that sensitization is initiated either from untampered martensite, precipitated carbides (mode 1 and 2) or from rapid cooling sequence due to low welding heat input producing ferrite-ferrite sensitized region. In mode 4 however, the sensitization may occur under very slow cooling associated with welding at excessive high heat input. High temperature austenite may sensitize on cooling if the cooling rate is sufficiently slow.

Mode 4 is least common of the four types. It normally exists within a narrow band at the border between HTHAZ and LHAZ in the vicinity of A_1 peak temperature isotherm. The occurrence of sensitization with such a narrow band suggests that very specific conditions must be fulfilled for mode 4 sensitization to manifest. The onset of the mode 4 sensitization is influenced by the cooling rate as well as the kinetics of the decomposition of austenite below the A_1 temperature. Du Toit et al suggested that mode 4 sensitization can be prevented by ensuring that the welding heat input does not exceed 1.5 kJ/mm.

Techniques for the control of sensitization

The incident of intergranular stress corrosion cracking within the HAZ is closely linked to the depletion of chromium content at the adjoining grain boundaries. It has been reported that at times, even in very solution, sensitization may induce intergranular corrosion attack (Amuda and Mridha,2011).It is therefore important that the phenomena is prevented rather than controlled ones it creeps in. Several techniques have been explored developed and practiced to prevent sensitization. These options are: Control of Interstitial (C+N) elements in steel, creating a high ferrite number, the use of stabilizing techniques, control of heat input and cooling rate.

Control of Interstitial (C+N) elements in steel

Since sensitization is promoted by the precipitation of carbides and nitrides at the grain boundaries due to the consumption of the matrix chromium by the interstitial constituents, then the concentration of these elements should be reduced to the level permitted by stoichiometry equilibrium that cannot initiate carbide precipitation. The solute solubility of carbon in ferritic stainless steel is very low, it is therefore recommended that the interstitial elements in stainless steel should be a maximum of 0.03wt%.

Creating a high ferrite number

The influence of ferrite factor in controlling sensitization in ferritic stainless steel was first reported by Kaltenhauser (Amuda, 2011). The ferrite factor is a scaling factor based on the strength of ferrite -stabilizing and austenite-stabilizing elements, which predicts the tendency for ferritic microstructure to develop in welds. Kaltenhauser developed an equation known as Kaltenhauser ferrite factor (KFF) to determine the tendency to form martensite in the weld metal. For low chromium steels, it is less than 13.5 and for medium -chromium steel, KFF number it is 17. Higher ferrite factor ensures that the steel is completely ferritic in the weld metal with improved corrosion resistance due to absence of intergranular martensite. The intergranular martensite induces residual stresses in the adjacent grain boundaries leading to poor impact resistance and accelerated initiation of cracks (Van Warmelo et al,2007).

Therefore, an appropriate controlled KFF number sensitization may be reduced or even eliminated.

The use of stabilizing technique

Resistance to intergranular corrosion (IGC) in austenitic stainless steel is enhanced through the addition of stabilizing elements. Since the mechanism of sensitization in austenitic stainless steel has been found applicable to ferritic stainless steel as well, then the stabilization technique adopted in austenitic stainless steel has also been applied to ferritic stainless steel. The stabilization treatment involves the addition of elements such as titanium and niobium during the AOD/VOD steel making process. These elements preferentially form stable MC-type carbides or nitrides. So far, titanium and niobium or combination of both are used to prevent sensitization since tantalum is quite expensive and vanadium is not effective due to slow formation of vanadium carbonitride precipitation reaction. Sensitization is still possible in properly stabilized alloys, particularly at extremely rapid cooling rate as experienced during the cooling cycle of fusion welding (Williams, 2005).

Control of heat input and cooling rate

In ferritics, it has been established that low heat inputs welding results in very fast cooling rates during the early stages of the weld thermal cycle, and these can suppress austenite nucleation.

2.13 Effect of shielding gas

The primary purpose of the shielding gas is to protect the molten weld pool from environmental contamination (Bergquis *et al.*, 2011). The oxides that often form as a result of poor purging and in stainless steels adversely impact on the corrosion resistivity due to different electro-potential between stainless steel alloy and the oxide (Huang and Yang, 2013). Effective post weld chemical cleaning of oxides by pickling is too complicated, time consuming and costly. It is consequently important to use an effective shielding gas to avoid oxidation (Durgutlu, 2004). The gas also promotes a stable arc and uniform metal transfer. In GMAW process shielding gas not only affects the mechanical/metallurgical properties of the weld but also determines the shape and penetration pattern. The quality, efficiency, and overall operating acceptance of the welding operation are basically dependent upon the shielding gas, since it affects the mode of the metal transfer in GMAW process. Moreover, shielding gas composition, during welding, affects microstructure of joined materials and hence their mechanical properties.

In addition, quality of the welded joint, metal transfer rate, and efficiency of welding process vary based on shielding gas composition. Martin (2020) conducted research whereby the gas flowrate of CO_2 was varied and it was discovered that changing the rate of shielding gas on the nozzles section influences the process taking place in the welding area. When varying the gas flow rate transfer of filler metal drops, stability of the welding process as well as the chemical composition of the weld metal which further influences the properties of the joint weld.

There are changes in the transfer frequency of electrode metal drops and chemical composition of the weld metal. Accurately selected gas shielding method and consumption of gas allows controlling the filler metal transfer and chemical composition of weld metal making the process of welding uninterrupted and forming necessary properties of the weld joints. Moreover, appropriate choice of shielding gas and use of an optimum flow rate results in better quality in terms of increased productivity, reduced gas consumption and improved weld geometry properties, microstructure and mechanical properties (Mvola and Kah, 2017).

Different kinds of shielding gases are often preferred for different processes and applications. The purging gas also acts as a current pathway between the arc and work piece (Bitharas *et al.*, 2018). Although the quality of the weld joint is dependent on several welding parameters (such as heat input, thickness of base metal and joint geometry), shielding gas plays a prominent role. The cost of helium is ten times that of argon, however helium produces a more stable arc than argon (Kang *et al.*, 2009). In addition, helium gives higher deposition rate and consequently increases the traveling speed and productivity (Shinde and Telsang, 2016).

Helium gas is not often used in mass production because of its high cost ; it is only employed in research or high end value-products (Chen *et al.*, 2017). To decrease costs, helium content is reduced as much as possible or new alternative gas supply methods are developed. Wang et al.(Wu *et al.*, 2016) used He-Ar mixture as a shielding gas in TIG welding of SiCp/6061 Al composites and reported that adding 50% volume of helium in the shielding gas improves not only the arc stability but also provides seams with high quality appearance (Xi-he *et al.*, 2009).

Chaudhari (2014) studied the effect of welding process parameters on tensile strength of the 3Cr12 stainless steel welded with ER 309L welding wire. One of the parameters that were investigated included the effect of gas flow rate on tensile strength; the gas flow rate was varied from 14 to 18 L/min with an increment of 1. It was observed that the tensile strength increased with an increase in gas flow rate. This research project focuses on varying the shielding gas (helium) flow rate, with the intention of observing the effect it has on the mechanical properties, deposition rate, and type of arc, microstructure, quality, and soundness of the weld.

This study seeks to obtain sound welds, defect free and good metallurgical and mechanical properties which will further improve the efficiency of fabricating the railway wagons giving rise to increase in productivity. According to the literature review which outlines the railway wagons applications, description of the ferritic stainless steel which also includes its microstructural evolution, effect of alloying elements and the effect of the shielding gas that will be varied to obtain the optimum gas flow rate to be utilized.

Chapter 3: Experimental procedure

3.1. Introduction

In this chapter, the aim of the experiment, the materials, fabrication of the testing samples and the detailed experimental methods employed are discussed. The analyses of the method and the testing standards used are presented. These includes welding, cutting, machining of the welded 3Cr12, welding parameters used, and safety precautions undertaken. The material characterization employed are also discussed. The aim of the experiments was to compare the effect of gas flowrate on welding of 3Cr12 with 308L welding wire. This was achieved by performing macro and microstructural analysis, XRD analysis, corrosion testing, tensile testing, impact testing and hardness testing.

3.2 Materials and welding process

Test samples of size 400 mm × 200 mm × 6 mm were cut from 3Cr12 ferritic stainless-steel plate. The 3Cr12 steels were procured from Macsteel in a fully annealed condition. The 3Cr12 ferritic stainless steel was welded using the ER- 308L austenitic stainless steel welding wire of 1.2 mm diameter. Chemical composition of the base metal and filler wire are shown in Table 3-1. The filler metal has high Cr and Ni content to ensure that there is microstructural control of the stainless-steel phases.

Table 3-1: Typical composition of 3CR12 ferritic stainless steel.

Elements (wt. %)	C	Cr	Mn	Si	Mo	Ni	Cu	S	P
Plates	0.009	11.41	0.86	0.76	0.005	0.74	0.14	0.001	0.02
308L Electrode	0.01	19.75	1.77	0.37	0.03	9.64	0.04	-	-

A 6 mm bevel butt joint was prepared to be welded by making use of a Miller GMAW welding machine as shown in Figure 3-1. Figure 3-2 illustrates the welding wires that was utilised during the welding process.

Figure 1: Miller GMAW welding machine with helium cylinders.

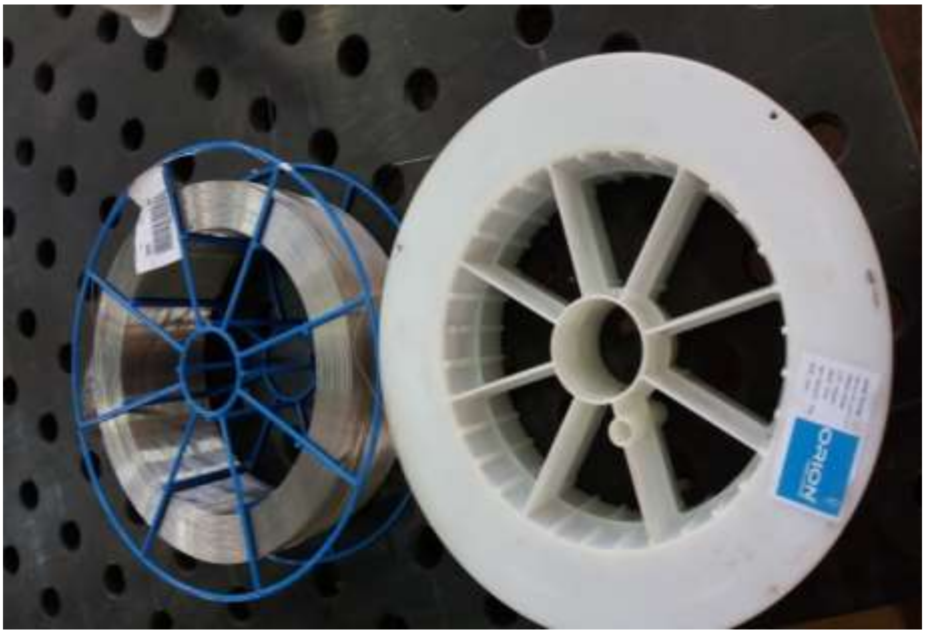

Figure 3-2: 308L welding wire spool.

The edges of the plates were cleaned with acetone to remove any contaminations before welding . Weld joint configuration was prepared as a double- butt joint of 45° internal angle, 2 mm root gap, 1 mm root face. The welded sample is presented in Figure 3-3. Welding paramaters used to join the plate are given in Table 3-2. The helium shielding gas flow rate was varied in increment of 5 L/min, from 10, 15, 20 up to 25 L/min .

Figure 2: welded 3Cr12 plate with 308L welding wire.

Table 3-2: Parameters used to weld the 3Cr12 stainless steel with 308L welding wire.

Gas flowrate(He)	**Voltage(V)**	**Current(A)**	**Wire feed speed mm/min**	**Time taken to weld 200mm**	**Welding speed mm/min**	**Heat input(HI) kJ/mm**
10L/min	26.7	86	4412	60	200.0	0.6
	25.7	88	4412	81	148.1	0.7
15l/min	25.2	98	4412	78	153.8	0.8
	25.6	84	4412	75	160.0	0.6
20L/min	26.5	102	4420	55	218.2	0.6
	26.6	97	4420	64	187.5	0.7
25L/min	24.9	76	4140	103	116.5	0.8
	25.1	70	4140	120	100	0.8

3.3 Non-Destructive Testing

3.3.1 Magnetic Particle inspection fluorescent Testing

Magnetic particle inspection testing (MPI) is used for the detection of flaws in ferromagnetic materials and is primarily used for crack detection. The specimen is magnetised either locally or overall, and if the material is sound the magnetic flux is predominantly inside the material. If there is a surface-breaking flaw, the magnetic field is distorted, causing local magnetic flux leakage around the flaw (British., 2002). This leakage flux is displayed by covering the surface with very fine iron particles applied either dry or suspended in a liquid. The particles accumulate at the regions of flux leakage, producing a build-up which can be seen visually even when the crack opening is very narrow. Thus, a crack is indicated as a line of iron powder particles on the surface. The method is applicable to all metals which can be strongly magnetised – ferritic steels and irons, but not generally austenitic steels (British., 2002).

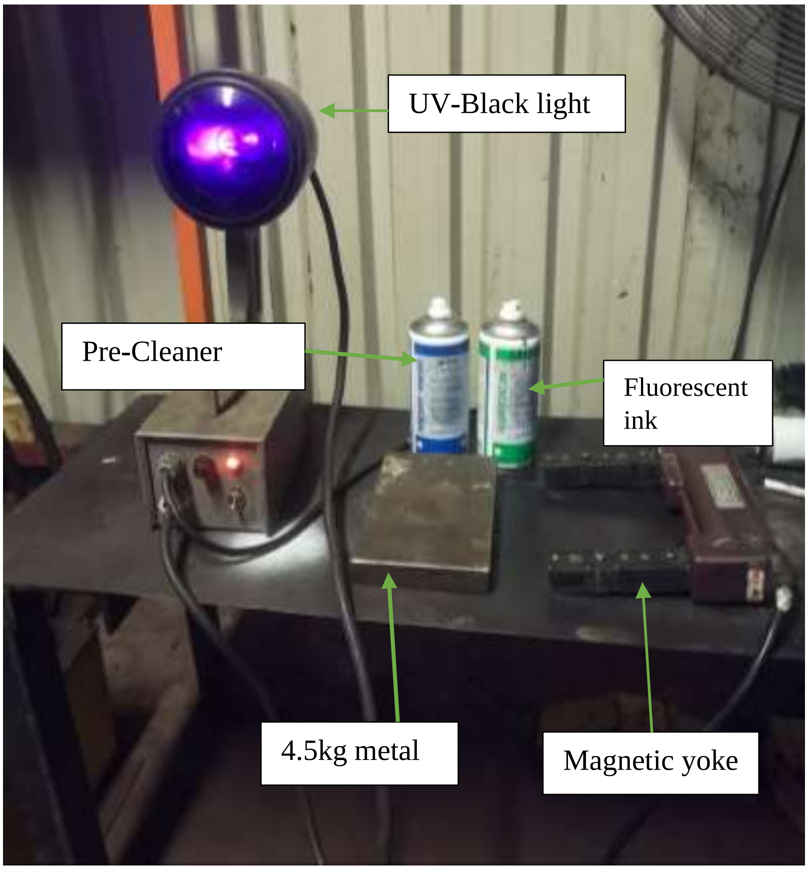

Figure 3-4: Fluorescent NDT testing equipments.

The surface was cleaned by spraying of pre-cleaner on the surface indicated on Figure 3-4. The 4.5 kg iron was used for quality to ensure if the magnetic yoke works. The UV black light was used to check if there were any discontinuities on the material before the test started. The magnetic yoke was further used to magnetise the welded plates to produce a magnetic field with lines of force at a large angle to the expected direction of the cracks to be detected, so that it is usual to apply the magnetisation more than once in different directions, for example in two directions mutually at right-angles, but methods of swinging the field direction during magnetisation are available. The magnetisation was produced by applying a permanent or electro-magnet to the surface (magnetic flow);by using a combination of two magnetic fields, a swinging or rotating magnetic flux can be produced, which will detect a crack in any orientation.

The iron particles dry powder suspended in a liquid (magnetic ink) were applied while the magnetising current is still flowing, but residual magnetisation is sometimes used, when the particles are applied after magnetisation (British., 2002). Magnetic inks (particles suspended in a liquid) are used more widely than dry powders. The magnetic ink was applied by low-pressure spray. It was ensured that the use of plenty ink was fulfilled and to allow time for the particles to flow over the surface and migrate to any cracks (British., 2002). Fluorescent particles, which require UV-A illumination, are widely used and coloured particles are also available. The indications of cracks and results obtained was preserved by photography.

3.4 Metallographic preparation

Metallography is the knowledge of material science, microscopy, and knowledge about sample preparation in practice in addition can further be explained as the study of the physical structure and the components of metals, using microscopy. The primary objective of metallographic examinations was to reveal the constituents and structure of metals and their alloys by means of the light microscope. Metallographic examination identifies and study the different structural elements and properties of each material. To study a structure of a material is necessary to carry out careful sample preparation. Microstructures have a strong influence on the properties and successful application of metals and alloys. The practical sample preparation may be divided into the following steps: cutting, mounting, grinding, polishing and etching. After preparation, the samples were analysed using optical microscopy.

3.4.1 Cutting /Sectioning

Welded samples were cross-sectioned into small specimen with dimensions 10 × 25 mm × 6 mm. Figure 3-5 illustrates how the material was cut from the welded plates for both micro-Vickers hardness profile as well as the microstructural analysis by making use of Struers Discotom-100/-10 cutting machine shown in Figure 3-6.The cutting of the samples was performed with a cutting wheel designed by Struers which contains relatively small abrasives particles, in order to produce fine surface and a minimum deformation. Wet abrasive sectioning was employed which involved the use of a recirculation system to supply a stream of coolant to the sample during the cutting process. This helps to prevent heat damage and to remove cutting waste from the wheel and specimen.

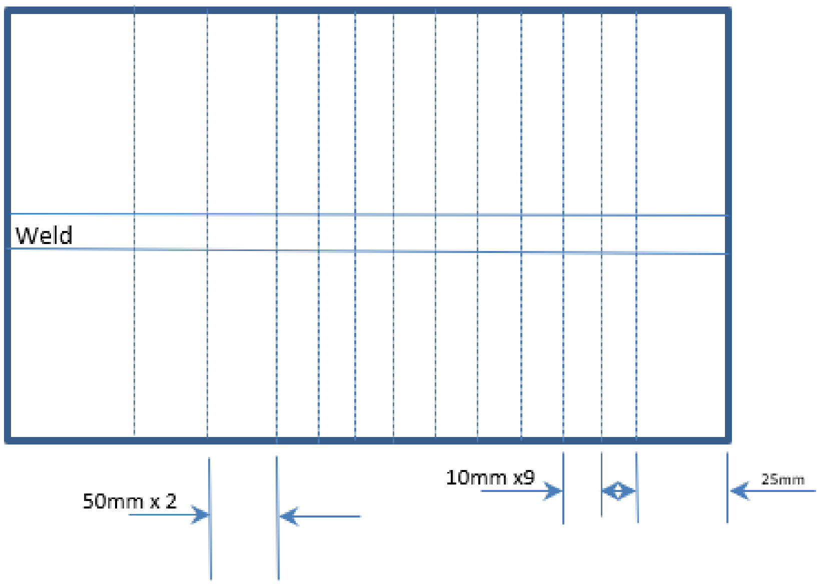

Figure3-5: measurements of the sectioned welded samples for test samples .

*Note: As per the testing standards the outer 25 mm should be discarded.

Figure 3-6: Cutting machine used to section the welded plates.

3.4.2 Mounting

After the metallographic samples were cut to an appropriate size, mounting of the samples was necessary for subsequent handling and metallographic polishing. Struess hot mounting Cito-press machine shown in Figure 3-7 was used to mount the samples whereby the samples were then pressed together using heat and hydraulic pressure (Alberto, 2008). Multi-fast Bakelite resin was utilised to mount the samples by ensuring that the samples were encapsulated with polymeric material.

Figure 3: Mounting machine.

3.4.3 Grinding

The purpose of this grinding machine as illustrated in Figure 3-8 was to grind the surface of the sample, to remove any visible scratches and contamination for microstructural analysis purposes. The sample was fixed in a sample holder and pressed onto the grinding medium grinding paper, grinding wheel with a grinding and polishing head. The grinding and polishing medium sits on top of a working wheel. A series of grinding steps follows whereby each new step makes use of even finer grinding medium, to proceed step-by-step towards the grade of polished surface desired. During the whole process, a lubricating and cooling fluid ensures that the sample is cooled, and waste material is washed away.

To ensure the complete elimination of the previous grinding scratches found by visual inspection, the direction of grinding was changed by 90^o from the one stage of grinding to the next stage. In addition, microscopic examination of the various ground surfaces during the grinding sequence may be worthwhile in evaluating the effect of grinding. Each ground surface should have scratches that are clean-cut and uniform in size, with no evidence of previous grinding scratches. Cleaning before going to next stage grinding is always helpful.

Figure 3-8: Grinding/polishing machine.

The samples were ground by making use of Struess grinding/polishing tetragramin machine following the standard operating procedures for stainless steel. SiC grinding paper of size ranging between P80, P120, P220, P1000 and P1200 µm was used. It is compulsory to start with paper of the biggest grain size and end with the finest one. Each step took about 1-2 minutes for accuracy. The sample was rotated at 90° and washed carefully between each step to remove any contamination or debris.

3.4.4 Polishing

Polishing is the final step in producing a surface that is flat, scratch free, and mirror-like in appearance. Such surface is necessary for subsequent accurate metallographic interpretation, both the qualitative and quantitative. The polishing technique used should not introduce extraneous structure, such as disturbed metal, pitting, dragging out of inclusions, and staining. The polishing step used the machine shown in Figure 3-8 and explained under grinding step. The polishing process consisted of three steps which includes 9 µm,3 µm and 1 µm which makes use of diamond abrasives. Dia-Duo was used for cooling and as lubrication. Samples were washed with water between the steps and the last one. Final polishing was carried out on a colloidal cloth with a silica suspension for 2 minutes. The samples were rinsed with water, sprayed with ethanol to avoid water marks on the surface and dried with a hair dryer.

3.4.5 Etching

Metallographic etching was used to reveal structural characteristics of a metal. This step is necessary to see the microstructure of the material since these structural characteristics are not visible in the as polished mirror like surface in the metal. The principle of etching multiphase alloys is based on the preferential attack or preferential staining of one or more phases, because of differences in chemical composition and, because of differences in grain-orientation. Before it was etched, the samples were inspected from polishing defects, such as scratches, pits, relief polish, comet tails, pulled out inclusions, and voids.

The chemical etching was accomplished by immersing the sample in the etchant until the required structure was revealed. Etching was done in petri-dish with loose covers to prevent excessive evaporation of the solvent. The samples were etched with Viella etchant (1g picric acid, 100 ml ethanol and 5 ml HCl) which attacks the heat affected zone and the parent material. The samples were further etched with aqua regia (10 ml HNO_3 and 30 ml HCl) to reveal the weld microstructure. Distilled water and cotton cloth was used to clean the sample whereas ethanol was utilized for easy drying. The specimens were stored in a properly labelled container in a dry environment.

3.5 Characterization

3.5.1 Optical microscope

Micro-structural analysis was carried out for several purposes, the most common one is to analyse the microstructure of the material. It is also common to examine for metallurgical abnormalities such as excessive grain growth, third phase precipitates, inclusions etc. The microstructures examination of the prepared specimens was observed and analysed under Olympus GX 71 microscope as shown in Figure 3-9.

Figure 3-9: Optical microscope

3.5.2 Stereoscope

Olympus Stereo Microscope illustrated in Figure 3-10 was used to capture the images and measure the area of the weld pool.

Figure 3-10: Olympus stereo microscope.

3.5.3 Scanning Electron Microscope

The Scanning Electron Microscope (SEM) as shown in Figure 3-11 uses electrons to form an image. The SEM produces images of high lateral resolution, which means that closely spaced features can be examined at a high magnification of the samples is relatively easy since most SEMs only require the sample to be conductive (Khokhar, 2005). The combination of higher magnification, larger depth of focus, greater resolution, and ease of sample preparation makes the SEM one of the most heavily used instruments in materials research areas today.

Figure 3-11: Scanning Electron Microscope machine.

Material examination by SEM can yield the following information: Morphology- The shape and size of the particles making up the object. (SEI, BEI) Crystallographic Information -How the atoms are arranged in the object. (EBSD) Composition- The elements and compounds that the object is composed of and the relative amounts of them (EDS or WDS). Carl Zeiss 460 Scanning Electron Microscope was utilised to analyse the corroded sample after Huey corrosion test was conducted, to evaluate if the grain boundaries are attacked by the acid during the test of the samples and the evidence of chromium depletion if it occurred (Khokhar, 2005).

3.5.4 X-Ray Diffraction

Crystal structures are studied through the diffraction of photons, neutrons, and electrons. The diffraction depends on the crystal structure and on the wavelength of incident radiation (Khokhar, 2005). Non-destructive analysis, minimal or no sample preparation requirements, ambient conditions, quantitative measurement of phase contents, texture and other structural parameters such as average grain size, strain and crystal defects.

Composition and phase identification of the specimens was achieved by X-ray diffraction (XRD) for all the welded sample. Figure 3-12 shows the Panalytical Empyrcan XRD model that is equipped with a Cu-kα X-ray source was employed for phase identification. The source with a wavelength of 1.54 nm was accelerated at a voltage of 45 kV, current of 40 mA and scanning from 20˚ to 120˚ angles at a step size of 0.02˚. High score software was used to predict the phases.

Figure 3-12: X-ray diffractometer machine.

3.6. Mechanical testing

The successful employment of metals in engineering applications relies on the ability of the metal to meet design and service requirements and to be fabricated to the proper dimensions (Bailey, 2009). The capability of a metal to meet these requirements is determined by mechanical properties (Bailey, 2009). Mechanical tests that were performed on the welds included hardness, impact and tensile testing. These tests were used to qualify the welds and to verify if the properties met the BS EN 10088-2:2014 specification for 3Cr12 stainless steel.

3.6.1 Hardness testing

Hardness may be defined as the ability of a material to resist permanent indentation or deformation when in contact with an indenter under load (Bailey,2009).Hardness is not an intrinsic property. The value of this property is the result of a defined measurement procedure, thus depending on the hardness method used, the hardness value will be different (Alberto, 2008).

All the hardness tests involve the use of a specifically different indenter, significantly harder than the test sample. The indenter is pressed into the surface of the sample using specific force. Either the depth or size of the indent is measured to determine the hardness value. Hardness values are widely used for quality control of materials because they are quick and considered to be non-destructive tests when the marks or indentations produced by the test are in low stress area (Alberto, 2008).

In this dissertation a micro-Vickers hardness was carried out on a flat metallographic polished sample surface by making use of Emco-Durascan machine presented in Figure 3-13. Vickers hardness is a measure of the hardness of the material, calculated from the size of an impression produced under load by a pyramid-shaped diamond indenter. This indenter is a square-based pyramid with an angle of 136° between opposite faces as shown in Figure 3-14. The two diagonals of the indentation left in the surface of the material after removal of the load are measured using a microscope and their average is calculated. The advantage of the Vickers hardness test is that is accurate and only one type of an indenter is used for all materials.

A load of 5gf was used to indent the sample with a dwell time of 10s. Hardness profile measurements were taken across the base metal, the heat affected zone, and the weld as shown in Figure 3-15. SANS 6507 (1-4):2006 standard testing method was used for hardness testing. A hardness profile was conducted, and the average was taken in order to achieve the overall hardness property of the fabricated samples.

Figure 3-13: Micro-Vickers hardness machine.

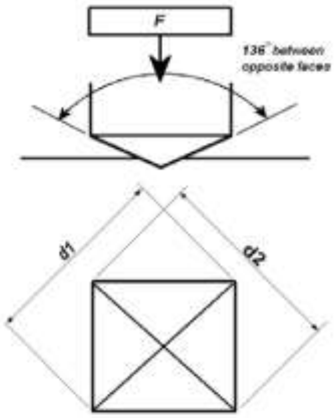

Figure 3-14: *Vickers pyramid diamond indenter (Alberto, 2008).*

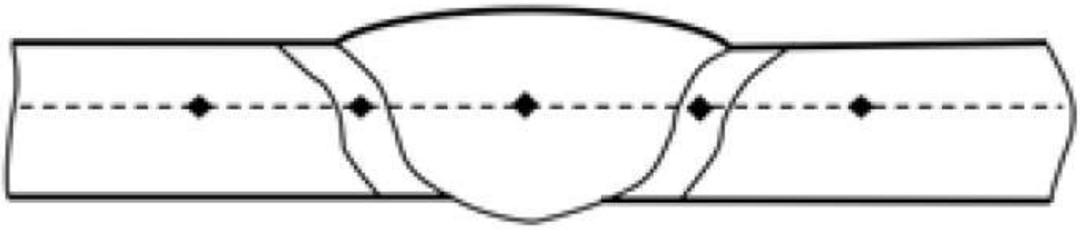

Figure 3-15: *Hardness profile indentation on the weld, HAZ and the parent material throughout the samples.*

3.6.2 Impact testing

Toughness is defined as the ability of a material to absorb energy. The Charpy non-standard V-notch impact specimen was used for characterizing the ductile-to-brittle transition behaviour of welded specimens in accordance with ASTM E23 guidelines as shown in Figure 3-16. The non -standard impact specimens with dimensions of 6 mm × 10 mm × 55 mm were machined. These specimens were tested under three different test temperatures (-7°C,-20°C and 25°C) and the impact notch toughness at each test temperature determined from the energy absorbed during fracture. The impact energy absorbed by the samples was tested by making use of SANS148-2:2013 standard testing method.

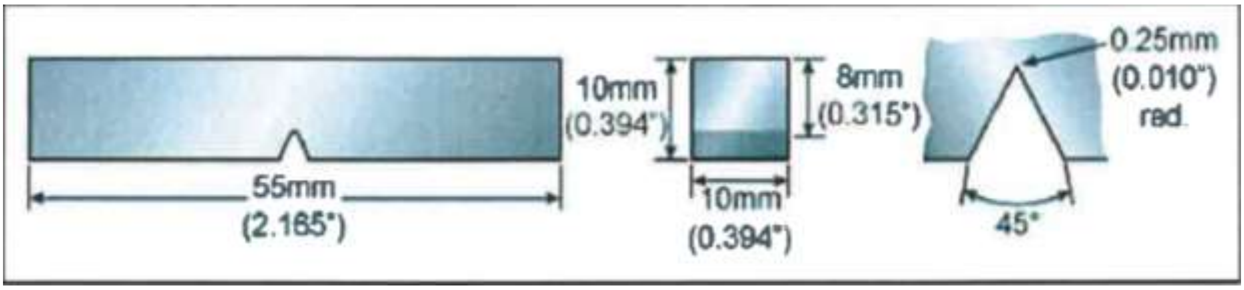

Figure 3-16: machining specification for Charpy V notched samples(ASTM,2018).

3.6.3 Tensile testing

Tensile strength test is one of the most common testing method used to determine the mechanical behaviour of material under statics, axial tensile or stretch loading. The tests were performed under ambient conditions to determine the tensile properties of the material. The tensile testing was carried out on 4 samples of 3Cr12 grade steels welded by GMAW process. The transverse tensile specimens were prepared as per ASTM E8 guidelines as shown in Figure

3-17. Figure 3-18 shows the machined tensile testing welded sample. Tensile tests were carried out on a 100 kN computer controlled universal testing machine. The cross- sectional area and pre-determined gauge length was measured to be 40 mm before testing each sample. The specimen was then loaded onto a machine set up for tensile loads and placed in the proper grippers so that the tensile specimens undergo deformation. Once loaded, the machine was used to apply a steady and continuous tensile load. With application of tensile load, specimens undergo deformation and ductile fracture took place at a particular load and the values were recorded to calculate ultimate tensile strength of the sample.

Tensile tests were conducted to evaluate the strength and ductility of the weld at room temperature. Tensile results will include the yield strength, ultimate tensile strength, and percent elongation as fracture stress, the strain rate of the machine is 0.1mm/mm. Figure 3-19 shows the machine used to conduct the test.

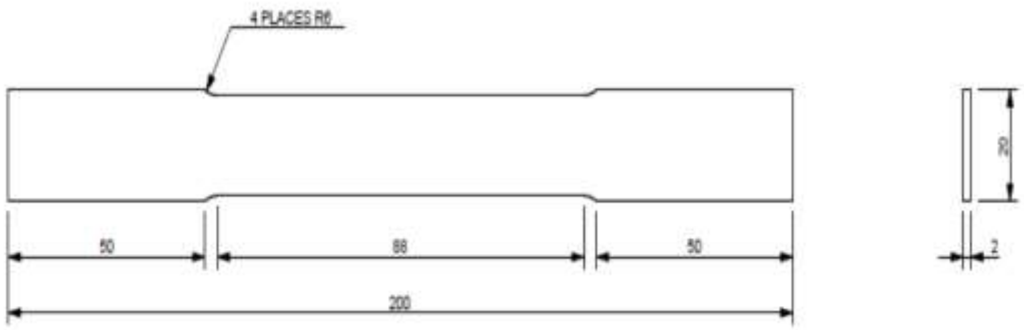

Figure 3-17: Tensile ASTM machining guidelines (ASTM,2018).

Figure 3-18: Machined tensile testing welded samples

Figure 3-19: Tensile testing machine.

3.7 Corrosion testing

3.7.1 Huey test

Welded samples were cross-sectioned into small specimen with dimensions 10 × 25 mm × 6 mm, grinded and polished in accordance with section 3.3 (grinding and polishing). The simplest and the longest-established methods of estimating corrosion losses in a plant and equipments is weight loss analysis. A weighed sample of the metal or alloy under consideration is introduced into the process and later removed after a reasonable time interval. The sample is then cleaned of all the corrosion products and is reweighed. The weight loss is converted to a corrosion rate (CR) which was calculated according to Equation 3-1:

$$\textit{Corrosion Rate (CR)} = \frac{Mass\ loss\ (g) * K}{Alloy\ density\left(\frac{g}{cm3}\right) * Exposed\ area(A) * Exposure\ time(hr)} \quad \ldots\ldots\ldots\ldots(3\text{-}1)$$

Huey test was performed according to ASTM 262-86 practice C of intergranular corrosion tests for stainless steels. Samples were subjected to a boiling solution of 65% HNO_3 for 48 hours, with fresh solution used at each interval. Five intervals of changing the solution were adopted.

The method is designed to sensitize the material and to find grain boundary segregation and precipitation.

The degreased and polished specimens were placed in a 1L Erlenmeyer flask containing boiling solution of 65% nitric acid with condenser. Volume of the solution for the test was 20ml. Samples were placed in the Erlenmeyer flask once the acid started boiling. After completion of each period, specimens were cleaned and weighed after drying. The corrosion rate during each boiling period was calculated from the difference of weight of the specimens before and after the test and by using Equation 3-1. Evaluation was done by measuring the initial mass of the samples, at each of the five intervals the mass loss was measured. The average of the mass loss was calculated and subtracted from the initial mass in-order to check how much mass was lost.

The typical sensitization treatment is 650°C – 700°C (1200 – 1290°F) for 30 – 120 minutes with air cooling. In this temperature range, the precipitation of a secondary phase or carbide on grain boundaries is accelerated. This results in the depletion of the adjacent grain boundary area of chromium with $M_{23}C_6$ precipitation, or molybdenum in the case of phase precipitation. Depletion of Cr leads to the grain boundary area being susceptible to attack while the bulk of the material remains immune to corrosion.

3.7.2 Electro etching

To eliminate any inaccuracies electro etching was conducted with Villella etchant for further examination of intergranular corrosion to observe if sensitization occurred on the material. Each sample was subjected to a current of 3.7 A, voltage of 63V as well as an exposure time of 1 minute in the solution, thereafter the optical microscope was used to view the microstructures after the test.

Chapter 4: Results and Discussion

4.1 Introduction

In this chapter the results of the experiments conducted during the study are presented and discussed. The trends and the correlations are observed and presented. Chapter 3 depicted how the metallography representation of the welded 3Cr12 was achieved with different gas flowrates. Several test analyses were done to investigate the objective of this study. The tests included the microstructural and macrostructural analysis, XRD, corrosion testing, micro-hardness profiling, tensile testing, and impact testing.

4.2 Non-Destructive Testing-Fluorescent Magnetic Particles Inspection

Figure 4-1 illustrates the results obtained after the non-destructive testing was conducted on all the welded samples. All the gas flowrates 10L/min, 15L/min, 20L/min, and 25L/min showed no form of defects or any abnormalities. It was observed that the welded samples of 3Cr12 plates with 308L welding wire using helium as a shielding gas yielded sound, quality and defects free welded samples at gas flowrates of 10L/min, 15L/min, 20L/min and 25L/min.

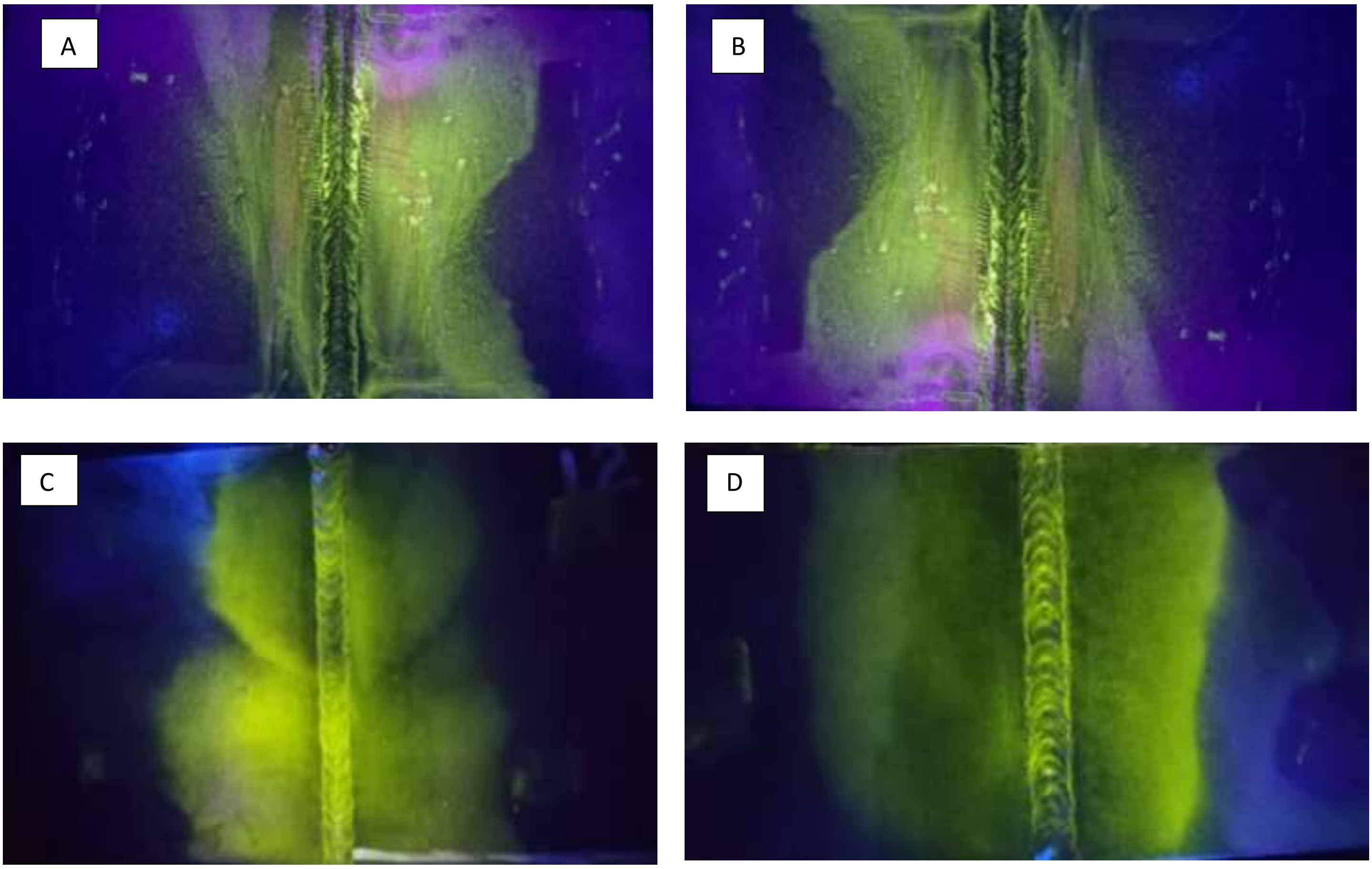

Figur4-1: Fluorescent magnetic particle inspection conducted on (A) 10l/min (B) 15l/min(C) 20l/min(D)25l/min

4.3 Macrostructural analysis

Macrostructural analyses were obtained by making use of a stereoscope to verify any welding discontinuities such as lack of fusion, lack of penetration cracks and any defects in the welded area. In addition, it was used to measure the weld deposition width obtained at different gas flowrates as schematically shown in Figure 4-2

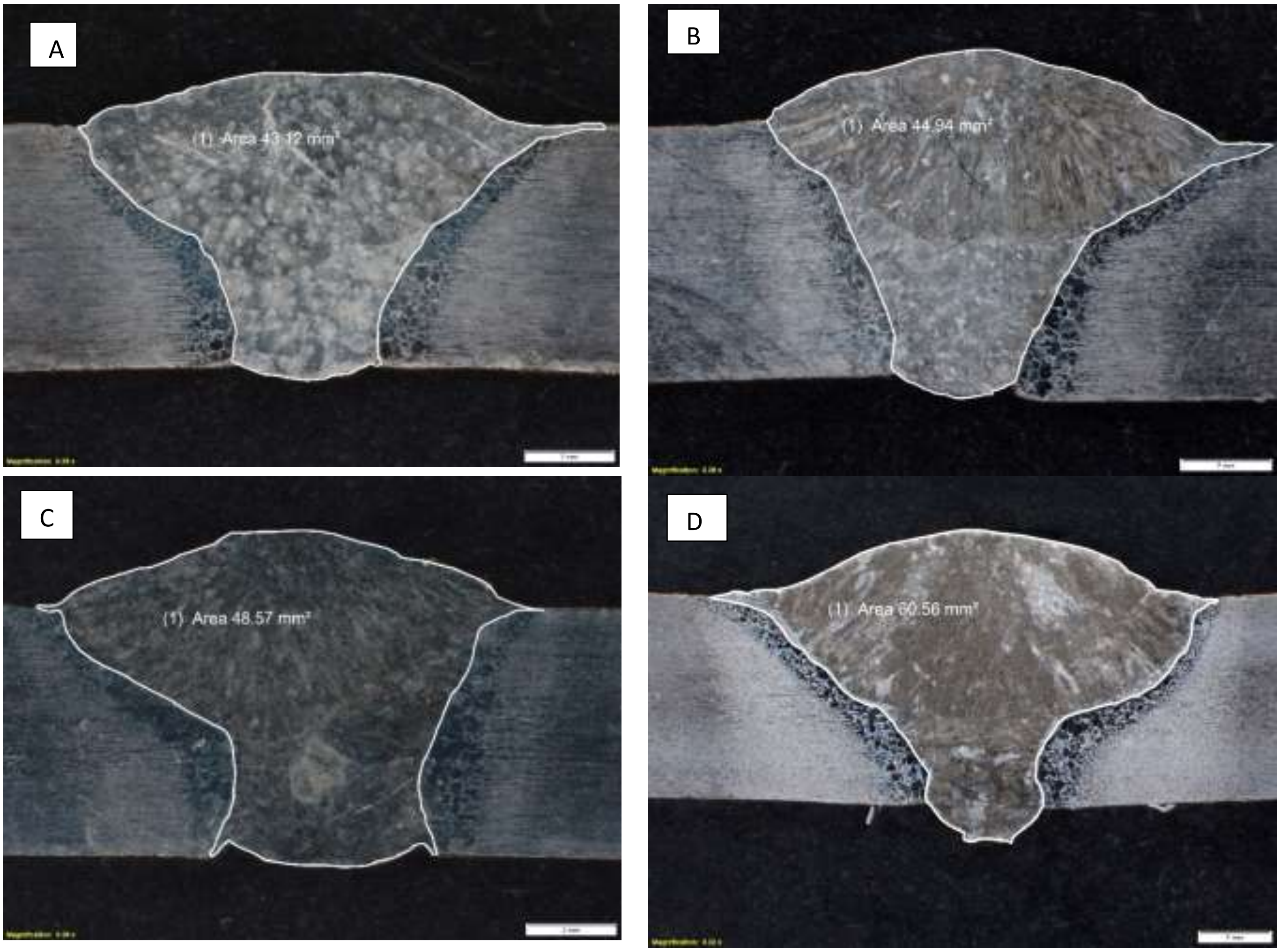

Figure 4-2: *Macroscopic view of the welded joint cross section area of the measured weld beard of a)10l/min, (b) 15l/min, (c) 20l/min and (d) 25l/min.*

Weld sample areas produced at varying gas flowrates (10L/min, 15L/min, 20L/min, 25L/min) yielded areas of 43.12 mm^2, 44.94 mm^2, 48.57 mm^2 and 60.56 mm^2 respectively. From the obtained macrostructural results, it was found that the weld joint prepared at a gas flowrate of 25L/min had higher weld deposition area as opposed to the other gas flowrates. Mohammed *et al* (2002) observed that an increase in gas flowrate increased the deposition of the weld on their carbon steel. Thus, an increase in gas flow rate led to increasing weld deposition rate. The macrostructural analysis showed no discontinuities on all the samples, and good fusion and penetration was observed on all the samples. This was attributed to the selection of the shielding gas since helium consists of a very high thermal conductivity (Nuclear power, 2012).

4.4 Microstructural analysis

Microstructure provides the different phases, the orientation of grains and grain boundaries. The phases found in a microstructure can predict the behaviour of materials. The captured images from the optical microscope illustrated the microstructures of the parent material, Low Temperature Heat Affected Zone (LTHAZ), the High Temperature Heat Affected Zone (HTHAZ) and the weld, for 10L/min, 15L/min, 20L/min and 25L/min. The general microstructure of the parent material consisted of equiaxed ferrite grain structure of a typical ferritic material consisting of ferritic phase with an average grain size of 9µm (Figure 4-3).

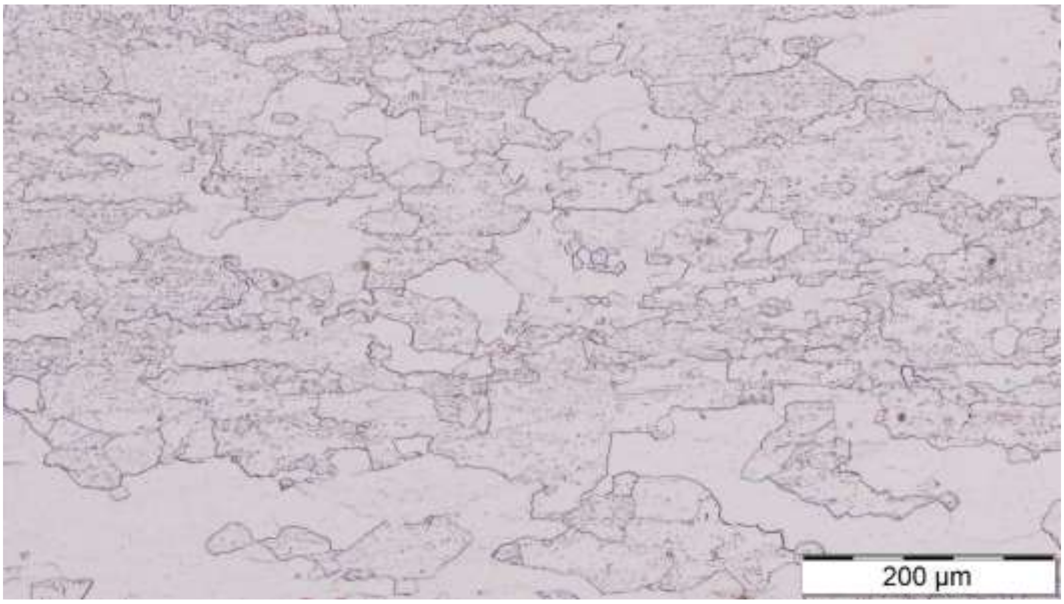

Figure 4-3: 3Cr12 parent material

Using the chemical compositions of the 3Cr12 as the parent metal and the filler metal (308L), the Schaeffler diagram was used to estimate the composition of the microstructural phases contained in the weld metal. The nickel and chromium equivalents that are part of the Schaeffler diagram were calculated using Equation 4-1 and Equation 4-2 for the parent metal and the filler metal were plotted and illustrated in Figure 4-4.

The red dot represents the expected microstructure for the 308L filler wire material only. The blue dot represents the 3Cr12 stainless steel plates only. According to literature the percentage dilution of parent metal is 30%-40% the weld and this is plotted on the tie line between the parent and filler dots with a green dot (Koli, 2019)

From the Schaeffler diagram the HAZ microstructure is expected to be predominantly ferrite but some martensite could be expected. This is expected due to the location of the blue dot, because the HAZ should consist of mostly parent material that melted and then cooled down rapidly. From the Schaeffler diagram the phases were found to be 85% ferrite with 15% martensite in the HAZ, whereas at the weld the phases that were present were 45% austenite,45 %martensite and 12% ferrite. Proper amount of ferrite in the weld metal is essential as the ferrite structure inhibits hot cracks in the weld metal (Kou., 2003). This is because ferrite can dissolve harmful elements such as sulfur and phosphorus which can segregate to the weld metal and increases the risk of cracks when the residual stresses increase. Kou (2003) stated that weld metal containing between 2-10 % ferrite structures in a stainless-steel weld metal is desirable.

$Ni_{eq} = \%Ni + 30 \cdot \%C + 0.5 \cdot \%Mn$ .... *(4-1)*

$Cr_{eq} = \%Cr + \%Mo + 1.5 \cdot \%Si + 0.5 \cdot Nb + 2 \cdot \%Ti$ ....(*4-2*)

Table 4-1: Ni_{eq} and Cr_{eq} of the 3Cr12 and 308L used for the welding

	3Cr12	AISI 308L
Ni_{eq}	1.44	9.20
Cr_{eq}	12.94	19.30

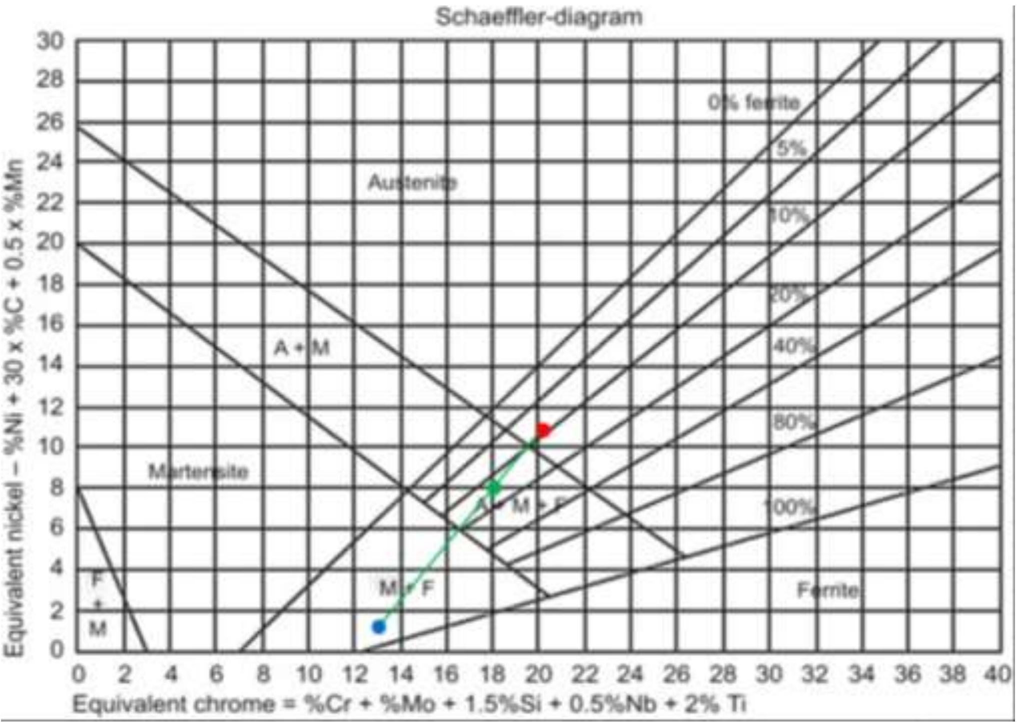

Figure 4-4: Schematic figure of the calculations with the Schaffler constitutional diagram (Lancaster, 1999)

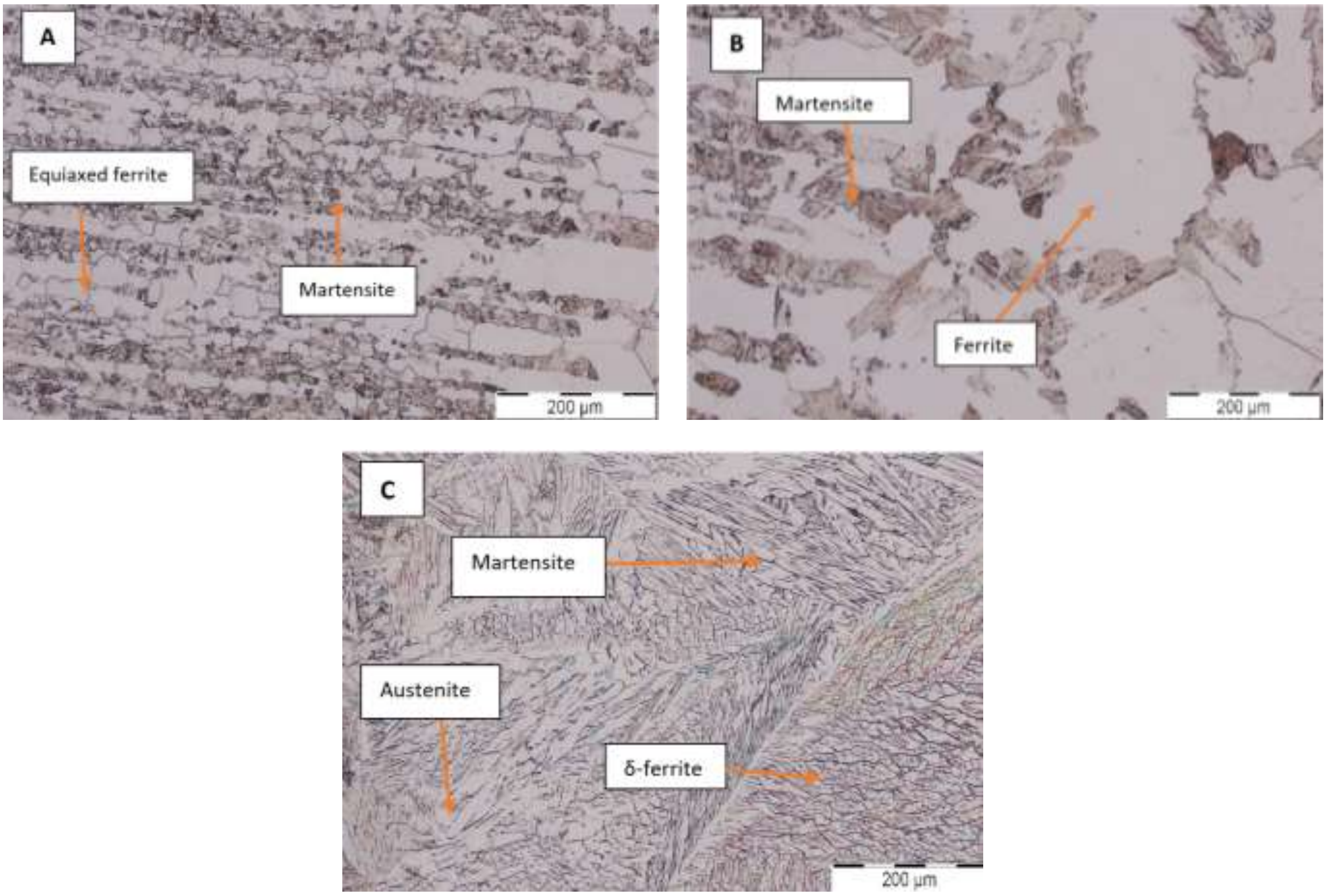

Figure 4-5: Microstructure for sample welded at 10L/min gas flowrate (A) Low temperature heat affected zone. (B)High temperature heat affected zone, (C) the weld

When the gas flow rate was 10L/min in Figure 4-5, the low temperature heat affected zone contained fine grained structure of ferrite (62%) and martensite (38%) whereas the high temperature heat affected zone comprised of coarse grains of ferrite (49%) with embedded blocky untempered martensite (51%) on the grain boundaries. The average grain size of the LTHAZ and HTHAZ was found to be 9µm and 11µm respectively. On the other hand, the weld showed a dendritic morphology containing martensite (10%), austenite (32%), and ferrite (58%) phases with an average grain size of 6µm.The difference in grain sizes between the LTHAZ, HTHAZ and the weld is due to the susceptibility of the HTHAZ to the heat that is generated during welding since it is adjacent to the weld fusion as opposed to LTHAZ which is further away from the fusion weld. The study conducted by Praktigno *et al* (2020) varied the helium gas flowrate (12L/min, 18L/min, 24L/min and 30L/min), and similar trend to this study was observed in regard to the HAZ as well as the observed weld morphology and microstructure was observed. The formation of martensite in the HAZ and weld is due to the temperature increase introduced by the weld pool followed by rapid cooling. The temperature range of HTHAZ is 1200°C-1430°C whereas the temperature range of LTHAZ was found to be 800°C-980°C. Research by Lippold (2005) indicated that martensite in ferritic stainless steel has shown to have both beneficial and detrimental effect, although martensite can introduce metallurgical notches, for purposes of wagon wear plates the harder phase promotes beneficial wear resistance.

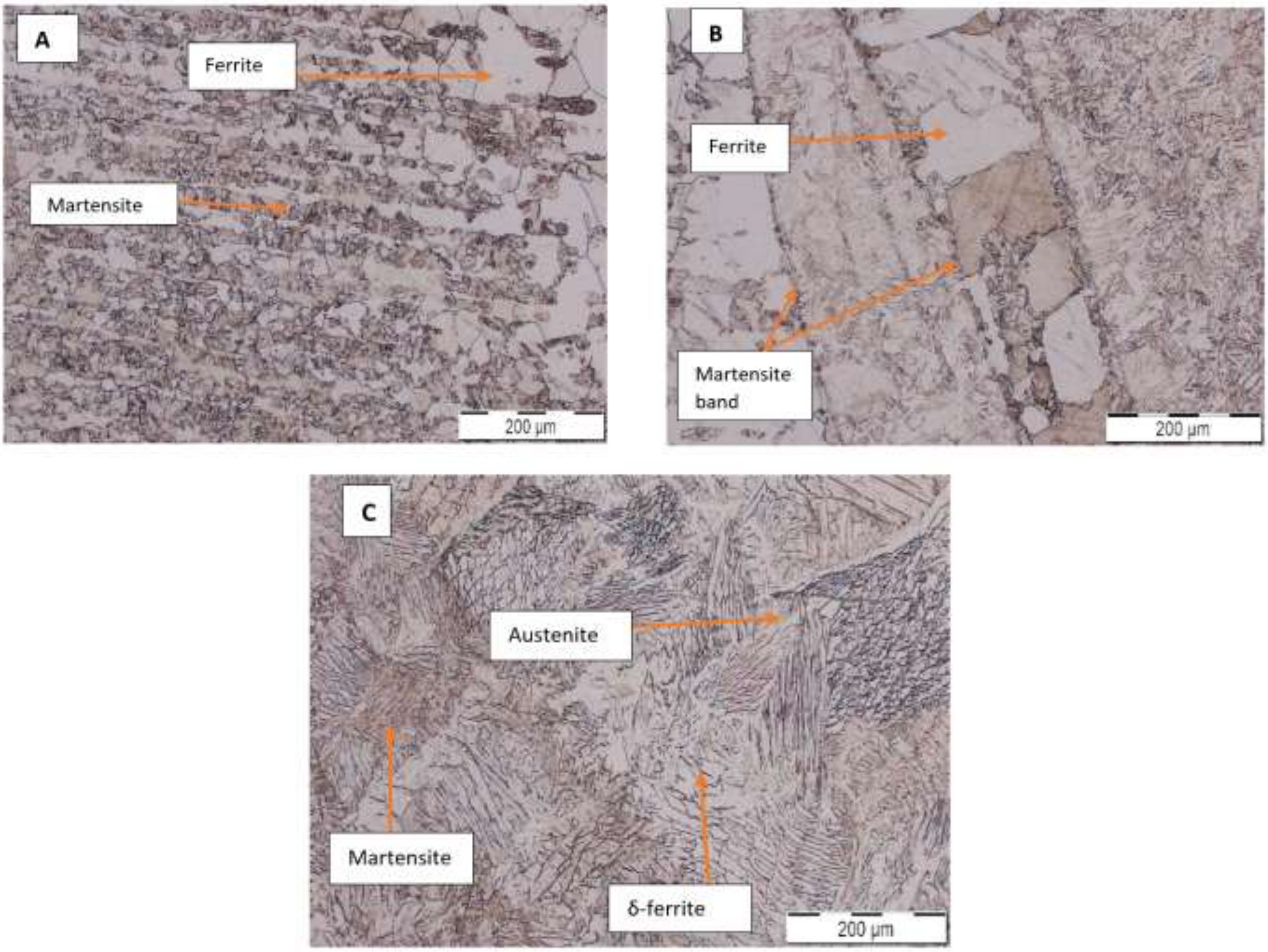

Figure 4-6: Microstructure for sample welded at 15L/min gas flowrate (A) Low temperature heat affected zone (B) High temperature heat affected zone, (C)the weld

In Figure 4-6 as the gas flowrate increased to 15L/min the low temperature heat affected zone showed equiaxed ferrite (57%) with martensite (43%) with the average grain size of 8µm. The LTHAZ also showed more distribution of martensite phase as opposed to 10L/min. HTHAZ showed a martensite band which indicates that there was overlap of runs during the welding process, coarse grained ferrites were still observed with an average grain size of 11µm. The weld exhibited more pronounced grains exhibiting widmastatten growth morphology as compared to the 10L/min. Delta ferrite (46%), martensite (21%) as well as austenite (33%)

were also observed on the weld. As the gas flowrate increases it accelerates the cooling process preventing the heat to be spread uniformly across the sample. This agrees with Kou (2003) where it was found that continuous cooling metal, lead to the transformation of ferrite to austenite. It was also found that the appearance of the continuously cooled specimen has all the characteristic of the widmanstatten structure.

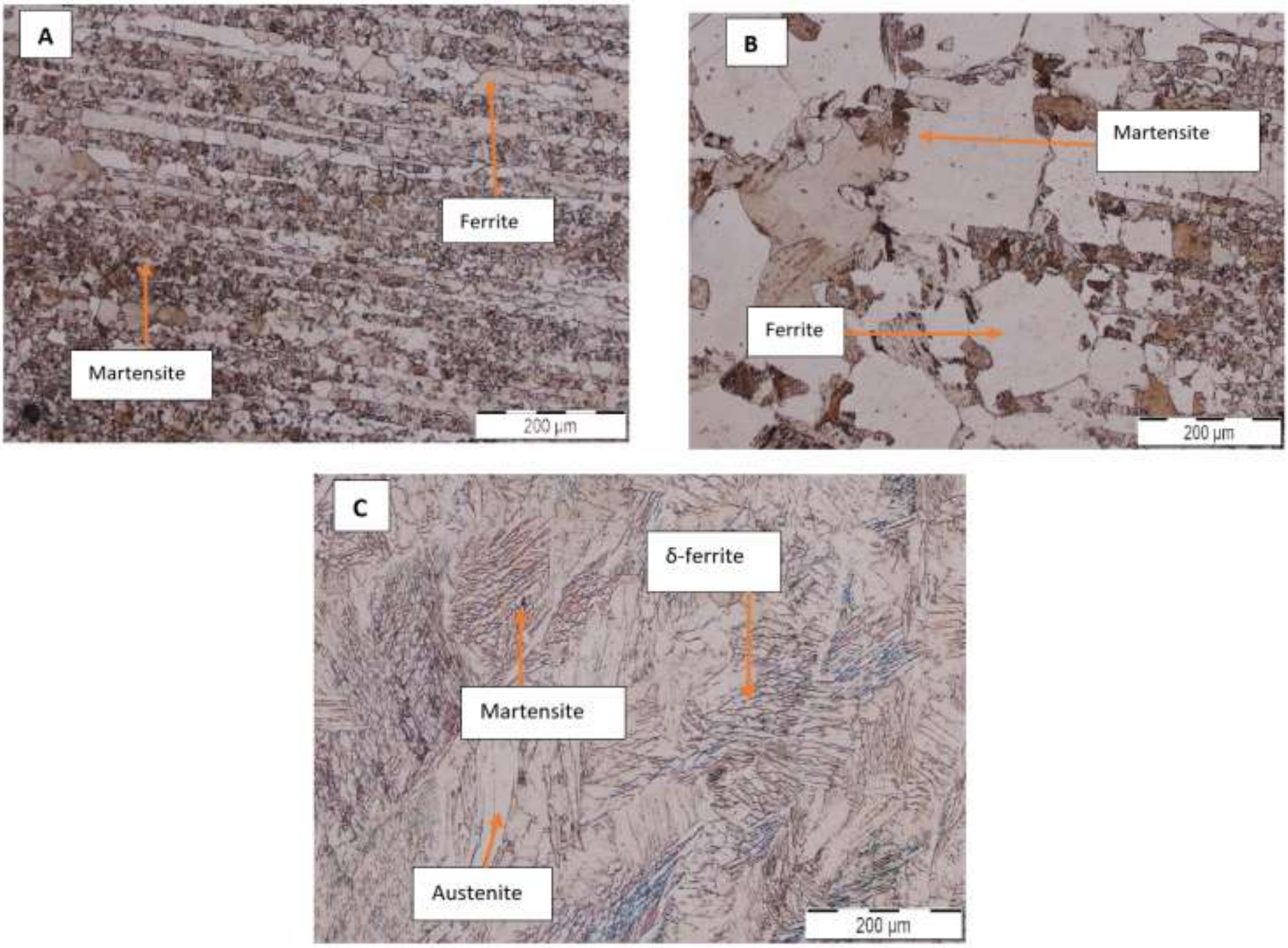

Figure 4-7: Microstructure for sample welded at 20L/min gas flowrate (A) the weld (B) High temperature heat affected zone, (C) Low temperature heat affected zone.

At 20L/min martensite (48%) and ferrite (52%) phases were also observed at the LTHAZ.This zone consisted of fine grained ferrite with untempered martensite intergranular and transgranular martensite as witnessed in the study by Grobler (1987). The HTHAZ grains were coarser ferrite (48%) with an average grain size of 11µm containing intergranular and transgranular martensite (52%). The weld consisted of three phases which were austenite (31%), delta ferrite (33%) and untempered martensite (36%) with the average grain size of the weld was found to be 6µm.

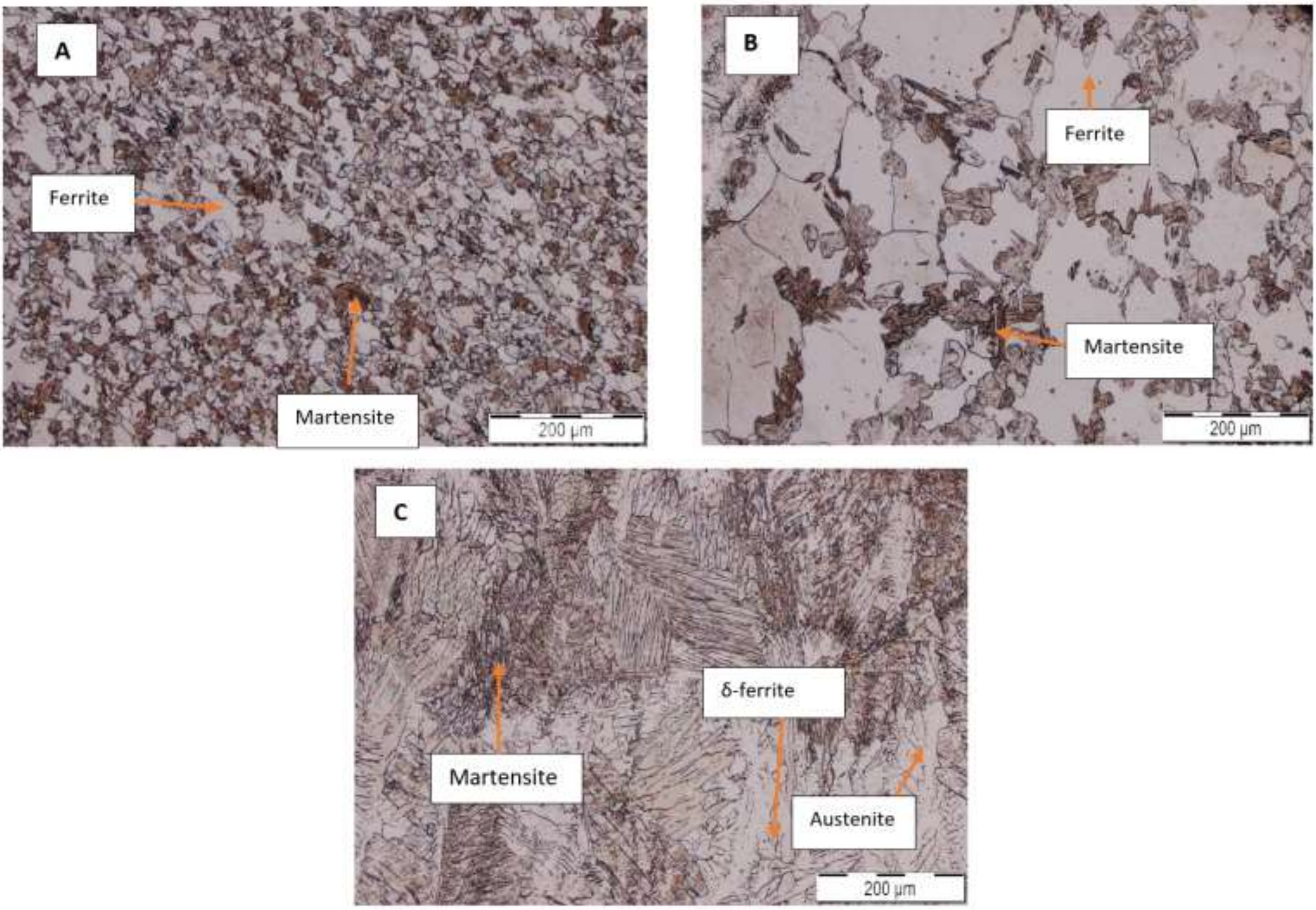

Figure 4-8: *Microstructure for sample welded at 25L/min gas flowrate (A) Low temperature heat affected zone. (B)High temperature heat affected zone, (C) the weld*

At 25L/min it can be seen from Figure 4-8 that there was a higher content of martensite (57%) than ferrite (43%) in the LTHAZ. More martensite was also observed on the grain boundaries as well as the inside of the grains for the HTHAZ with phase analysis of 35% and 65% for martensite and ferrite, respectively. On the other hand, the weld zone showed phase content of martensite, ferrite and austenite being 43%, 32% and 25% respectively. The weld zone showed more content of martensite as opposed to the 10L/min, 15L/min and 20L/min which was reported to be 10%, 19% and 38% respectively. The observed results are due to high cooling rates that transforms more of austenite to martensite at a faster rate, this is expected as stated in the hypothesis which states that an increase in gas flowrate increases the cooling rates which further transforms more ferrite to martensite upon cooling. Finally, when the gas was at the highest flowrate of 25L/min, it was discovered that high content of martensite on the grain boundaries was obtained. The higher the gas flowrate, the higher the cooling rates which results in increasing martensite content, this is further substantiated by the highest hardness values obtained on the weld.

Overall discussion on all the microstructure of different flowrates.

During welding, with increasing gas flow rate the continuously transported helium has a compression effect on the arc results in a more compact arc resulting in denser weld bead. The temperature field around the arc results in a more compact arc and a denser distribution of welding temperature. The helium arc transfers more energy to the weld which lead to penetration depth. Penetration increases slightly with gas flowrate from 10L-25L/min because the helium density with low gas density helium is not entirely transported to the arc.

Ferrite to austenite transformation occurs by a diffusion-controlled process, in which Ni diffuses in the ferrite towards the advancing austenite, and Cr is rejected by the advancing interface (Leone and Kerr, 1982). The austenite-ferrite interface becomes non-planar and has widmastatten appearance (Leone and Kerr, 1982). During welding the HTHAZ zone was heated within the ferrite phase field. Due to the very high peak temperature range of 1300°C-1510°C in this zone excessive ferrite grain growth occurred, with subsequent transformation of some of the ferrite to austenite during subsequent cooling cycle. The grain growth zone is adjacent to the weld fusion, and it experience temperatures that are exceeds then AC_3 transformation temperatures (Abe et al., 2008). All precipitates that hinder the growth of the grains melt/dissolve at this temperature, resulting in grain coarsening. At the maximum peak temperature (T_p>1250°C) delta ferrite grain could nucleate, when cooling the 3Cr12 steel at the cooling rate range of 100-150°C/s martensitic microstructure is instantaneously formed upon cooling.

4.5 XRD results

Samples welded under varying gas flowrates (10 L/min, 15 L/min, 20 L/min and 25L/min) were subjected to X-ray diffraction for phase identification. Figures 4-9 to 4-12 shows XRD patterns of the welded samples. The phases that were identified in the samples are mainly ferrite (BCC) and austenite (FCC). However according to the microstructural analysis, martensite is an expected phase that is formed in the HAZ and the weld, yet it was not detected during the phase analysis due to the low carbon composition of 3Cr12 which led to the formation of low carbon martensite. SEM results showed in Figure 4-19 and Figure 4-20 confirmed the presence of martensite in the microstructure. In high carbon concentration entrapped in the martensite lattice, the c/a ratio is large enough that, in an XRD pattern ferrite and martensite peak are well separated to each other to facilitate the measurement of the peak positions. Some carbon must have dissolved in the Fe-lattice (i.e., ferrite phase) has some interstitial carbon which translate to the minor changes in the lattice spacing of the Fe (Zahiri, 2017).

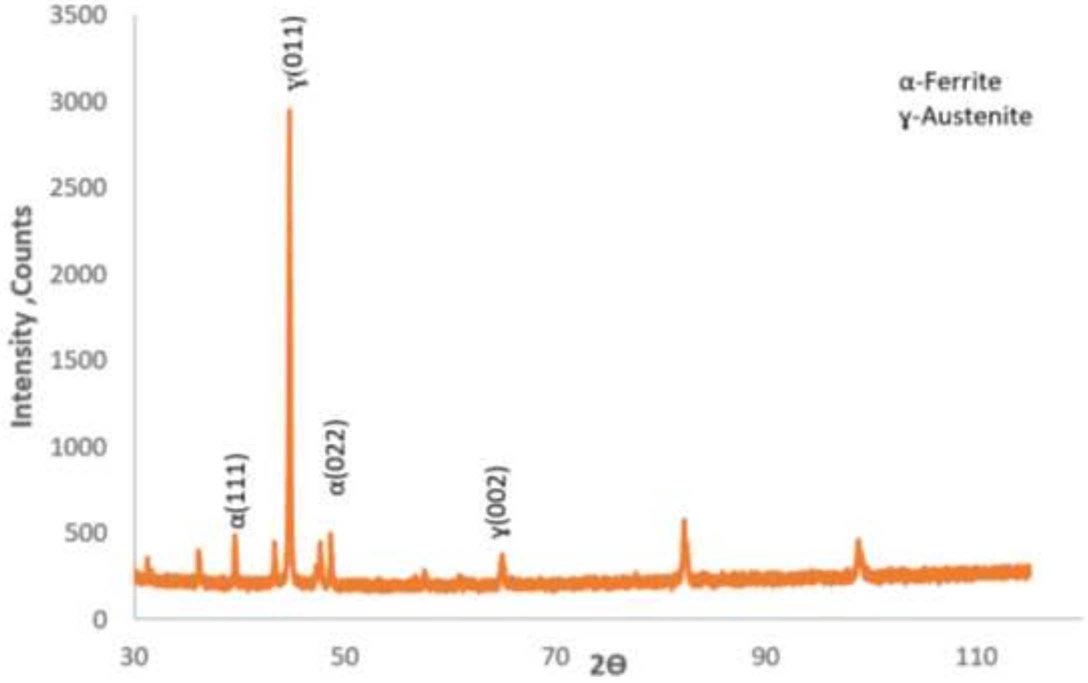

Figure 4-9: XRD spectrum depicting ferrite and austenite peaks for 10L/min gas flowrate

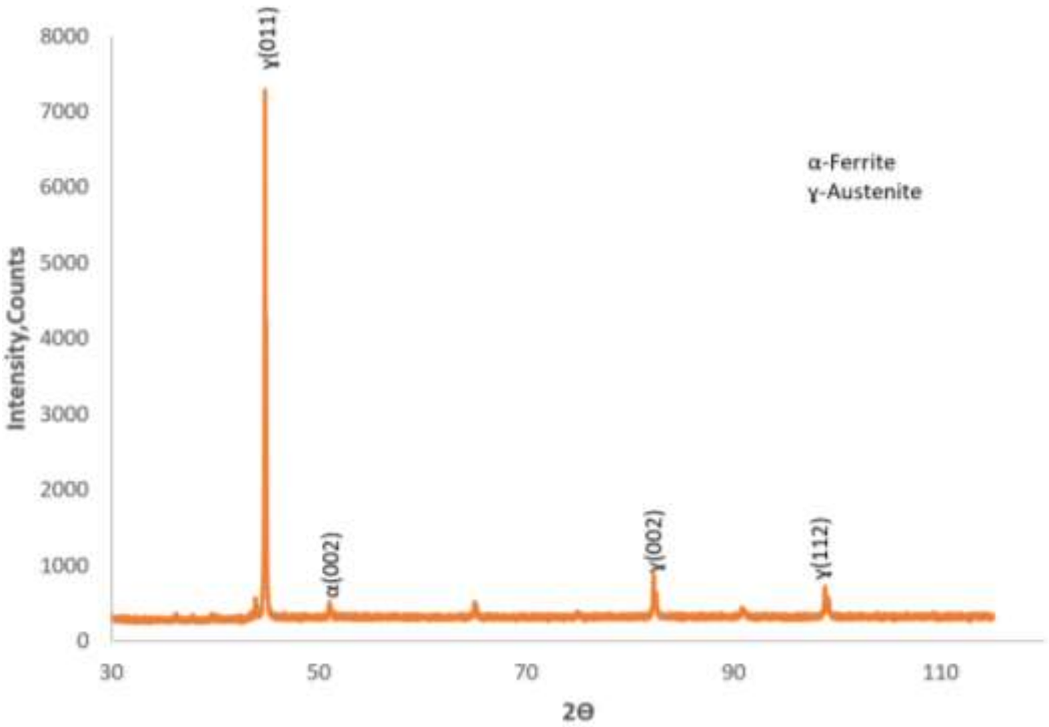

Figure 4-10: XRD spectrum depicting ferrite and austenite peaks for 15L/min gas flowrate

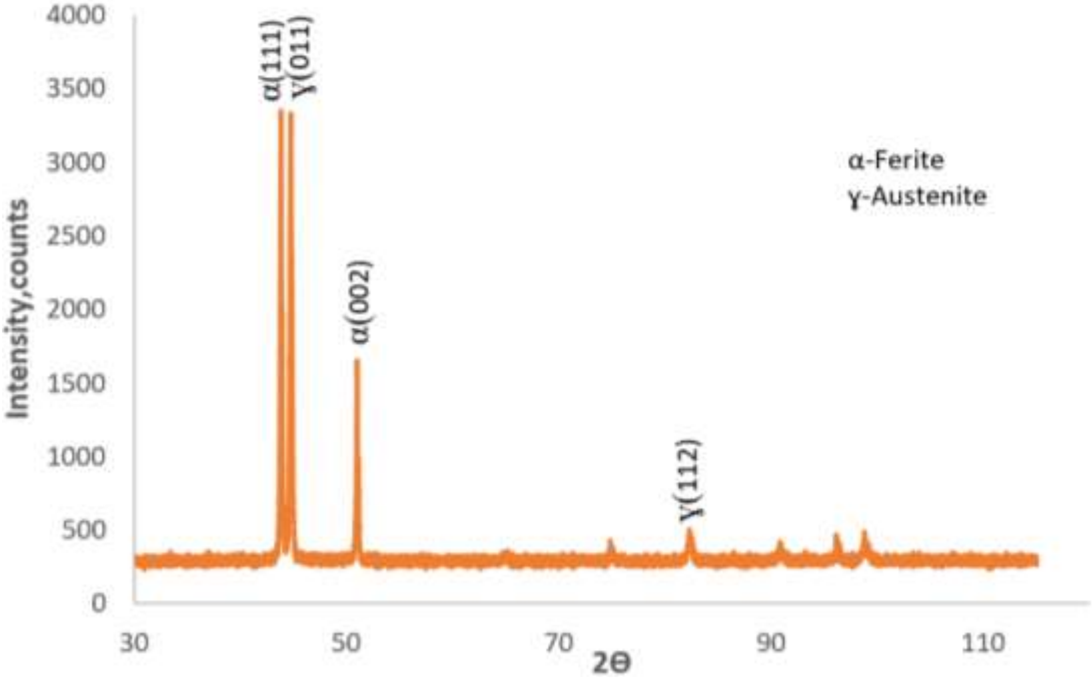

Figure 4-11: XRD spectrum depicting ferrite and austenite peaks for 20L/min gas flowrate

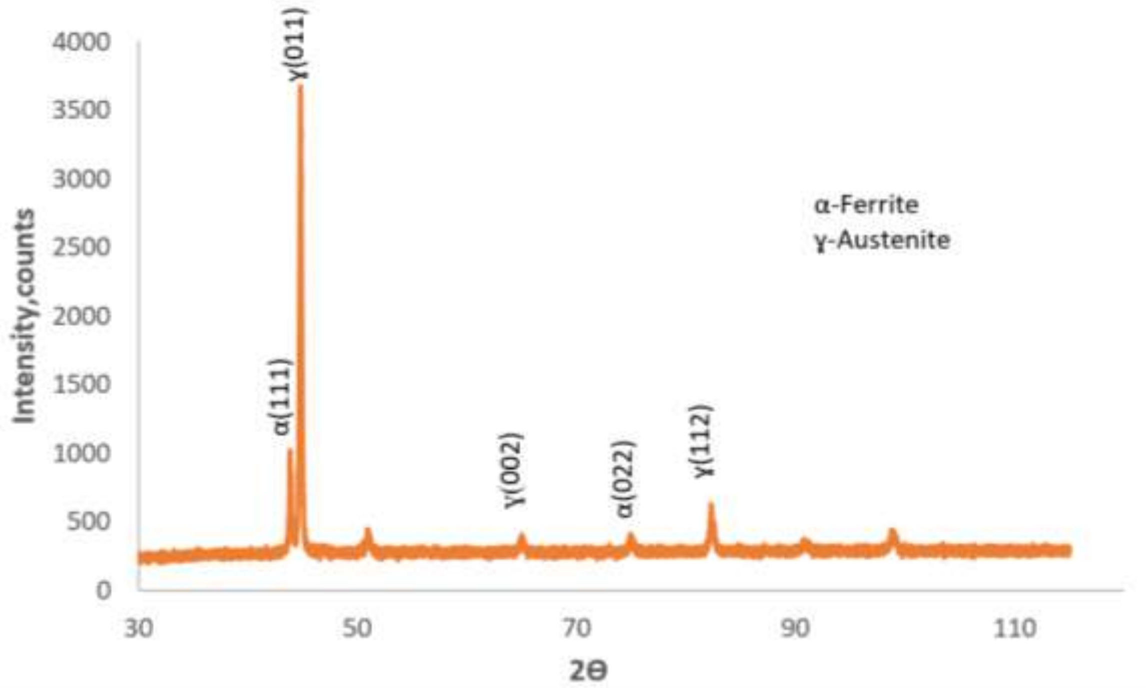

Figure 4-12: XRD spectrum depicting ferrite and austenite peaks for 25L/min gas flowrate

4.6 Hardness results

Vickers micro hardness machine was used to determine the hardness profile of the material. The micro-hardness profile across the mid thickness of the welded joint which included the base metal, heat affected zone and the weld is presented in Figure 4-13. The hardness results show the variations across the joint. Average hardness is outlined in Table 4-2. The increase in gas flow rate impacted on the hardness of the material, with high hardness values observed at high gas flowrate.

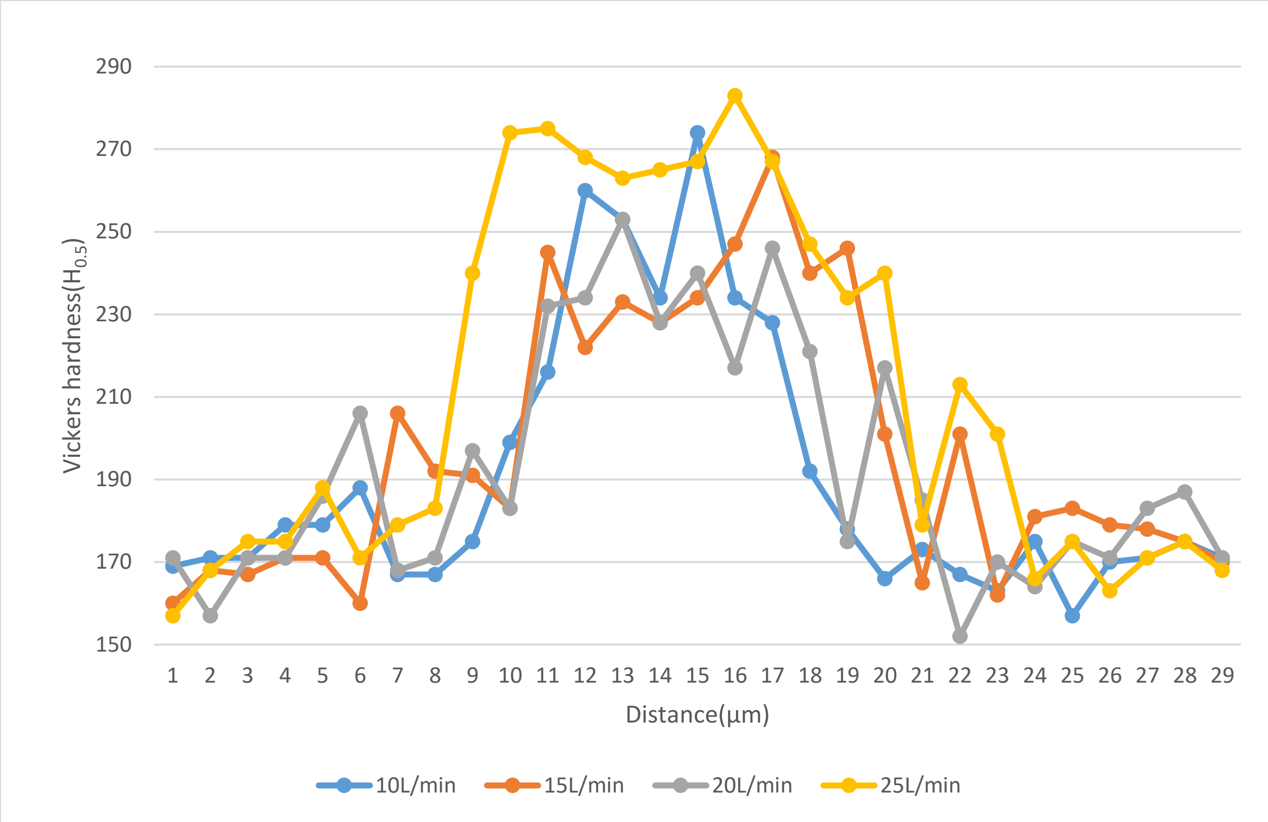

Figure 4-13: Micro-Vickers hardness values across the weld.

Table 4-2: Average micro-Vickers hardness.

Gas flowrate	10L/min	15L/min	20L/min	25L/min
Parent Metal (H_v)	171	172	170	171
HAZ(H_v)	186	191	188	207
Weld (H_v)	243	236	234	268

Hardness profile clearly indicates that there is a hardness increase in the weld region for all the gas flowrates. The HAZ microstructure contains ferrite and martensite. The martensite was formed due to the high temperature (above 723°C) that was transferred during welding and the successive rapid cooling that it received from the parent material. The rapid cooling transforms the austenite to martensite. The presence of martensite resulted in increased hardness within certain parts of the HAZ. From Table 4-2, it can be observed that there is increasing average hardness from the parent metal to the heat affected zone and the weld. This increase in hardness in the weld for all the gas flowrates in the weld is due to the higher cooling that is associated with higher gas flow rates which leads to fine grained microstructure in the weld and the intergranular formation of martensite, hence the hardness increased.

The profile for all the gas flowrates 10L/min-25L/min showed that the parent materials hardness ranges between 170 -179H_V.However, as the indenter started hitting the LTHAZ as well as HTHAZ the hardness increased and then dropped. This was due to the softer ferrite phase that is also contained in both the HTHAZ and the LTHAZ. The hardness increased as the weld zone was reached and decreased within the HTHAZ and LTHAZ until the base metal was reached. Similar trend was observed in all the gas flow rates, with the highest hardness observed at 25L/min. This observation is expected since the weld exhibited small grains with an average grain size of 6µm as opposed to 9µm and 11µm that were observed in LTHAZ and HTHAZ respectively, in addition more martensite was seen on the 25L/min weld microstructure hence the hardness is higher in that region.

4.7 Tensile results

The tensile test samples were tested at room temperature to evaluate the strength of the welds. Table 4-3 presents the tensile properties whereas Figure 4-14 illustrates the stress-strain curve where the linear slope shows the elastic deformation. The yield strength represents the point in which the material starts to undergo permanent plastically deformation.

Table 4-3: Tensile properties of the welded samples at different gas flowrates in comparison to the parent material.

Gas flow rate (L/min)	Ultimate tensile strength (MPa)	Yield strength (MPa)	Elongation (%)
10L/min	389	308	19
15L/min	396	297	17
20L/min	398	307	12
25L/min	442	368	13
Parent metal	**433**	**361**	**37**

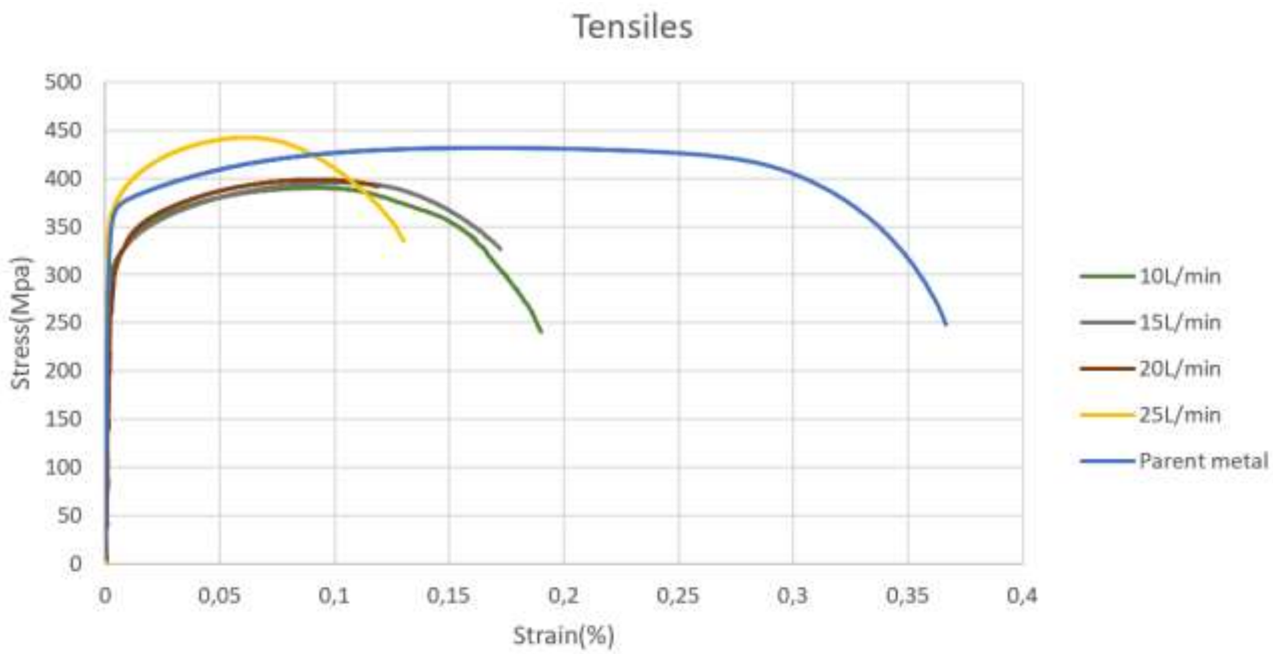

Figure 4-14-: Stress Vs Strain curve for the welds at 10L/min, 15L/min, 20L/min and 25L/min in comparison with the parent metal.

The fracture of the tensile sample was consistently on the parent material as shown in Figure 4-15 suggesting that the joints are strong enough. Welded joints showed lower ductility as opposed to the parent material for all the welded samples.

Figure 4-15: Fracture points for the tensile samples.

A significant drop in tensile strength as opposed to the BS EN 10088 standard was observed in all the samples although this effect was complicated by the presence of both grain boundary martensite and retained austenite. It is apparent that the degradation of toughness and ductility in chromium stainless steel welds is not related strictly to grain size. Thomas and Robison (2002) suggested that intragranular precipitates due to rapid cooling also contributed to decreased tensile strength.

Based on the obtained tensile results it was observed that as the gas flowrate increases the ultimate tensile strength increased. Sanjay *et al.*, (2016) in his research established that an increase in gas flowrates lead to an increase in ultimate tensile strength (UTS). At a gas flowrate of 10 L/min,15L/min,20L/min, and 25L/min UTS of 390 MPa, 396 MPa, 398 MPa and 442 MPa was obtained. According to BS EN1008 standard the minimum UTS that 3Cr12 steel should possess is 450 MPa. All the samples obtained ultimate strength that is below the minimum tensile strength with sample 25L/min recording the highest ultimate tensile strength of 442MPa but also below the minimum UTS recommended by the BS EN 10088 standard. In comparison to the parent material, the weld at 25L/min superseded the parent material. However, the ductility of the parent material reported was 37% elongation. The high UTS that was obtained at 25L/min was due to the high flowrate that stabilised the arc so that the welding wire melted faster. This further accelerated the cooling process of the weld pool. Herman *et al*. (2020) illustrated that the increase in gas flowrate increases the ultimate tensile strength as opposed to decrease in gas flowrate.

The elongation showed that at lower gas flowrate of 10L/min elongation was found to be higher yielding 19%. At 15L/min, elongation dropped to 17%, and dropped further to 12% at 20L/min. Finally the ductility was found to be 13% at 25L/min, increasing only by 1% from 20L/min. Therefore, as the gas flowrate increases the elongation drops. High temperature heat affected region reach peak temperature at 1300°C and causes grain growth of ferrite grains. Lippold (2005) argued that although carbon content of ferritic stainless steel is very small, on rapid cooling the formation of intergranular martensite take place along the grain boundaries. Formation of martensite in the HAZ even in small amounts results in a loss of ductility. Rapidly cooled samples were found to exhibit inferior toughness relative to the samples of equivalent grain size that were slowly cooled (Hunter and Eager, 2000).

4.8 Impact results

Charpy impact test samples were sectioned in the transverse direction. The impact test was conducted to determine the toughness of the material by measuring the absorbed energy under different temperatures (-20°C, -7°C and 25°C), results are recorded in Figure 4-16.

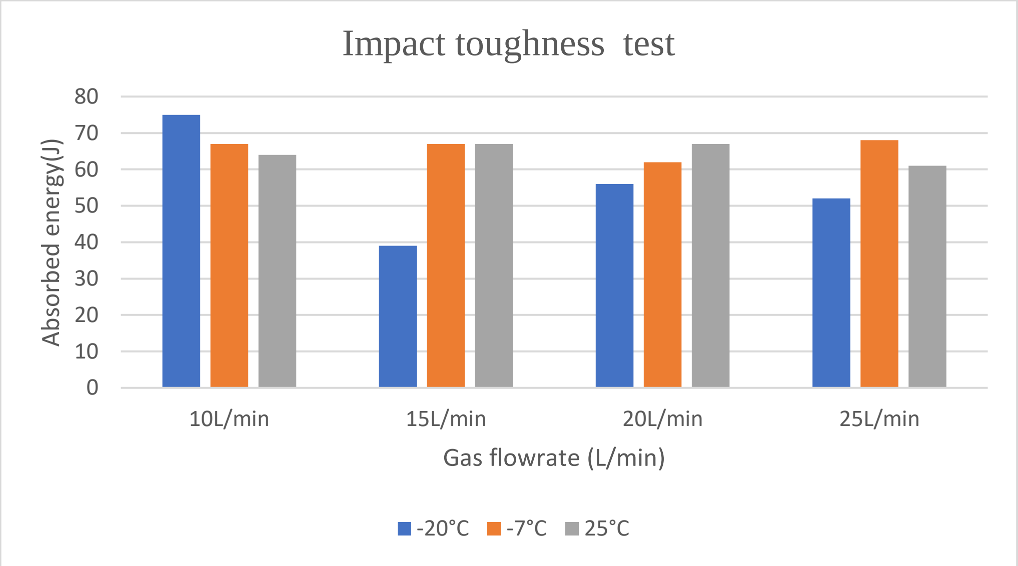

Figure 4-16: Energy absorbed at 10L/min,15L/min,20L/min and 25L/min obtained at -7°C, -20°C, and 25°C tested temperatures.

As the gas flowrate increased in all the tested temperatures (-20°C, -7°C and 25°C) the obtained energy absorption at 10L/ min ,15L/min,20L/min and 25L/min gas flowrates were found to meet the minimum requirement of the absorbed energy stipulated by the standard. BS EN 1008 states that a minimum of 34 J is expected from 3Cr12 material.

At -20°C all the samples obtained an energy absorption above 34 J which is specified in the BS EN 10088 standard, at 10 L/min, 15L/min, 20 L/min and 25L/min an energy absorbed was found to be 75J, 39J, 56J and 52 J respectively. Similarly, trend was seen at -7°C where at 10 L/min, 15 L/min and 25 L/min and 25 L/min obtained relatively the same energy of 67 J, lowest 67 J, 62 J and 68J respectively. Finally at 25°C the different gas flowrates of 10 L/min, 15 L/min and 25 L/min managed to obtain and absorbed energy of 64J, 67J, 67J and 61J respectively.

Using helium as a shielding gas result in a hotter arc and provides a suitable cooling rate for transfer from ferrite to austenite, which should improve the impact toughness of the weld the results indicate that the samples can withstand impact in different environment. Wright and wood (2001) in their research have shown that duplex ferritic-martensitic microstructure based on the Fe-Cr-Ni and Fe-Cr systems respectively, have superior impact toughness properties relative to either ferritic or fully martensitic steels of similar composition.

4.9 Huey corrosion results

Boiling nitric acid is a strongly oxidizing environment to detect the chromium depleted regions as well as intermetallic precipitations, like sigma phase in the stainless steels. The area of the sample was calculated and presented in Table A-1; Table A-2 shows the weight measured at different time intervals as tabulated in the appendix. Table A-3 illustrates the mass loss of all the gas flowrates whereas Table A-4 and Figure 4-17 below shows the calculated corrosion rates of different samples.

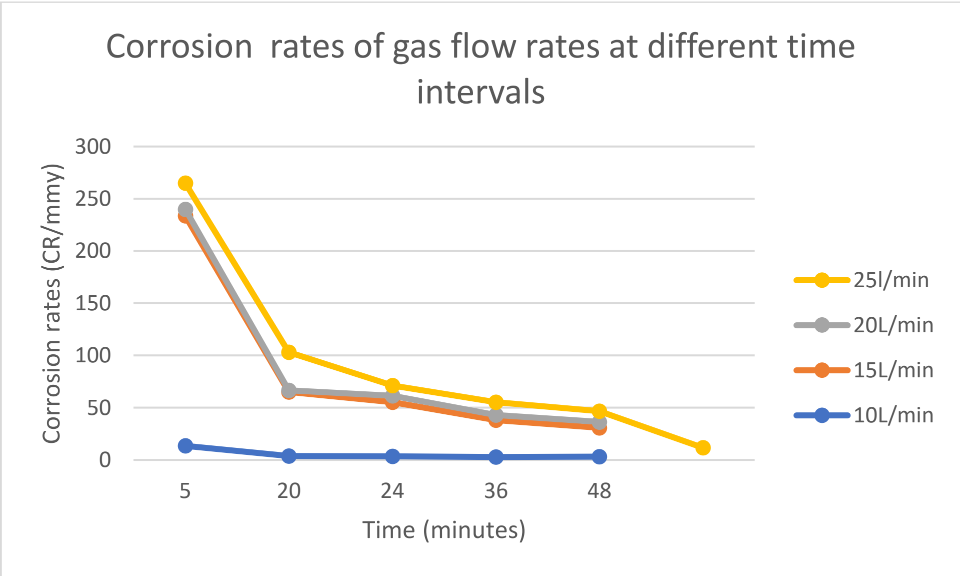

Figure 4-17: Corrosion rates of gas flowrates at different time interval

Corrosion rates in Table A-5 were calculated according to Equation 4-3 and Figure 4-18 shows the comparison of obtained average corrosion rates at different gas flowrates:

$CR = \frac{M*K}{\rho*A*T}$ ………. *(4-3)*

Whereby:

M-Mass loss(g)

k-constant=8.74X10^4

ρ*-Alloy density (g/cm*^{3}*)*

A-Exposed area (cm^2*)*

T-Exposure time(hr)

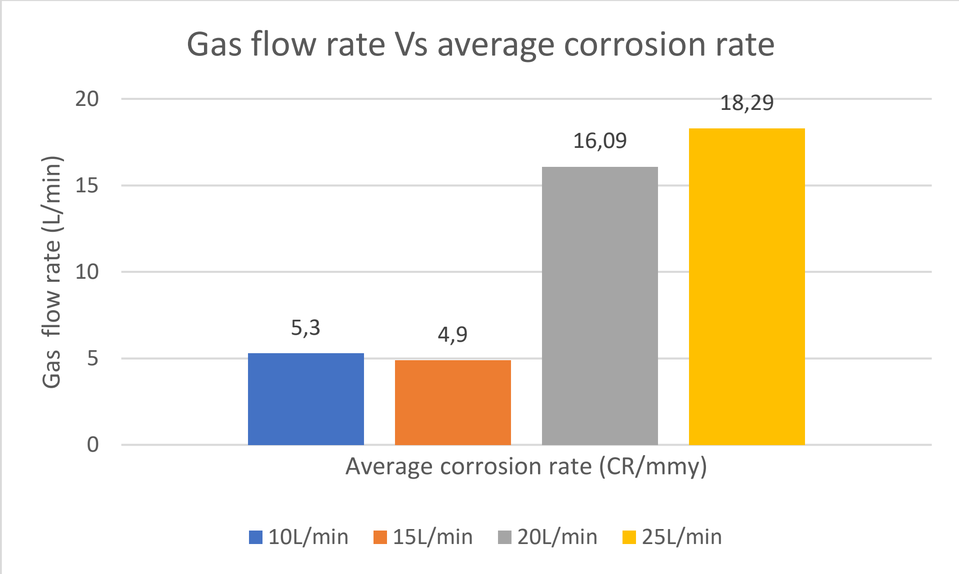

Figure 4-18: Corrosion rates for different gas flow rates.

The Huey corrosion showed that no intergranular corrosion was observed (Figure 4-19), insignificant mass loss was observed on all the samples. According to the evaluated microstructural images captured no mass loss was observed on the grain boundaries. No continuous ditches were found of any samples as a result no sensitization occurred on any of the sample. Therefore, welding of 3Cr12 with helium gas at different gas flowrates is not susceptible to the intergranular corrosion. There are several factors that can be used to limit sensitization during the welding process. Low heat input which ranges between 1kJ/mm 1.5kJ/mm as well as the use of low carbon welding wire minimizes the risk of sensitization by slowing down the carbide precipitates. These are the ways that can be used to limit sensitization during welding.

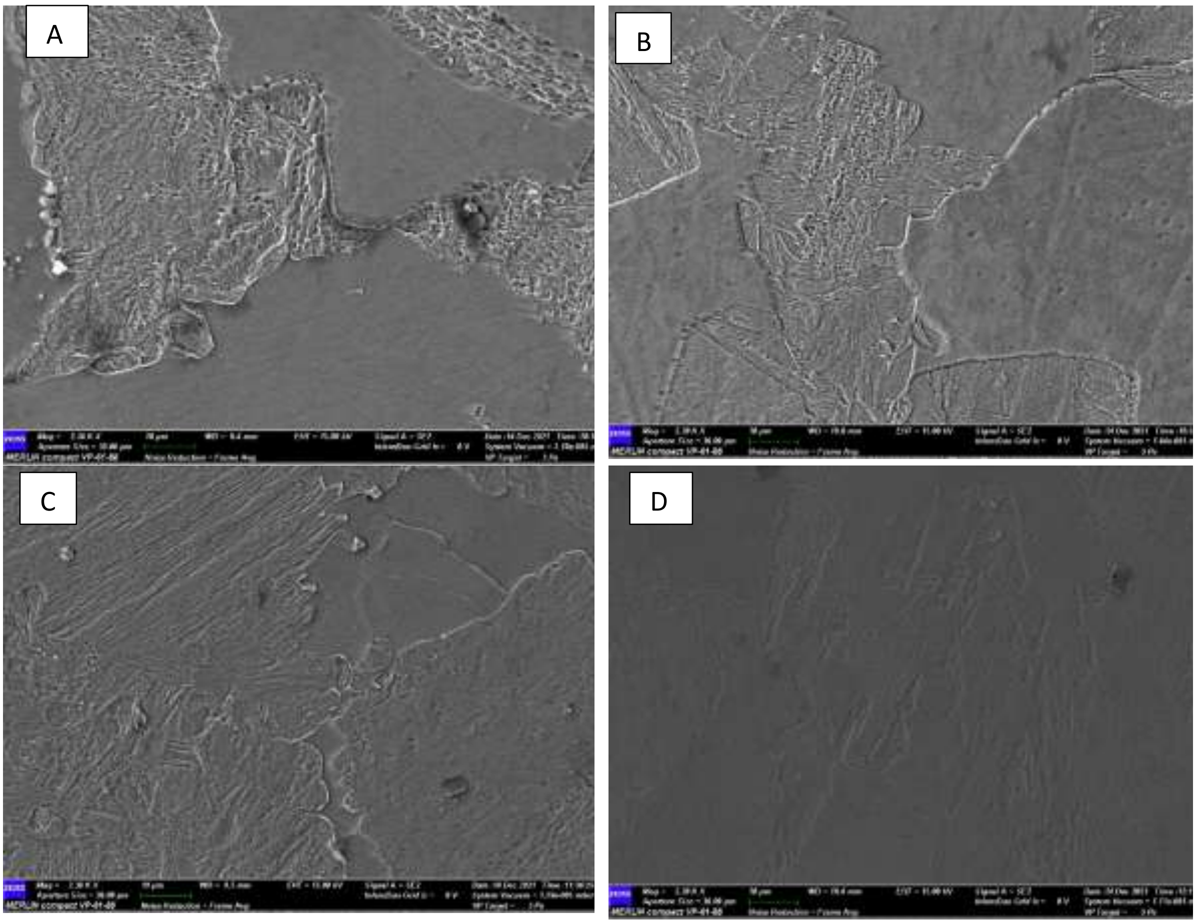

Figure4-19: SEM micrographs of the different gas flowrates after Huey corrosion testing (a)10l/min, (b) 15l/min, (c) 20l/min and (d) 25l/min.

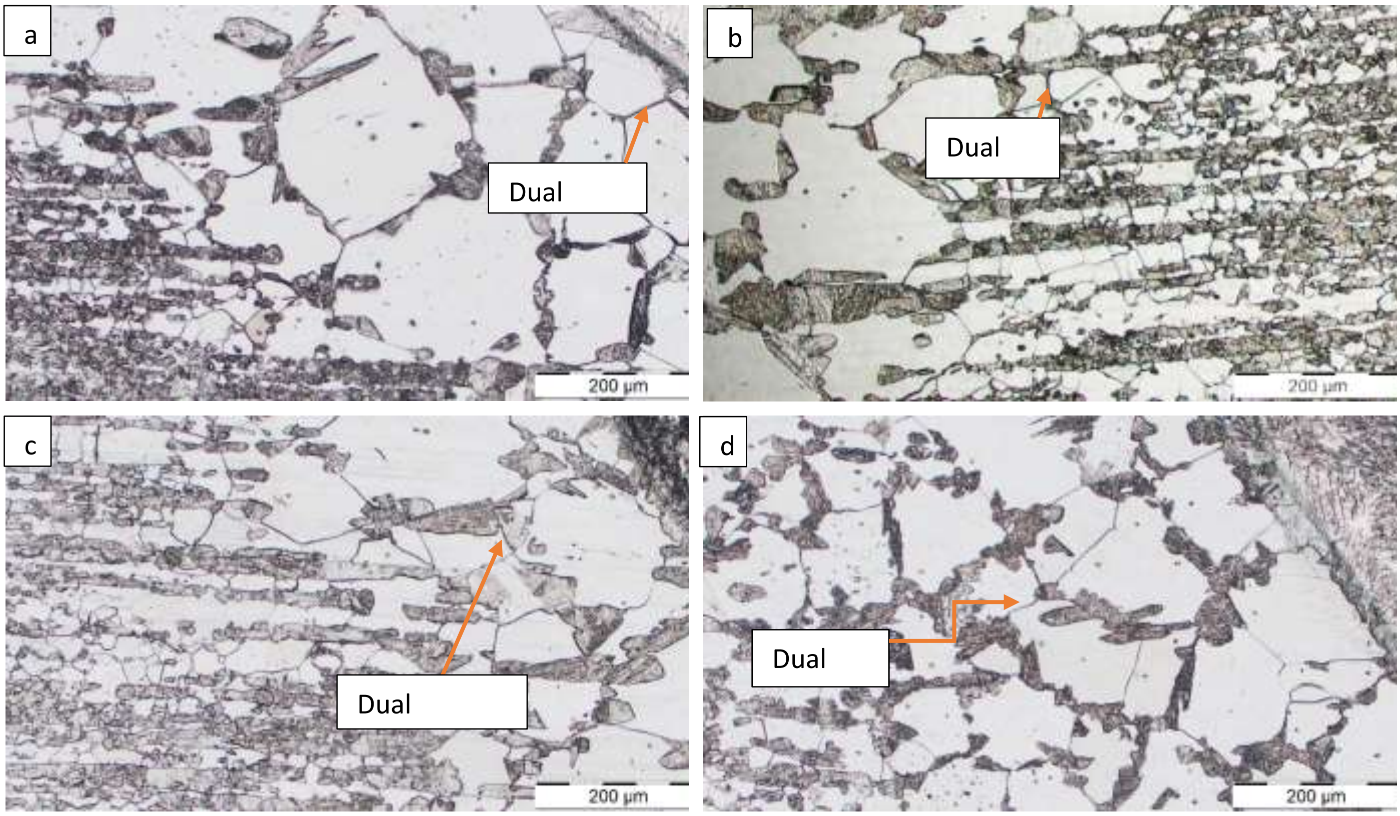

Figure 4-20: Microstructures of the different gas flowrates after Huey corrosion testing (a) 10l/min, (b) 15l/min, (c) 20l/min and (d) 25l/min.

Vilella etchant was recommended for electro-etching of this material as it exposes the structure and the observation of sensitization way better than the oxalic acid. All the gas flow rates did not show any continuous ditch however duals were observed and indicated on Figure 4-20. According to literature dual and step are accepted for material application and sensitization is meant to occur when a continuous ditch is visible, no ditch was observed on the samples, therefore no sensitization occurred. This agreed with the Huey tests that were conducted showing that there was no sensitization.

Figure 4-20 shows the samples which were electro-etched to check for sensitization which would be represented by a ditch structure. From the micrographs, there were duals on some grain boundaries, which are indicated by pronounced grain boundaries, but the grains are not surrounded by duals hence there is no sensitization in any of the samples. This suggests that the heat input used was high enough to completely fuse the two materials but still low enough to not cause sensitization. There is grain growth which can be seen at the HTHAZ which is due to the heat input from the welding process. The high temperature caused grain growth and rearrangement of dislocations in the crystal structure, resulting in the recrystallisation of grains to form new coarser grains.

The gas flowrate was varied from 10L/min to 25/L/min with increments of 5L/min and on all samples, it was observed that the microstructure on the weld was austenite with a combination of martensite and ferrite for all the samples. At the heat affected zone was found to have high temperature heat affected zone which is closer to the fusion zone, and it consisted of coarse grains of ferrite as opposed to lower temperature heat affected zone (LTHAZ) this is due to the susceptibility of the HTHAZ to the heat that is generated during welding.

(Grobler, 1987) reported that the low carbon ferritic steel has poor weldability as after welding, there is martensite that forms on the grain boundaries which increases the hardness but decreases the ductility and corrosion resistance. The heat affected zone (HAZ) has grain growth which decreases the toughness and ductility of the material. The relationship between grain size and yield strength can be explained using the Hall-Petch equation which says that increasing grain size decreases yield strength (Li, *et al*., 2016). Grobler (1987) stated that decrease in yield strength results in a decrease in ductility. There are also chromium carbides that form (Du Toit *et al*., 2007).

Heiring (2019) suggested that coarser grains result in decreased hardness, yield strength, tensile strength, impact, and fatigue strength (Herring, 2019). It would be expected that the hardness would increase with increasing distance from the parent metal due to the presence of martensite in the weld which the conducted test revealed. Referring to Figure 4-13, the average hardness is highest in the weld and lowest in the parent metal. The hardness profile does not show a linear increase from the parent metal to the weld. This is because microhardness can indent specific phases within the HAZ, the indentations with the higher hardness are most likely martensite whilst the one with the lower hardness show the ferrite phases.

Chapter 5

5.1 Conclusion

In this project, the welding process was carried out by varying the gas flowrate of helium as the shielding gas during the welding of 3Cr12 with 308L welding wire. From the tests conducted, the following conclusions were drawn:

- Defect free and sound welded samples were obtained from the welding of 3Cr12 with 308L welding wire at all gas flow rates. The base metals fused properly with the austenitic filler, good penetration was achieved, and no cracks were detected.
- The sample consisted of a low-temperature HAZ which has fine grains and a high-temperature HAZ which consists of coarser grains with a microstructure of ferrite and intergranular martensite on the grain boundaries.
- The weld for all samples showed an austenitic microstructure with a combination of martensite and sigma ferrite.
- XRD results showed the presence of BCC ferrite and FCC austenite across the welded samples, however martensite was not detected due to low carbon stainless steel used.
- No sensitization was observed on the welded samples hence no intergranular corrosion will occur on them. Heat input played a very important role as a weld parameter in joining ferritic stainless steel. The heat input was kept at the correct range of not promoting sensitization, it was kept low to avoid excessive grain growth within the HAZ. Thus, use of low HI is recommended in welding steel. The 308L welding wire contains low carbon hence the limitation of sensitization.
- The weld zone exhibited higher average hardness than the parent and the HAZ regions of the sample. The obtained hardness for the parent metal has an average that is about 171H_V which meets the specification.
- Tensile properties proved that welding decreases the superior of the tensile properties to meet the minimum requirements throughout all the samples although the helium shielded samples have superior tensile properties. The tensile test revealed that the material is ductile with 441MPa being the maximum stress that the material, at 25L/min, can withstand. The obtained tensile stress and elongation for the 10L/min, 15l/min, 20L/min and 25L/min samples are less than the minimum tensile stress (460MPa) and the minimum elongation (18%) that is in the mill specification.

- The impact properties exceeded the specification minimum of 35kJ of absorbed energy required for the material.
- Helium is much lighter; hence the increased gas flowrate (25L/min) is necessary to yield optimum results. Therefore 25L/min was found to be more optimum gas flowrate from the obtained results.
- The use of helium as the shielding gas at 25L/min during welding yields preferably suitable metallurgical, mechanical and corrosion properties for welding of 3Cr12 with 308L welding wire.

5.2 Recommendations

- High speed camera should be incorporated to capture the melt pool during welding of the samples at each gas flow rate, measure and compare the different gas flowrates.
- A similar design of experiment should be conducted on 309L currently used welding wire and compare the obtained results with the alternative welding wire contained in this study.

References

Abbruzzese G, B. M., 2004. *Structural Application of Stainless Steel*. Italy: Centro Sviluppo *Materiali*.

Abioye, T., 2017. *The effect of of heat input on the mechanical and corrosion properties of AISI 304 electric arc weldments*. British of journal of applied science and technology, 20(11), pp. 1-10.

Alberto, J., 2008. *Mechanical properties of hybrid laser MIG welding and spot welding on lap joint.*Sweden: Lulea University of Technology.

Amuda, M., 2011. *An overview of sensitization dynamics in ferritic stainless steel welds*. Advance Materials and Surface Engineering Research Unit, 2011(10), pp. 1-9.

Antila ,S ., Heikkinen , H. 2014. *Structural Application of Ferritic Stainless Steel.* Finland: The Research Fund for Coal and Steel.

Apurv, C., 2014. *Influence of heat input on mechanical properties and microstructure of austenitic 202 grade stainless steel weldments*.Transactions on Applied and theoretical mechanics , 9(5), pp. 222-228.

Arun, N.J., 2013. *Influence of gas tungsten arcwelding parameters on aluminium 5083 alloy*. International Journal of Engineering and Innovative Technology , 3(3), pp. 113-118.

Atlas, 2013. *Atlas Steel.* [Online]
Available at:
https://www.atlassteels.com.au/documents/Atlas%20Technical%20Handbook%20rev%20Aug%202013.pdf
[Accessed 03 January 2021].

ASTM, i., 2018. *Standard Test Methods for Notched Bar Impact Testing of Metallic Materials.* 3 ed. West Conshohocken: ASTM International.

ASTM, S., 2018. E8 *Standard Test Methods of Tension Testing of Metallic Materials*. American Society for Testing and Materials,3(1).

Atma, R., 2014. *Determination of distortion development during TIG welding of low carbon steel plate*. Engineering Research , 1(4), pp. 23-29.

Bailey, J. A., 2009. *Mechanical testing and evaluation.* Newyork: ASM Metal Handbook.

Bang, K. C., 2008. *Effect of welding parameters on tensile strength of weld metal in flux cored welding.* Science and Technology of Welding and Joining, 13(7), pp. 508-514.

Baughurst., 2011. *Welding defects, causes and correction.* Australia: Aspec Engineering.

Bergquist, E. L., Huhtala, T.,Karlsson, L.,2011 '*The effect of purging gas on 308L TIG root-pass ferrite content',* Welding in the World, 55(3–4), pp. 57–64.

Bitharas, I.,Mepherson,N.A.,Mcghie,W.,Roy,D.,Moore,A.J.,2018. 'V*isualisation and optimisation of shielding gas coverage during gas metal arc welding*', Journal of Materials Processing Technology, 255 pp. 451–462.

Bolarinwa, J. A. G., (2018). *Review of Gtaw welding parameters*. Minerals and materials characterization, 6(5), pp. 541-554.

Bomi, K., Soojin,K.,Heesan., K.,2018. *Effects of Alloying Elements (Cr, Mn) on Corrosion Properties of the High-Strength Steel in 3.5% NaCl Solution*. Hindawi, 2(18), pp. 1-14.

British,I., 2002. *The British Institute of Non-Destructive Testing :What is NDT.* [Online] Available at: https://www.bindt.org/What-is-NDT/Magnetic-particle-inspection-MPI/ [Accessed 22 november 2021].

Capudean, B., 2020. *Metallurgy Matters: Welding's effect on strengthened steel.* [Online] Available at: https://www.thefabricator.com/thewelder/article/metalsmaterials/metallurgy-matters-welding-s-effect-on-strengthened-st

Chaudhari, P. D. and More, N. N.,2014.E*ffect of Welding Process Parameters On Tensile Strength*, 4(5), pp. 1–5.

Chen, C.,Wei,X.,Zhao,Y.,Yan.K.,Jia,Z.,2017. *Effects of helium gas flow rate on arc shape, molten pool behavior and penetration in aluminum alloy DCEN TIG welding*, Journal of Materials Processing Tech,3(1),pp. 38-50

Chuang, YY., Chang, Y.A.,1987. *A thermodynamic analysis and calculation of the Fe-Ni-Cr phase diagram*. Metall Mater Trans,18 (13) 733–745

Columbus., 2007. *3Cr12 technical sheet ,* Middleburg: Columbus stainless steel.

Cortie, M., 1993. *Development of ferritic stainless steel*. SAAIM, pp. 165-170.

Dahmen, M., Dhasanur, K., Lindner, S.,2015.*Sensitization of laser-beam welded martensitic stainless steels*, Physics Procedia. 78, pp. 240–246.

Demo, J., 1971. *Mechanism of high temperature embrittlement and loss of corrosion resistance in AISI type 446 stainless steel*. Corrosion, 27(12), pp. 531-544.

Duffey, M. J., 2016. *Metallurgical characterization and weldability evaluation of ferritic and austenitic welds in armor steels,* United State: The Ohio State University.

Durgutlu, A.,2004.*Experimental investigation of the effect of hydrogen in argon as a shielding gas on TIG welding of austenitic stainless steel*, Materials and Design, 25(1), pp. 19–23.

Du Toit, M., Van Rooyen, G. T. and Smith, D.,2007. *An overview of the heat-affected zone sensitization and stress corrosion cracking behaviour of 12 % chromium type 1.4003 ferritic stainless steel*, Welding in the World,51(10),pp.41-50

Easterling, K., 1992. *Introduction to the Physical Metallurgy of Welding.* 2nd ed. London: Buttersworth Heinemann Ltd.

Enterprise, R. T., 2002. *Google.* [Online] Available at: http://www.revotechnologies.net/uploads/1/6/0/7/16078520/unit_ii-_mt1.pdf [Accessed 17 December 2021].

Ethan, 2021. *Mewelding.* [Online] Available at: https://mewelding.com/carbon-arc-welding-caw/ [Accessed 17 December 2021].

Florida, U. O., 2006. *Google.* [Online] Available at: https://mae.ufl.edu/designlab/Lab%20Assignments/EML2322L-Welding.pdf

[Accessed 20 November 2021].

Ghazviloo, H., 2010. *Effect og gas shielded flux cored arc welding parameters on weld width and tensile properties of weld metal in low carbon steel.* Applied science, 10(7), pp. 658-663.

Gomes , 2020. *The 10 Common Weld Defects You Should Know.* [Online]
Available at: https://sentin.ai/en/10-common-weld-defect-imperfections-discontinuities/
[Accessed 04 January 2022].

Gooch, T., 1984. *Welding of 3Cr12 corrosion resisting steel.* Johannesburg, Inuagural internatinal 3Cr12 conference

Grobler, C., 1987. *Weldability studies on 12% and 14% chromium steels,* Pretoria: University of Pretoria.

Herring., 2019. *Grain size and its influence on material properties.* [Online]
Available at: heat-treat-doctor.com/documents/grainsize.pdf
[Accessed 17 April 2020].

Hoffman, J., 1984. *The welding of a titanium stabilized 12 percent chromium ferritic-martensitic steel.* 2 ed. France: ASM.

Huntley, R., 1984. *Pipeline girth welding using the flux cored arc welding process*. Welding in energy related projects, 1(21), pp. 120-138.

Industries, S., 2021. *SMI steelmor.* [Online]
Available at: https://www.steelmor.co.za/the-role-of-alloying-elements-in-stainless-steel/
[Accessed 29 December 2021].

Huang, H. Y. and Yang, C. W.,2013 '*Influence of activating flux and helium shielding gas on an austenitic stainless steel weldment*', Metallurgical and Materials Transactions, 44(3), pp. 730–737.
Industries, S., 2021. *SMI steelmor.* [Online]
Available at: https://www.steelmor.co.za/the-role-of-alloying-elements-in-stainless-steel/
[Accessed 29 December 2021].
Janunkar, R., 2017. *Effect of welding speed on strength of welded joint using TIUG welding process.* Technology ,engineering and research, 2(1), pp. 337-342.

Joao., 2014. *Scientific Research and Essay.* [Online]
Available at: https://www.researchgate.net/figure/Schematic-flux-cored-arc-welding-process_fig2_269399548
[Accessed 01 July 2022].

Kah, P.,Mvola,B.,Martikainen,J. and Suoranta,R. (2014) '*Real Time Non-Destructive Testing Methods of Welding*', 3(8) pp.13-19.

Kaltenhuser, R., 1971. *Improving the engineering properties of ferritic stainless steel*. Metals engineering, 11(2), pp. 41-47.

Kang, B. Y.,Prasad,Y.,Yarlagadda,K.P.,Kang.M.J.,Kim,H.J.,2009a.*Characteristics of alternate supply of shielding gases in aluminum GMA welding, Journal of Materials Processing Technology* 209, pp. 4716–4721.

Kang, B. Y.,Prasad,Y.,Yarlagadda,K.P.,Kang.M.J.,Kim,H.J.,2009b.*The effect of alternate supply of shielding gases in austenite stainless steel GTA welding,* Journal of Materials

Processing Technology, 209(10), pp. 4722–4727.

Keskitalo, M.Sundvist,J.,Mankyjarvi,K.,Powell,J.,Kaplan A.F.,2015.*The influence of shielding gas and heat input on the mechanical properties of laser welds in ferritic stainless steel'*, Physics Procedia. 78(5), pp. 222–229.

Khokhar .,2005. *Quantitative analysis of multi-phase systems -steels with mixture of ferrite and austenite* , Sweden: Linköping University.

Knusten, R., 1989. *A microstrutural examination of duplex ferrite-martensite corrosion resisting steel*, Capetown: University of Cape town.

Koli,Y.,Yavaraj,N.,Vipin,T and Aravindan,S.,2019.*Investigations on weld bead geometry and microstructure in CMT, MIG pulse synergic and MIG welding of AA6061-T6*,Material research express.6(12),pp.65-70.

Larry, F., Jeffus ,V.,Johnson,L., 1988. *Welding: Principles and Applications.* 2 ed. Texas: Delmar.

Leon,L.,Kerr W.,1982.*The ferrite to austenite transformatiom in stainless steels,*welding research supplement.2(3),pp.13-22

Lesson, S., 2020. *About us:Material Science.* [Online]
Available at: https://studentlesson.com/arc-stud-welding-definition-machine-applications-types-working/
[Accessed 12 November 2021].

Lincoln, 2014. Gas Metal Arc Welding Guidelines. *The welding expert.*

Lippold, J.C.,Kotecki,D. J., 2005. *Welding Metallurgy and Weldability of Stainless Steel.* 2 ed. Canada: John and Wiley & Sons Inc.

Liu, S. T., 1989. *A study of droplet rates for various transfer modes*. Welding and joining research , pp. 53-58.

Li, Y., Bushby, A. J. and Dunstan, D. J., 2016. *The Hall–Petch effect as a manifestation of the general size effect.* London, Royal Society.

Materia, 2022. *Total Materia.* [Online]
Available at:
https://www.totalmateria.com/page.aspx?ID=CheckArticle&site=kts&LN=TR&NM=232
[Accessed 07 July 2022].

Malcom, 2000. *The Welding Institute.* [Online]
Available at:
https://www.researchgate.net/publication/238705366_Geometry_and_Microstructure_of_Metal_Inert_Gas_and_Friction_Stir_Welded_Aluminium_Alloy_5383-H321?enrichId=rgreq-4df5868c8375aa48fc7bc63f85a1b1e9-XXX&enrichSource=Y292ZXJQYWdlOzIzODcwNTM2NjtBUzoyNzY0NjQ2N
[Accessed 01 July 2022].

Martin L.,Marcus,T.,Uwe,F and Sacha,R.,2020.*Influence of the CO_2 content in shielding gas on the temperature of the shielding gas nozzles during GMAW welding*.Journal of Manufacturing and Materials Processing,4(113),pp. 2-13.

Messler Jr, R.W.,Savage,W.F.,1999. *Principle of Welding Process.* 1st ed. Singapore: John

Wileyand Sons Inc.

Metalwork, 2020. *Student lesson.* [Online]
Available at: https://studentlesson.com/arc-stud-welding-definition-machine-applications-types-working/
[Accessed 01 July 2022].

Meyer, A. M. and Meyer, M. (2000) '*Interstitial diffusion from the weld metal into the high temperature heat affected zone in 11- 12 % chromium steel welded joints* .Weld World 52,pp.42-49.

Molabe, 2018. *Determining the optimum welding of 3Cr12 stainless steel ,* Johannesburg: University of Johannesburg.

Moslemi, N.,Redzaan,N.,Ahmed,N.,Hor,T.N.,2015. *Effect of Current on Characteristic for 316 Stainless Steel Welded Joint Including Microstructure and Mechanical Properties, Procedia CIRP*. 26, pp. 560–564.

Mvola, B. and Kah, P.,2017. *Effects of shielding gas control : welded joint properties in GMAW process optimization*, pp. 2369–2370.

Paktechpoint, 2016. *Paktechpoint.* [Online]
Available at: https://paktechpoint.com/shielded-metal-arc-welding-with-coated-electrodes-smaw/
[Accessed 01 July 2022].

Pagani, S., 1984. *The development of the weld metal composition of 3Cr12 in relation to mechanical and electrochemical requirements.* Johannesburg, Inuagural International 3Cr12 conference.

Paniagua, M., 2007. *Effect of active and non-active fluxes on mechanical properties and microstructure in sub-merged arc welds of A-36 steel plates*. Materials and manufacturing processes, 223(11), pp. 851-863.

Profile, S. E. E. (2013) '*Welding New Generation Steel PB2 Using Conventional Welding with and without PWHT with Use of Temper Bead Technique*', 5(1)pp.1-4.

Poorhaydari, K. and I. G., 2005. *Estimation of Cooling Rate in the Welding of Plates with Intermediate Thickness*. Welding Research, 1(1), pp. 149-155.

Rivlin V. G. and Raynor G. V, (1980).*Critical evaluation of constitution of aluminium-iron-nickel system,* International Metals Reviews,25(1) pp.79-93

Seong., S. Y., 2013. *Role of grain boundary carbides in cracking behaivior of Ni base alloys*. Nuclear Engineering and Technology, 45(1), pp. 74-81.

Shamail.,2015. *Presence of golden ratio relationships in Fe–Fe_3C, Cu–Zn and Cu–Sn alloy systems.*International Journal of Design and Nature and Ecodynamics, 10(2), pp. 174-181.

Shinde, N. V. and Telsang, M. T.,2016.*Effect of Alternate Supply of Shielding Gases of Tungsten Inert Gas Welding on Mechanical Properties of Austenitic Stainless Steel*, Journal of The Institution of Engineers (India)*:* Series C. India, 97(3), pp. 299–307.

Shojaati, M. and Beidokhti, B.,2017.*Characterization of AISI 304 / AISI 409 stainless steel joints using different filler materials*, Construction and Building Materials.147, pp. 608–615.

Sun, H., 2008. *Effects of oxide activating flux on laser welding of magnesium alloy*. Science and technology of welding and joining, 13(9), pp. 305-311.

Sundqvist, J.Manninen,T.,Heikkinen,H.,Anttilas,S.,Kaplan,A.F.,2018.*Laser surface hardening of 11 % Cr ferritic stainless steel and its sensitisation behaviour,* Surface and Coatings Technology.344 , pp. 673–679.

Strawstrom, C., 2002. *An improved depleted zone theory of intergranular corrosion of 18-8* stainless steel. 2 ed. London: Mechanism and mitigation.

Streicher, M., 1973. *The role of carbon ,nitrogen and heat treatment in dissolution of Iron-chromium alloys in acids*. Corrosion, 29(9), pp. 337-360.

Tewari, S., 2010. *Effect of welding parameters on the weldability of materials*. International journal of engineering science and tehnology , 2(1), pp. 512-516.

Thomas, C.R.,Apps.R.L ., 1980. *Weld heat affected zone properties in AISI 409 ferritic stainless steel.* 4 ed. London: ASTM International.

Thorat, S., 2016. *Automobile Engineering.* [Online]
Available at: https://learnmech.com/atomic-hydrogen-welding-working-advantages-and-application/
[Accessed 02 01 2022].

Tomari, H. M., 1982. *Intergranulare stress corrosion cracking of 13%/ and 18% Cr ferritic stainless steel in high temperature putrity water*. Corrosion, 38(5), pp. 293-294.

TVS, 2007. *Welding master.* [Online]
Available at: https://www.theweldingmaster.com/welding-defects/
[Accessed 04 January 2022].

TWI, 2003. *Who we are :TWI industries and technical knowlegde.* [Online]
Available at: https://www.twi-global.com/technical-knowledge/faqs/flux-cored-arc-welding-fcaw
[Accessed 27 December 2021].

Van Warmelo, M., 2007. *Susceptibility of 12% Cr steels to sensitization during welding of thich gauge plate.* 1 ed. Australia: University of Wollongong.

Welding IS, 2021. *Weldingis.com.* [Online]
Available at: https://www.weldingis.com/gtaw-welding/
[Accessed 01 July 2022].

Welding metallurgy, 2012. *Welding metallurgy.* [Online]
Available at: https://www.nrc.gov/docs/ML1215/ML12157A607.pdf
[Accessed 01 July 2022].

Williams, J., 2005. *Susceptibility and prevention of HAZ sensitization and intergranular stress corrosion cracking in various 12% Cr steels.* United States, Proceedings of the Iron and steel Technology Conferences.

Yuri, T., 2000. '*Effect of welding structure and ferrite on fatigue properties for TIG welded austenitic stainless steel at cryrogenic temperatures*'. Cryrogenics, 40(6), pp. 251-259.

Wu, J.,Wang,W.,Attallah,M.M.,Loretto,M.H.,2016.*Microstructure and strength of selectively laser melted AlSi10Mg*', Acta Materialia, 117, pp. 311–320.

Xi-he, W.,Ji,T.,Shao,W.,Dong,F.,2009. *Investigation on TIG welding of SiCp-reinforced* *aluminum – matrix composite using mixed shielding gas and Al – Si filler*,499, pp. 106–110.

Zahiri, B., 2017. [Online]
Available at:
https://www.researchgate.net/post/How_to_identify_low_carbon_martensite_or_martensitic_ferrite_in_01C_steel_through_XRD/58e7bcd7eeae397f5d4cd432/citation/download
[Accessed 11 January 2022].

Zhang, R., 2006. *Electron beam welding with activating flux*. Transactions of Japan Welding Research Institute, 35(3), pp. 12-19.

Appendix A
Huey corrosion results

Table A-1: Calculated area of the samples size before testing.

Gas flowrate(l/min)	Area/cm^2
10	1,6
15	1,6
20	1,36
25	1,6

Table A-2: Weight measured at different time interval.

Gas flowrate (l/min)	Initial mass(g)	Mass(g) after 5 hrs	Mass (g) after 20 hrs	Mass (g) after 24hrs	Mass (g) after 36 hrs	Mass (g) after 48hrs
10	10,188	10,187	10,187	10,187	10,187	10,186
15	19,278	19,262	19,260	19,260	19,260	19,259
20	5,811	5,811	5,811	5,810	5,809	5,808
25	10,818	10,816	10,815	10,814	10,813	10,810

Table A-3: Mass loss at different time intervals.

Gas flow rate(l/min)	M5/g	M20/g	M24/g	M36/g	M48/g
10	0,001	0,0011	0,0012	0,0015	0,0022
15	0,0163	0,0182	0,0184	0,0189	0,0197
20	0,0004	0,0004	0,0019	0,0021	0,0034
25	0,0027	0,0029	0,0044	0,0054	0,0083

Table A-4: Corrosion rates of gas flowrates at different time interval.

Gas flowrate (l/min)	CR5/mmy	CR20/mmy	CR24/mmy	CR36/mmy	CR48/mmy
10	13,50	3,71	3,38	2,81	3,09
15	220,10	61,44	51,76	35,45	27,71
20	6,35	1,59	6,29	4,63	5,63
25	36,46	9,79	12,38	10,13	11,67

Table A-5: Average corrosion rates

Gas flow rates (L/min)	Average corrosion rates(CR/mmy)
10	5.30
15	4.90
20	16.09
25	18.29